
UNIVERSITÀ POLITECNICA DELLE MARCHE
FACOLTÀ DI INGEGNERIA

Corso di Laurea Magistrale in Biomedical Engineering

# Biomedical Application of Hyperspectral Imaging in Medicine

Relatore:
**Lorenzo Scalise**

Tesi di Laurea di:
**Silvia Discepolo**

Correlatore:
**Paolo Castellini**

A.A. 2020/2021

# THANKSGIVING

Prima di passare alla trattazione del lavoro volevo dedicare poche parole per ringraziare tutte quelle persone che ci sono state in questi due anni, che in un modo o nell'altro mi hanno portato a essere la persona che sono ora.
Questo traguardo lo voglio dedicare prima di tutto a me stessa, alla mia forza, alla mia testardaggine e al mio sorriso. Ringrazio me stessa perché in un periodo difficile sono riuscita a portare a termine questo traguardo, per me molto importante.

Il primo ringraziamento è per Lara, la mia sorella gemella, la mia fotocopia e la mia ragione di vita. Ti ringrazio perché sei stata la prima a credere in me. Io e te abbiamo condiviso sempre tutto insieme, eccetto che la vita scolastica. Ci siamo divise fin dalle superiori e poi abbiamo continuato a prendere strade differenti, ma ci siamo sempre sostenute in questi anni e mai lasciate sole. Sei sempre stata per me, il mio punto di riferimento per la tua caparbietà, per il tuo carattere e la tua forza di riuscire a dimostrare sempre a tutti quanto sei forte e quanto vali. Ti voglio ringraziare perché tu sei il mio porto sicuro e il mio riparo. Ti ringrazio per avermi dato la forza quando mi mancava, per avermi strappato un sorriso quando mi scendevano le lacrime, e per avermi sempre detto di continuare anche quando tutto mi sembra veramente difficile e volevo mollare.

Questo traguardo lo dedico alla mia famiglia, a Mamma, a Papà e a Daniele. A te Papi spero di aver dimostrato, anche scegliendo una strada diversa dalla tua, che sono brava e che puoi essere fiero di me. A te mamma voglio ringraziarti perché sei stata sempre una delle poche persone che ha creduto in me, mi hai sempre detto che avevo una bella "testa" matematica, che il percorso che avevo scelto era la strada giusta e adatta a me. Ti ringrazio mamma, perché hai gioito con me per i miei successi e mi hai insegnato a stringere i denti e a continuare a andare avanti, perché per raggiungere un obiettivo non sempre tutto va bene. A te Dani, ti ringrazio perché per me e Lalli sei stato il primo esempio da seguire essendo il nostro fratello maggiore, e forse proprio perché abbiamo avuto te come guida siamo le persone che siamo ora.

Poi ci sei tu Alessandro. Sicuramente se sono arrivata fin qua è anche grazie a te, che da due anni a questa parte mi hai preso la mano e hai continuato questo viaggio insieme a me. Ti ringrazio per tutti i momenti down che ci sono stati, ti ringrazio per tutti quei momenti in cui ero giù, tu mi guardavi, mi chiamavi il tuo genietto e mi tiravi su'. Ti ringrazio perché sicuramente questo percorso senza di te sarebbe stato ancora più difficile.

Voglio ringraziare anche a te, Vittorio. Ti ringrazio perché ci sei sempre stato, ti ringrazio per aver creduto in me, facendomi vivere una delle esperienze più importanti per la mia vita fino ad ora. Ti ringrazio perché quel lavoro mi ha fatto sicuramente perdere tante ore di sonno, ma mi ha fatto anche crescere tanto come persona.

Poi ringrazio a voi amiche mie, Claudia, Lavinia e Michela, che mi avete sempre sostenuta. Stiamo crescendo insieme e ci siamo sempre incoraggiate l'una con le altre. Ognuna di noi ha preso strade differenti, ma ormai da anni siamo l'una la spalla dell'altra. Ringrazio a te, Silvia che dal primo giorno che ti ho conosciuta a lavoro ho trovato in te il mio specchio. Ti ringrazio perché in questi mesi abbiamo condiviso tanto e so che ci saremo l'una per l'altra per molto tempo ancora. Ringrazio anche a te, Gina, la mia ultima scoperta universitaria, la mia compagna di progetti, di ansie e di pomeriggi interi passati a studiare insieme davanti a uno schermo di un computer. Ti ringrazio per aver assecondato la mia pazzia e le mie preoccupazioni.

Infine un ringraziamento necessario è per il Professore Paolo Castellini e il dipartimento di meccanica dell'Univpm. Grazie a Voi, ho riscoperto la bellezza dell'Università, dei laboratori e la voglia di condividere e di scoprire ogni giorno cose nuove.

# ABSTRACT

Hyperspectral imaging is a hybrid modality that combines both spectroscopy and digital imaging [1]. Unlike other techniques, such as RGB, this method allows the continuous acquisition of a spectrum for each individual pixel, not just in the visible range [1]. The final data from this approach are presented in the form of a "hyperspectral cube" identified by two spatial and one spectral dimension [1] . Over time, this modality has been widely used in a number of sectors, such as agriculture, forensics, industry, medicine and disease diagnosis, due to its ability to discriminate and identify the spectral content of chemical compounds that make up a substance [1]. The main objective of this study is to verify how a hyperspectral system can be used in different biomedical fields. The first field examined is ophthalmology, in particular the combination of the Senop HSC-2 hyperspectral camera mounted on a Haag-Streit slit lamp eyepiece. Initially, a calibration procedure was performed using the Spectralon, appropriately inserted into the cavity of a mask simulating the human face. This first step made it possible to obtain the white reference target for all the subsequent acquisitions. Subsequently, discussing with a doctor specialized in ophthalmology, it was possible to understand whether this instrument could be valid as a medical device for the diagnosis and identification of ocular pathologies. The second field analyzed, using both the Senop-HSC-2 and HinaLea hyperspectral cameras, is dermatology. The spectral analysis of the variation in melanin content between light and dark colored skin and between a mole and healthy skin is conducted. Finally, the HinaLea hyperspectral chamber is used for the analysis of a wound caused by a vascular ulcer. The results of this study are manifold; first of all, a correct functioning of the hyperspectral chamber integrated to the slit lamp is observed for the analysis of the anterior segment of the eye. Some issues arise during the studying of the posterior segment due to the non-optimal compatibility between specialist’s lenses and slit lamp setup. For the dermatological analysis, there is a good ability of the hyperspectral system to discriminate not only light skin from dark skin, but also how a healthy and small mole in the 700 nm to 750 nm range shows different spectral characteristics to the surrounding skin. In the same way, during the analysis of wound a very good discriminatory ability of this system

emerged respect to the healed one and healthy skin. Limitations and disadvantages were found for each of these areas. During the acquisitions performed in the three different fields, the primary problem revealed is the difficulty in obtaining a clean and sharp image for all wavelengths. Consequently, for an acquisition as fast as possible and not disturbed by motion artifacts, caused by the patient for the long duration of the examination, it is necessary to choose a limited spectral range characterized by specific wavelengths

# INDEX

CHAPTER 1 I INTRODUCTION

# FIGURE LIST

# TABLE LIST

# CHAPTER 1 INTRODUCTION

## 1.1 Introduction

In this introductory chapter, starting from the physical principles that characterize spectroscopy and in particular the link between electromagnetic radiation and matter it is arrived to define the main topic of this thesis and therefore the hyperspectral imaging.
In section 1.7, in fact, the modalities of acquisition of a hyperspectral system and the components that constitute it, such as sensors, dispersive elements and filters, are initially described. Subsequently, referring to the areas in which this work is focused, sections 1.8, 1.9, and 1.10 explain how the use of hyperspectral imaging in ophthalmology, dermatology, and wound healing, respectively, brings improvements from a diagnostic and treatment point of view.

## 1.2 State of the art

Spectroscopy is the oldest of all optical methods of analysis and dates back to the discovery of Isaac Newton (1666) [2]. The astronomer was the first to methodically study the behavior of light he noticed that by passing a beam of white light through a glass prism, the prism broke down into an ordered series of colored rays [2]. This was the demonstration that the light that appears white is not actually monochromatic, but is the sum of a series of rays, each of which has a different wavelength [3]. More precisely, therefore, the white color corresponds to the absorption of all frequencies and their subsequent re-emission. In addition to the concept of scattering, Newton expounded the concept that light consists of corpuscles moving in a straight line. Along with the corpuscular theory Huygens (1690) introduced the concept of wave nature to explain optical phenomena such as interference between light sources and diffraction. The question of the undulatory nature was given by the fact that light, unlike sound, could also propagate in a

vacuum and this presupposed the conceptual need for a medium capable of transmitting and supporting light waves. In 1859 Maxwell was able to explain light in terms of a continuous transformation of electric and magnetic fields oscillating orthogonally with each other through his four equations [4]. The current concept of spectroscopy became popular in the mid-19th century thanks to the so-called father of spectroscopy, Joseph Von Fraunhofer, who, while working on the production of more efficient lenses for the manufacture of telescopes, determined the first real catalogue of 547 black lines, and saw that some of them were always in the same position as the bright lines in the spectrum produced when a flame is used to reheat certain salts [3]. The explanation that Fraunhofer (1814-1815) failed to provide regarding the causes of dark absorption lines was solved by Gustav Robert Kirchoff and Bunsen (1855), through their systematic study of the nature of light and the formation of empirical laws of emission and absorption, determined that the position of spectral stripes is independent of chemical bonding and temperature [3]. They realized that the dark stripes were due to the selective absorption of light by elements in the solar atmosphere [2].

Developments in spectral analysis since the work of these two inventors were very rapid and widespread in many areas of research [3].

In 1860, the various components of the spectroscope were designed. In chemistry, spectroscopy undoubtedly led to the discovery of many more chemical elements.

From a quantitative point of view, great progress was made in 1880 by Lockyer, who proposed an analysis based on the examination of the length, intensity and number of spectral lines [3]. Spectra are defined as continuous when all lines overlap a background consisting of all or part of the colors identifiable by the iris. This phenomenon is explained by Planck's theory of radiation emission. The German physicist showed that a heated body behaves in a similar way to systems in which matter and radiation are in equilibrium with each other [4]. This system was characterized by a set of resonant oscillators with a finite energy level multiple of the radiation frequency. Macroscopically, there is a continuous spectrum of emitted radiation with a wavelength that depends only on temperature [4]. The concept that light is a quantized quantity, composed of particles of light, called photons, was later taken up by Einstein [4]. Over time, the concept of spectroscopy has been greatly

expanded to include any interaction with radiative energy as a function of its wavelength or frequency. Spectroscopic data are generally represented in the form of a spectrum. Spectroscopy is not an analysis conducted only in the visible range, but covers the entire electromagnetic spectrum from radio waves to X-rays. As technological knowledge has evolved Hyperspectral Imaging has opened the door to many areas for more precise and quantitative knowledge of several substances through the integration of conventional imaging and spectroscopy.

## 1.3 Overview of spectroscopy

Spectroscopy is fundamental to the investigation of the structural properties of elements [1]. Based on the study of the energy exchange between electromagnetic radiation and the molecules of the sample under examination, this technique provides information on the composition of the elements [1] [5].

*Electromagnetic radiation* may be described according to wave or quantum nature [5].

According to the *undulatory nature*, electromagnetic waves are characterized by frequency, which indicates the number of oscillations made by the electromagnetic field in one second, by wavelength described as the spatial distance between two successive peaks of a wave, and by the speed of propagation of the wave in the medium in which it propagates (in vacuum the speed of propagation takes the value of $2.9976 \times 10^8$ m/s) [5].

According to *the corpuscular theory*, instead, electromagnetic wave propagate thanks to discrete packets of energy, called photons or quanta that propagate in a rectilinear way with sinusoidal motion with a frequency $\nu$ [5]. The characteristic quantity in this case is the energy E that each particle transfers in interaction with matter. This energy is proportional both to the frequency of radiation and to Plank's constant ($6.63 \times 10^{-34}$ Js), according to the equation (1.1):

$$E = hv = \frac{hc}{\lambda} = hf \quad (1.1)$$

Each electromagnetic wave differs from the others by its wavelength ($\lambda$) or by its oscillation frequency v [5]. Electromagnetic waves cover an extremely wide range of wavelengths extending from $10^{-10}$ μm to $10^{10}$ μm, within which several categories can be identified based on their effects and interactions with matter, summarized in the electromagnetic spectrum (fig. 1) [5]. Although it is a continuous spectrum, a purely conventional and indicative subdivision into various frequency ranges or bands is possible.

The visible part of the EM spectrum extends from wavelengths of 0.4 micrometers for violet to 0.7 micrometers for red, and covers a very narrow band of wavelengths. Moving progressively toward shorter wavelengths, one finds the regions belonging to the ultraviolet, X-rays, and gamma rays. In the opposite side to the latter we have the infrared band and then that of radio waves.

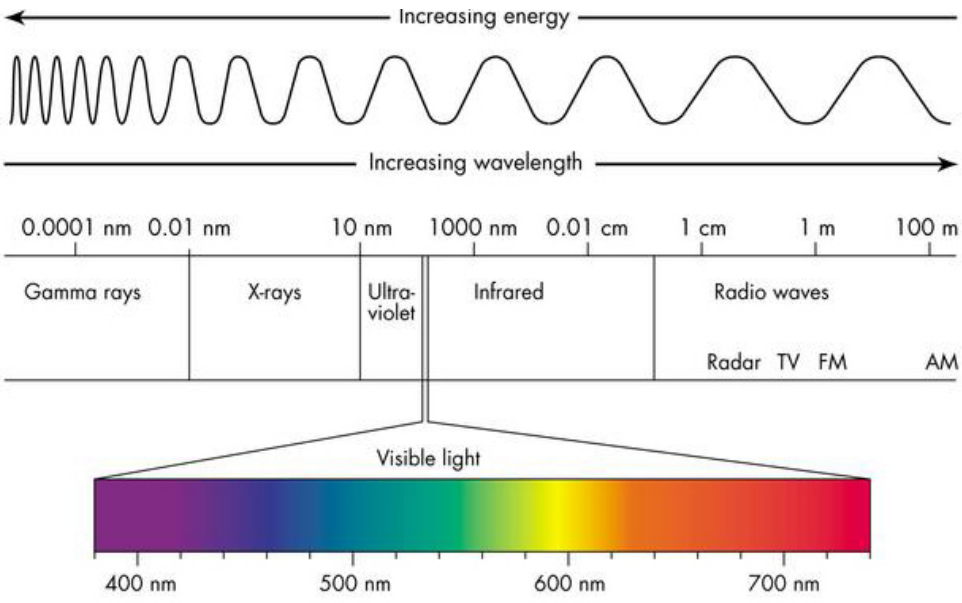


*Figure 1.1: Electromagnetic spectrum*

A spectrometer, also known as a spectrograph or spectrophotometer, is used to measure the spectrum. In particular, spectroscopy deals with the measurement of the light intensity of those regions extending from the near ultraviolet to the near infrared.

## 1.4 Visible Spectrum

The *visible spectrum*, as mentioned earlier, contains that very small portion of the spectrum characterized by wavelengths that are both sensitive to the human eye and the basis of color perception. In general, the visible spectrum includes the range of wavelengths between 380 nanometers and 780 nanometers [5]. The shorter wavelengths correspond to the blue-violet color range, while the longer wavelengths correspond to the red range. Consequently, considering these two colors and those in between, it is possible to find all seven colors described by Newton in the experiment he conducted [3].

The vision of colors by our visual system occurs at the level of the retina, the thin membrane of the eye in which nerve signals are generated in response to visual stimuli [6]. The retina is made up of cones and rods, which are also called photoreceptors because they are capable of picking up photons [6][7]. The outer segment of each photoreceptor is formed by hundreds to thousands of flattened membranous discs, filled with opsin, that contain visual pigments that have the ability to absorb and thus give rise to the first phase of light detection [7]. The inner segment of a photoreceptor, on the other hand, contains cell organelles and it is in synaptic relation with other cells.

The rods are responsible for peripheral vision as they are located outside the central part of the retina. They are very numerous and are responsible for night vision as they are very sensitive to light, even of low intensity [8]. The rods provide the central nervous system with information about the presence or absence of photons, but with no reference to wavelength, which is why they are unable to distinguish colors.

> Cones, on the other hand, are less numerous and vary in number between six and seven million, and are responsible both for the vision in conditions of daylight illumination and to color signals [7][8] . They are concentrated in the small central yellowish part of the retina known as the macula, and in particular in the fovea [6].

Three types of cone-shaped photoreceptors composed of three photopigments realize trichromatic vision of human colors [9]:

- **L cones or red cones** are more sensitive to long wavelengths, such as red light (610 nm). Maximum absorption occurs at 565 nm [10]. These cones make up 64% of the total cones.
- **M cones or green cones** are more sensitive to medium wavelengths such as green. Maximum sensitivity - peak  is about 540 nm [10]. These cones make up 32% of the total cones.
- **S cones or blue cones** are more sensitive to short wavelengths such as blue light. Maximum peak sensitivity occurs at approximately 445 nm [10]. These cones make up between 2% and 7% of the total cones.

These three types of cones, as can be seen earlier in percentage terms, are not present in the same proportion. S cones are a minority, and are totally absent from the center of the fovea, while the other two types of cones have on average the same frequency (fig. 1.2) [11].

The relative frequencies of these cones can vary considerably from eye to eye and even within the same eye between one portion and another. The sensitivity of the three cone types differs as a function of both wavelength and maximum value; the sum of the three functions gives the relative foveal sensitivity V($\lambda$).

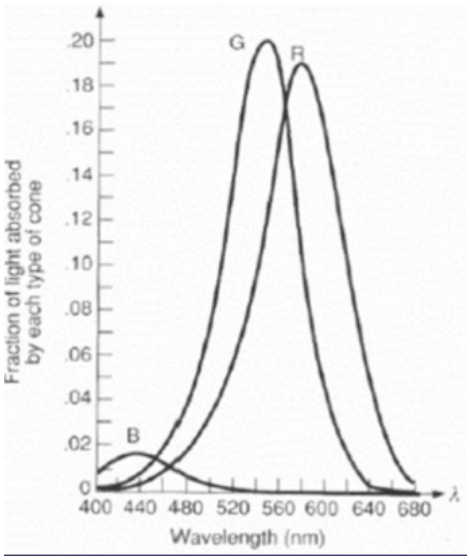


*Figure 1.2: Sensitivity of the three cones*

Based on the composition of the radiation emitted by the observed object, the three types of cone are activated in various combinations and percentages. From this and final processing in the brain results in the ability to distinguish different colors.
Under conditions of high light intensity, such as daylight with a luminance > 3 cd/m2, the photopic regime occurs (fig. 1.3)[7][12]. Light in this condition is mainly perceived by the cones in the center of the retina and the relative sensitivity V($\lambda$) is given by the T curve which peaks at 555 nm, which corresponds to the color green [7][13].

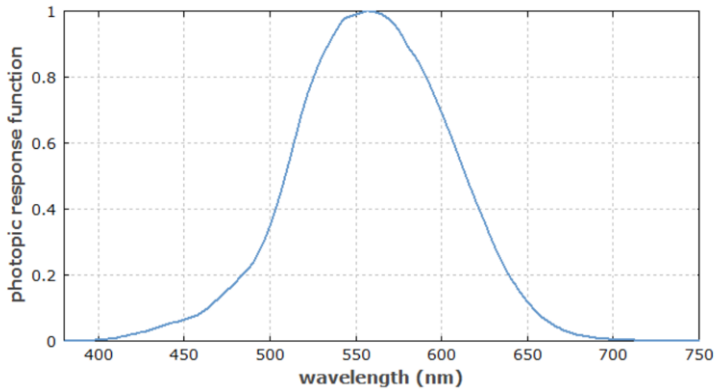


*Figure 1.3: Photopic vision*

Under conditions of low light intensity, such as the starry sky with a luminance of < 0.001 cd/m2, the scotopic regime occurs (fig. 1.4) [7][12]. In this regime, light is not perceived by the cones, but mainly by the rods at the edge of the retina [7][12]. The relative sensitivity V'($\lambda$) is represented by the N curve which has its maximum sensitivity at 507 nm, which corresponds to bluish green [13].

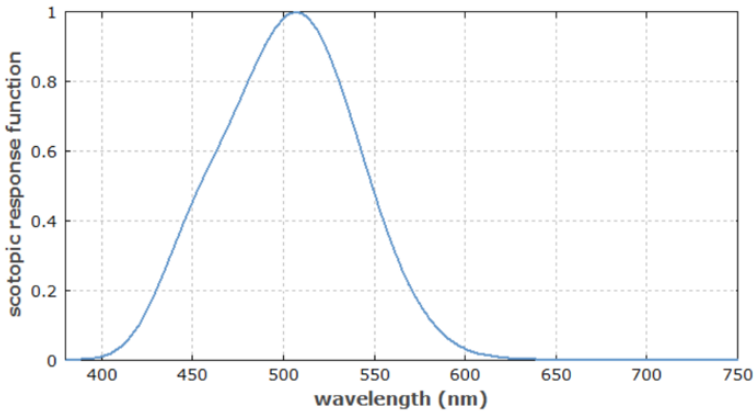


*Figure 1.4: Scotopic vision*

The two curves differ not only in the positioning of the peak, but also in the absolute values of sensitivity. In fact, the rods "working" in low conditions and being of much greater number are more efficient than the cones. However, the large number of rods compared to cones is at the expense of visual acuity.

## 1.5 Infrared Spectrum

Infrared radiation covers the range of the electromagnetic spectrum between 700nm and 1mm. These radiations are also known as thermal radiations, in fact they can be emitted by every "hot" body, but at the same time if absorbed they give rise to a development of heat. Knowing that the molecular vibratory motions are related to the wavelength of radiation, the study of emission and absorption spectra in spectroscopy is a very popular method for the investigation of molecular structures.

## 1.6 Physical principle of spectroscopy

Spectroscopy deals with the transitions that can occur between the different internal electronic states of the molecule and, by studying the absorbed radiation and the intensity of absorption of the various substances, allows precise qualitative and

quantitative analyses to be carried out using their different spectral signatures [1][5]. The spectrometer is the device that is able to measure the spectrum of electromagnetic radiation and show the properties of light as a function of its wavelength.

In this work the spectral ranges mainly investigated are near UV, visible and near infrared. The modes of sample presentation to the instrument can be of different types, and consequently the acquisition of spectra can be in transmittance, reflectance, transflectance and interactance [1]. In this thesis the reflectance acquisition mode is used where both the light source and the detector are positioned in the same part, and the spectral ranges investigated cover wavelengths from 500 to 900 nanometers in the first chamber, as we will see later, and from 400 to 1000 nm the second.

### 1.6.1 Bohr's theory

The energy of a molecule is a quantized quantity, as it cannot have just any values, but only very specific levels [5]. The total energy possessed by a molecule is considered to be the sum of several contributions of energies [5]:

- The *electronic energy* relates to how the electrons are distributed in the various available orbitals. At room temperature, all molecules are in the lowest energy state, the fundamental state.
- The *vibrational energy* relates to the oscillation of the atoms around an equilibrium position, corresponding to the bond distance.
- The *translational energy* relates to the kinetic energy due to the displacement of the entire molecule.
- The *rotational energy* relates to the spin state of the nuclei.

All the energies described above make up what is known as thermal energy. To arrive at the total energy, it is necessary to add the energy at the zero point, that is,

the energy that a given particle would have if all its forms of thermal energy were in the lowest possible state.
Thus the total energy is defined as the equation (1.2):

$$\varepsilon_{tot} = \varepsilon_0 + \varepsilon_{el} + \varepsilon_{vi} + \varepsilon_t + \varepsilon_{rot} \quad (1.2)$$

With the exception of the translational energy, the electronic, vibrational and rotational energies are quantized, i.e. they can vary only by discrete and well-defined quantities [5].

According to quantum theory, the energy associated with electromagnetic radiation is transmitted by indivisible packets, called photons or quanta. Within a few years, Rutherford's model (1911) was replaced by Bohr's model, which assumed that electrons moving around the nucleus in fixed orbits exchange energy by passing from a stationary to a non-stationary orbit. The electron, being then unstable, returns to its initial orbit, at a lower energy, emitting a photon with an energy equal to the energy difference between two orbits [5]:

$$\Delta E = E_2 - E_1 = h\nu \quad (1.3)$$

Where E2 and E1 represent the total energy of the atom in its final and initial energy states, respectively (fig. 1.5) [5]. The acquired energy is subsequently converted either to:

- Stretching: it is a rhythmic movement along the line joining atoms, as a consequence a change in bond length is produced.
- Bending: this movement results in a change of the bond angle deformation by changing the angle formed between the bonds.

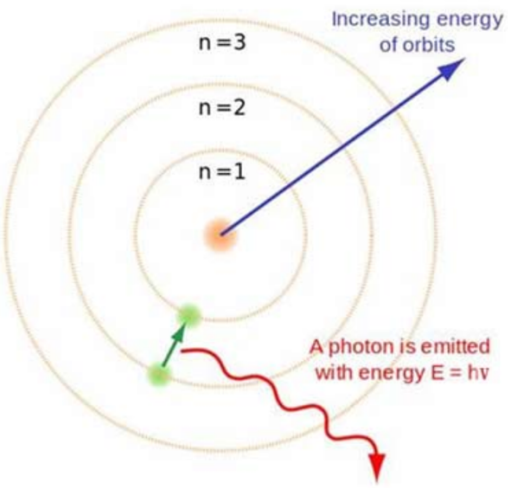


*Figure 1.5: Bohr's atomic model*

### 1.6.2 Interaction between light and matter

When light strikes a surface, part of the incident flux is reflected, part is transmitted, and part is absorbed. From the principle of conservation of energy, the sum of the transmitted, reflected and absorbed amounts is equal to the amount of incident energy [14] [15]:

$$\phi i = \phi r + \phi r + \phi a \tag{1.4}$$

In this regard, it is useful to characterize the behavior of different surfaces through the ratios of the flux of transmitted, reflected, and absorbed light to the incident light. The following quantities are referred to as reflection, absorption, and transmittance coefficients, respectively.

*Reflection coefficient or reflectance* $(\alpha)$ provides information on the behavior of an opaque surface with respect to the incident light flux, expressed as the ratio between the amplitude of the reflected wave and the incident wave. This is a very important and used parameter as it can describe the reflective properties of a target as a function of incident wavelength.

*Absorption coefficient or absorbance* $(\rho)$ is considered only in cases where absorption in the material medium is taken into account, and is defined as the ratio of the amount of absorbed flux to the amount of incident flux. [15]

*Transmittance coefficient or transmittance* ($\tau$ ) expressed as the ratio of the amount of light transmitted to the amount of light incident [15].

Also due to the principle of conservation of energy, the sum of reflectance, transmittance and absorbance is equal to 1.

The coefficients of reflectance, absorbance and transmittance take values between 0 and 1. In relation to these coefficients, different types of "ideal" bodies can be defined. These bodies are reported in tab. 1.1.

| Body | Transmittance | Reflectance | Absorbance |
|---|---|---|---|
| **Opaque** | 0 | - | - |
| **Transparent** | 1 | 0 | 0 |
| **Reflective** | 0 | 1 | 0 |
| **Black** | 0 | 0 | 1 |

*Table 1.1: Transmittance, Reflectance and Absorbance of some bodies*

Most solids are opaque, they can absorb and reflect the energy that comes to them but cannot transmit it.

$$\tau = 0 \qquad \rho + \alpha = 1 \tag{1.5}$$

Consequently, it is essential to describe the behavior of real surfaces by comparing them with an ideal system for which the laws that distinguish it are known.

Black bodies are able to absorb all the radiation incident upon them, irrespective of the frequency values they possess, and are able to emit isotopically in space. These bodies are characterized by maximum assertiveness and maximum emissive power. Spectral or monochromatic emissive power is defined as the thermal radiation emitted in all directions per unit area and per unit time in a given wavelength range. Unlike the black body, in real objects the radiation emitted at a specific frequency is a fraction of the ideal emission.

For both absorption, reflection and transmission coefficients, it is possible to define the respective spectral coefficients when a certain wavelength range of incident energy is to be taken into account ( $\alpha_\lambda$, $\rho_\lambda$ $\tau_\lambda$).

### 1.6.3 Main reflection mechanisms

Reflection and refraction are two phenomena that characterize the behavior of radiation at the surface dividing two mediums with different refractive indices, thus generating reflected and refracted radiation (fig. 1.6).
Reflection is the phenomenon by which light, hitting a surface that separates two media with different refractive indices, is reflected, propagating in the same medium from which it comes. An aspect of considerable interest considering the present work is that relating to the variation of the direction of reflected radiation depending on the composition of the surfaces. Two main models are used to calculate the reflected flux, the first is the perfectly specular reflection model, where the energy of the incident angle is equal to the energy of the reflection angle, while the second is the perfectly diffusing, or Lambertian, reflection model, where the radiance observed from any angle of absorption does not change [16][17]. As they are limiting cases they represent few exceptions, for real surfaces an intermediate case between the two previous ones is used.

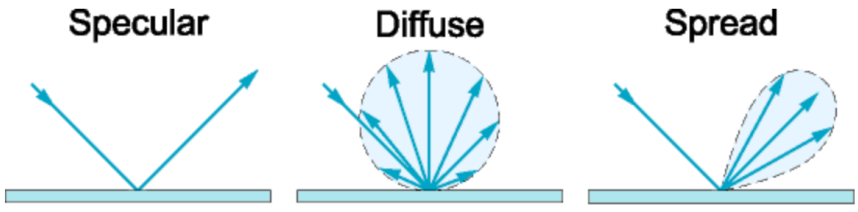


*Figure 1.6: Specular, diffuse and spread reflection from a surface*

a) In the *specular or regular reflection pattern,* light is reflected in only one specific direction. In this case, the angle of incidence, the angle formed between the normal to the surface at the point of incidence and the incident

ray, is equal to the angle of reflection, that is, the angle formed between the normal to the surface at the point of incidence and the reflected ray [14] [17]. The phenomenon whereby the angle of incidence is equal to the angle of reflection follows Snell's law (θi=θr) [14]. This type of reflection characterizes perfectly reflective surfaces, characterized by a reflection coefficient equal to 1, or at least those surfaces where it is possible to eliminate all irregularities with light wavelength fractions of μm [14].

b) *Lambertian surfaces* reflect light following Lambert's cosine law which states that the energy reflected in a specific direction by a section of the surface is proportional to the cosine of the angle between the direction and the normal to the surface. Lambert's law determines how much of the incident energy is reflected, and also the amount of energy reflected in each direction is constant [17]. Consequently it can be said that the reflected intensity does not depend on the direction that is considered, but it depends on the orientation of the emitting source relative to the surface [17]. The previous considerations lead to the conclusion that the radiance emitted by a Lambertian surface is constant as the angle varies, and thus a diffuse or isotropic radiation occurs. Consequently, when the wave impinges on matter, it is broken down and re-emitted in multiple directions, independent of its original direction, according to what is called the surface scattering profile. Diffusive reflection of electromagnetic radiation is a process that does not include any absorption or emission. This type of reflection is typical of rough or opaque surfaces.

c) In many cases the actual surface has an intermediate behavior between perfectly specular and perfectly diffuse such as Lambertian surfaces. *In mixed reflection*, the reflected radiation scatters in different directions, with a greater intensity contribution in the direction corresponding to specular reflection.

*d) Bidirectional reflectance distribution function:* In reality, few materials are not perfectly 'diffusive' or 'mirror-like'. The bidirectional reflectance distribution function (BRDF) measures the distribution of reflectance from non-Lambertian surfaces [17][18]. Mathematically, it is described as the ratio of

the observed radiance to the incident irradiance, taking into account all existing geometrical arrangements based on the angles incident $(\theta, \varphi)$ to the surface and the angles exiting $(\theta',\ \varphi')$ it according to the formula [17]:

$$F(\theta, \varphi, \theta',\ \varphi') = \frac{dL(\theta,\varphi,\theta',\varphi')}{dE(\theta,\varphi,\theta',\varphi')} \tag{1.6}$$

In the presence of a perfectly absorbent surface the value coincides with zero, while in the presence of surfaces with a perfectly specular reflection the value coincides with 1 (fig 1.7).

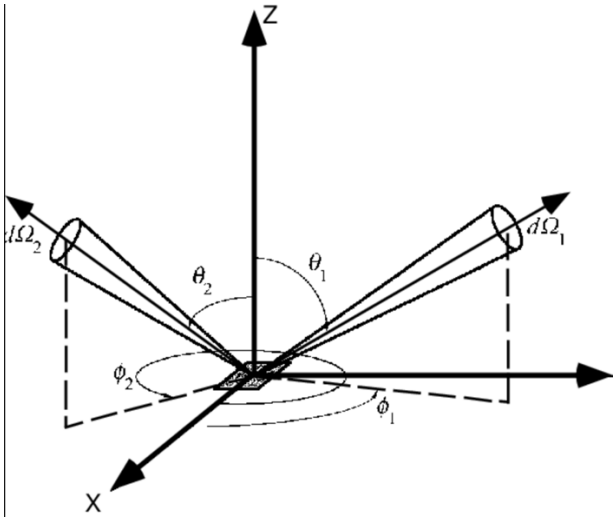


*Figure 1.7: BRDF*

### 1.6.4 Refraction mechanisms

Refraction is defined as the deflection that light rays undergo when crossing the separation interface between two different media (e.g. air-glass) (fig. 1.8). The abrupt change in the characteristics of the medium through which the wave travels varies its speed, and consequently the direction of propagation ($\theta_2$).
The value of the angle of deflection depends essentially on a property of the medium known as the refractive index and the angle of incidence of the light ray on the surface ($\theta_1$).

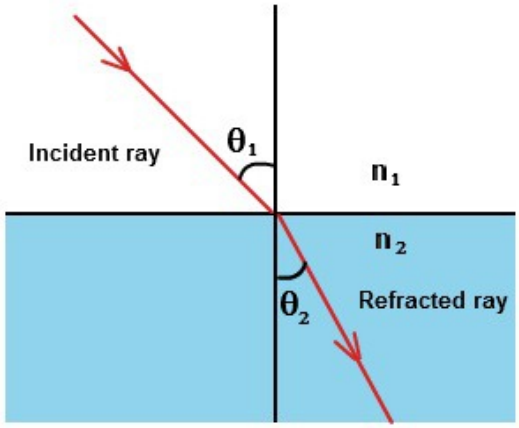


*Figure 1.8: Refraction mechanism*

The refractive index is expressed as the ratio between the velocities of the wave passing through the two media, in other words it aims to describe how fast the light ray passes through the material, and can be obtained by means of the following relationship:

$$\eta = \frac{c}{v} \tag{1.7}$$

Where η is the refractive index, c is the speed of light in vacuum or in air, and v is the speed in the medium. Since the speed in the medium is less than the speed of light in vacuum, it follows that for vacuum the refractive index is equal to 1, while for a transparent medium it is always greater than 1.

### 1.6.5 Interaction with the atmosphere: Diffusion phenomena

Unlike the reflection phenomenon where light is deflected elastically at the same wavelength in a particular direction, in scattering light is deflected in all directions by air molecules or small suspended particles. When a photon with a wavelength unsuitable for an electronic transition interacts with a molecule, it can be scattered

in three different ways, such as elastic scattering, anelastic scattering with energy transfer or with energy acquisition (fig. 1.9) [19].

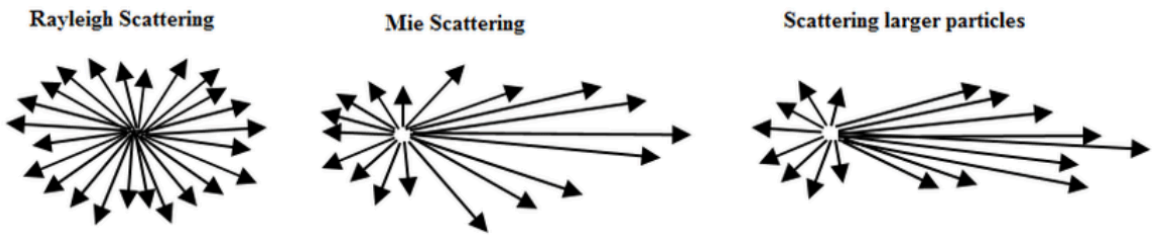


*Figure 1.9: Scattering phenomena*

a) *Rayleigh scattering* occurs as a result of elastic scattering of a light wave caused by particles that have small size compared to the incident electromagnetic wave and it is present in the higher layers of the atmosphere [19] [20]. Being a type of elastic scattering, the scattered radiation has the same frequency, and therefore wavelength of the incident one [19]. This scattering approximation was defined by Lord Rayleigh in 1871. [20]
b) *Mie scattering* refers primarily to the elastic scattering of light from atomic and molecular particles, whose diameter is comparable or larger, than the wavelength of the incident light (usually $\frac{d}{\lambda} > 10$)[19] [20] . For this reason this type of scattering finds application both in the optical study of colloids and in meteorology. Mie scattering occurs mainly in the lower layers of the atmospheres, where the most numerous particles are the large ones, clouds and water vapor are also present. In addition to the different wavelength dependence, the two types of Rayleigh and Mie scattering have a different angular distribution. Rayleigh scattering (fig. 1.10) has a distribution similar to that of a Hertzian dipole, where the scattered intensity is symmetrical with respect to the direction of the incident light [20]. In the second type of scattering, Mie (fig. 1.9), the distribution is characterized by a much more pronounced front lobe, which increases as the particle size increases. Forward scattering is an interference effect due to variations in the phase of the electric field on large particles.

c) During an *anelastic collision* the frequency of the scattered radiation can be different than that of the incident radiation, and in this case we speak of diffusion or of *Raman effect* (fig. 1.10) [19]. The difference in frequency between incident and scattered light is equal to that associated with a vibrational or rotational transition [19]. A photon scattered inelastically from a molecule leaves it in a different rotational or vibrational state, in fact, when the photon gains energy is dispersed at a higher frequency than the original one, or in the case of energy loss is dissipated at a lower frequency [19]. Thus, incident light induces the movement of bonding electrons, which, being in motion, re-emit light. The level at which they are located is so unstable that within 10-14 seconds, i.e. before any kind of collision can take place, the same radiation is spontaneously re-emitted and the system returns to its fundamental state.

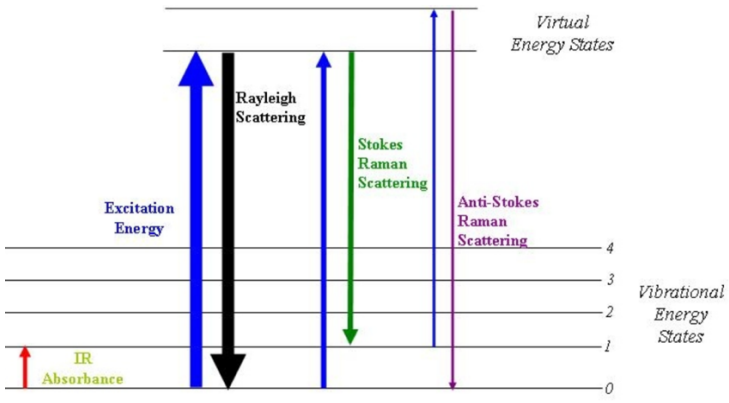


*Figure 1.10: Scattering Raman*

### 1.6.6 Interaction with the atmosphere: Absorption phenomena

Absorption means the ability of a body to be able to absorb the energy of an incident electromagnetic wave, as it is able to induce energy changes at molecular or atomic level [14]. For example, in the case of absorption of infrared components there is an increase in the kinetic energy of the molecules, resulting in an increase in the thermal energy of the medium. The absorbed energy can be used by the molecules

in the medium to make transitions between different energy levels. Thus, it can be concluded that absorption occurs in the presence of certain interactions between the incident radiation and the molecules and that it is strongly dependent on the frequency of the wave.

The part of the radiation that is transmitted, is that which escapes from the material after passing through it [15].

a) *For black body* the absorption coefficient assumes a value of 1, this implies that there is a perfect absorption of radiation incident on it. identified by a maximum emissive power (representing the thermal energy emitted by the surface considered in the unit of time per unit area) [W/m$^2$].
b) *For real bodies* characterized by a lower emissive power it is useful to define the ratio between the maximum emissive power of the surface and that of the blackbody.

A quantitative way to measure absorption is *transmittance* (T) [5]. In the case of absorption, the intensity I of the electromagnetic radiation leaving the sample will be lower when compared to the intensity hitting the sample Io. The ratio between the intensity of the outgoing radiation compared to the incoming one is called and being the ratio between two dimensionless quantities can assume values between 0 and 1, or otherwise be expressed in percentage terms [5]:

$$T = \frac{I}{I_0} \tag{1.8}$$

This quantity expresses the fraction of incident light that has passed through the sample without being absorbed, and is smaller in value the greater the absorption [5].

If the percentage transmittance value is 100, it means that the ray has not been weakened and no type has occurred from the substance [5]. If the percent transmittance value on the other hand is 0, it implies that the radiation has been completely absorbed [5]. The main drawback of transmittance is that it is not related

in any way with the concentration of the sample because it would be important to know how much the light decreases as the concentration of the sample increases. A more suitable parameter is the *absorbance* (A), defined by:

$$A = \log \frac{I_0}{I} \qquad 0<A<\infty \qquad \text{Or even:} \quad A = -\log T \tag{1.9}$$

This equation takes the assumption that incident light is neither reflected nor scattered, but all light is either transmitted or absorbed [21]. Absorbance is also related to both molar concentration and optical path according to the relationship, known as *Lambert-Beer's law* [5] [21]:

$$A = \varepsilon b c \tag{1.10}$$

Where , $b$ is the optical path expressed in cm, $c$ whose unit is M, is the molar concentration and $\varepsilon$ is the coefficient of proportionality and is an intrinsic characteristic of the molecule being analyzed, which depends on both the solvent used and the wavelength of the radiation [21]. The proportionality coefficient is also called molecular specific absorbance or molar extinction coefficient [5]. The value of the molar extinction coefficient depends on the wavelength of the absorbed radiation, the nature of the solvent, the chemical species it absorbs and is totally independent of temperature.

Thus, according to Lambert-Beer's law, absorbance is proportional to both the concentration of the absorbing substance and the thickness of the observed layer. It can be deduced that the higher the concentration of molecules passing from the fundamental to the excited state, the higher the absorbance (fig. 1.11).

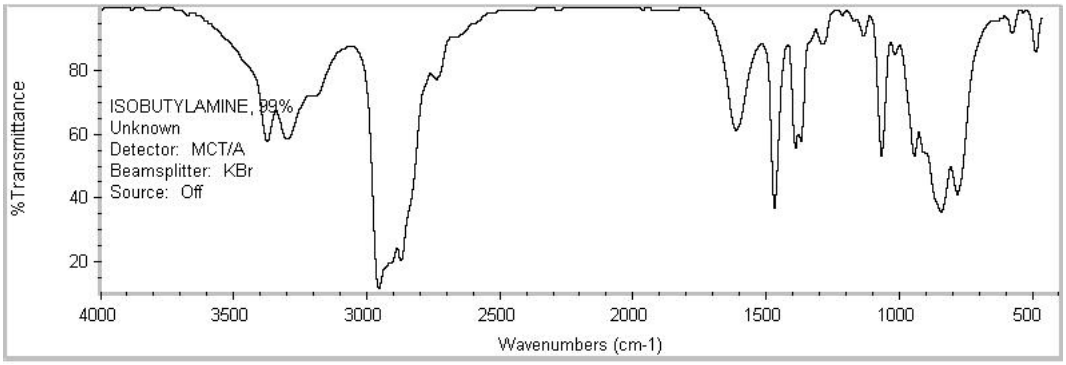


*Figure 1.11: Transmittance Spectrum*

## 1.7 Hyperspectral imaging

Hyperspectral technology (HIS) is a hybrid modality able to combine both imaging and spectroscopy techniques [1]. It can be used for more challenging applications to measure objects or scenes, in fact is capable to acquire a spectrum for every pixel in an image [1]. While the human eye has only three color receptors in the blue, green, and red, hyperspectral imaging measures the continuous spectrum of light for each pixel in the scene with fine wavelength resolution, not only in the visible but also in the near-infrared [22].

The acquire data is presented in a three dimensional dataset known as "hyperspectral cube", featured by two spatial dimensions and one spectral dimension (fig. 12, right) [1]. Spatially resolved spectral information can be used to reveal the chemical composition of the target in a non-destructive, non-contact manner [22].

The difference between a hypercube and an RGB color image is depicted in fig. 12. RGB imaging does not provide spectral information beyond the visible spectrum, which is of great importance for characterizing the chemical and physical properties of a sample [22][1]. From an RGB imaging system that returns the intensity values of the three channels R red ($622\,nm < \lambda < 780\,nm$), G green ( $492\,nm < \lambda < 577\,nm$) and B blue ($455\,nm < \lambda < 492\,nm$) for each pixel of an image, HIS systems allow the acquisition of multiple images, through the sampling of multiple channels at different wavelengths (fig. 1.12) [1].

The costs of an HIS system are far higher than RGB imaging systems. But the cost is generally offset by the great potential that HIS systems can offer.

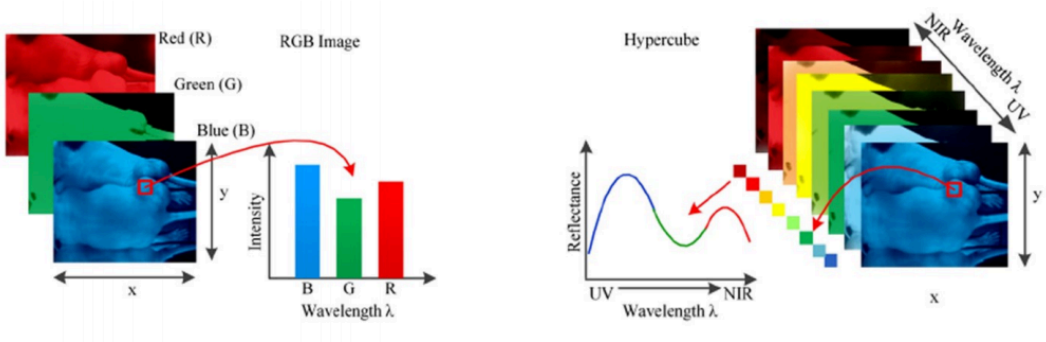


*Figure 1.12: Comparison between hypercube and RGB image. Hypercube is three-dimensional dataset of a two-dimensional image on each wavelength (right). RGB color image only has three image bands on red, green and blue wavelengths respectively (left).*

Depending on the number of wavelengths, a distinction can be made between the multispectral Imaging (MSI): if the number of wavelength is smaller than ten, and hyperspectral imaging if it is composed of hundreds of bands for each pixels [23].

### 1.7.1 Components of a hyperspectral system

An HSI system is mainly equipped of a light source, wavelength dispersion device, and area detectors (fig. 13) [1].

Light source illuminates the test specimen. The light is then projected through the front lens in an entrance slit. The width of the slit has a very great importance, in fact controls the amount of light entering the spectrograph [1]. Thereby, for each pixel interval along the line define by the slit, a corresponding spectrum is projected onto a column of detector array [1] . Each line is projected as a 2-D image into the detector, with a spatial dimension and spectral information. The slit acts as a field-stop to determine the instantaneous field of view (IFOV) in spatial directions.

Wavelength dispersion device can be a prism or a grating able to divide the incoming light into a series of narrow spectral bands that are then projected into a detector array [1].

Then, by scanning the whole tissue sample or moving the camera through the tissue sample, in a push broom or line-scanning mode, an HSI camera collects 2-D images for adjacent lines, creating a hypercube with one spectral and two spatial dimensions (fig. 1.13) [1].

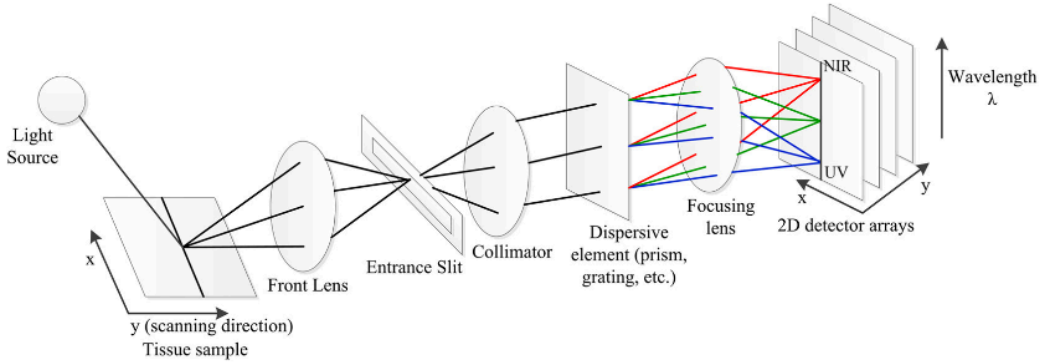


*Figure 1.13: Schematic diagram of a pushbroom hyperspectral imaging system*

### 1.7.2 Hyperspectral Imaging Acquisition Mode

The term acquisition mode refers to how spectral and spatial information is obtained [1]. There are several ways to acquire HSI volumes in practice, following are the main and most popular acquisition methods in hyperspectral imaging. Each of the following modes involves physical limitations that require a balance between different parameters such as spectral and spatial resolution, acquisition time (or temporal resolution), device compactness, and computational complexity [24].

*In spatial scanning* the spectral information one at time are acquired by passing light through a dispersive optical element, such as a grating or prism [4][25]. The two main spatial-techniques *are the point or whiskerbroom scanning* and *pushbroom or line scanning* (fig 1.14).

*Whiskerbroom scanning* is mainly used in remote sensing applications. Whiskbroom is a point scanning process relies on the use of a pinhole to scan the image point by point, which requires scanning across the two spatial dimensions of the image [25] . Whiskbroom tends to offer the highest level of spectral resolution, but at the same time is a slow acquisition mode, because requires the system to scan the target area in both the x- and y-axes [22][26].

*Pushbroom scanning* is characterized by detecting pixel spectra on a single spatial line at each moment in time [24]. A two-dimensional array of measurements is then created for each spatial line. One of the dimensions of the array corresponds to the spatial axis along the detected line and the other corresponds to the spectral axis [24]. As the scene is traversed in a scan direction perpendicular to the axis of the detected lines, multiple 2D arrays are collected. These arrays are, then, stacked together to originate a cube of hyperspectral image data. Scene scanning is usually accomplished by moving the imager or its field of view along the scene [25]. The speed of the movement should be synchronized with the capture rate in the imager [25]. Pushbroom systems can have compact size, reduced weight, simpler operation and a higher signal-to-noise ratio, and it is faster and more efficient since it requires scanning across only one spatial dimension of the image , but at the same time must use a fairly short exposure time to avoid the risk of inconsistencies at the spectral band level (saturation or underexposure) [22][25].

So the main advantages of spatial scanning is to acquire data with high spectral resolution over a wide spectral range [24]. However, a major restriction of spatial scanning techniques is the need for relative motion between the imaging system and the target [24].

*Spectral scanning or staring or area-scanning* represents the main compromise between spectral and temporal resolution, where spectral filtering is performed by tunable filters, such as a liquid crystal tunable filter or an acoustic-optical tunable filter [24] [25]. The tunable filter is placed before the illumination source or before the image sensor to capture a series of 2D images of the lens, each at a different

wavelength [25]. By stacking the images together, the hyperspectral cube can be constructed [25]. This technique stores the images in a band-sequential format

*Snapshot or single shot* is capable of collecting an entire cube of hyperspectral data with all spatial and spectral information in a single integration period [22]. This is a developing technology that still lacks support for higher spatial resolutions [22]. Due to the high acquisition speed without scanning, in addition to limited spatial resolution, spectral resolution is also compromised.

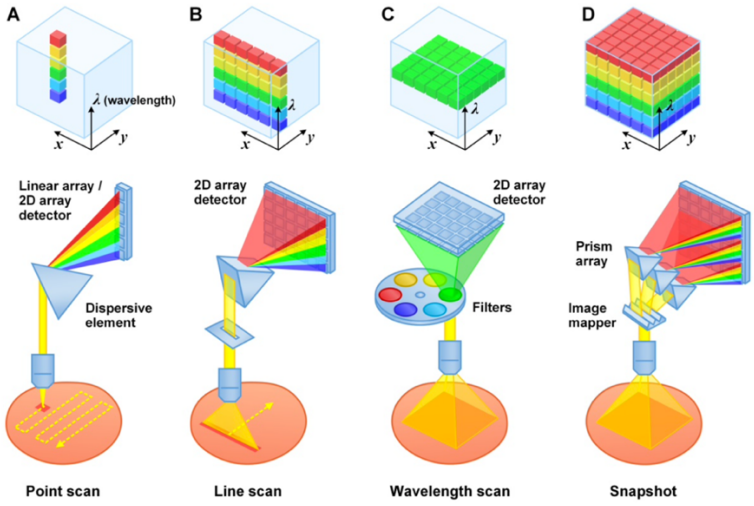


*Figure 1.14: Acquisition Mode*

In *time scanning* technique a superposition of spatial and spectral data is captured by acquiring a series of images over time [25]. The spectral information can then be extracted using mathematical operations [25]. An example of this technique is Fourier transform infrared imaging (FTIR) where the transformation of the images is performed after they have been a function of the interferometer's optical path difference [25].

While spatial scanning leads to data characterized by high spectral resolution over a wide range, this is certainly more complicated in spectral and temporal scanning due to hardware requirements such as tunable filtering or the acquisition of interferograms over a wide range of optical path differences [25].

In contrast to spatial and spectral scanning techniques that rely on cutting the hyperspectral data cube along orthogonal dimensions, the *spatial-spectral scanning* technique manages to combine the complementary properties of the previous techniques by simply moving a transverse camera across the slit of a basic spectroscope [25]. This method is characterized by the acquisition of diagonal slices of the hyperspectral cube, each of which contains a 2D spatial image of the target that is wavelength-encoded (fig. 1.15) [27].

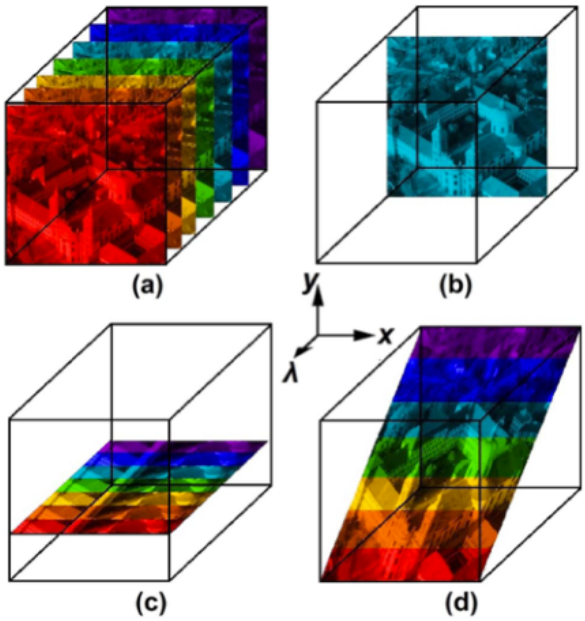


*Figure 1.15: Panel (a): scan less technique that generates a chromatically dispersed snapshot of the scene. Panel (b): spectral scanning technique that generates a temporal sequence of monochromatic snapshots of the sample, Panel (c):spatial scanning technique that collects a temporal sequence of ordinary striped slit spectra of the scene. Panel (d): the spatial scanning technique.*

### 1.7.3 Hyperspectral Imaging sensors

Regarding the concept of hyperspectral sensors, HSI systems are based on area image sensors (focal plane arrays) that represent arrays composed of up to several million detectors operating simultaneously and play an important role in data acquisition [22][23]. Some of the main parameters that characterize the performance of detector arrays and that must be taken into account in order to achieve good

image quality are signal-to-noise ratio, dynamic range, spectral quantum efficiency, and linearity [1].

Over the wavelength range of 250 nm to 1,200 nm (near-ultraviolet, visible and near-infrared light), two types of sensors are prominently used to achieve the conversion of incident photons to electrons, and are charge-coupled sensors and complementary metal-oxide-semiconductor sensors (fig. 1.16) [22].

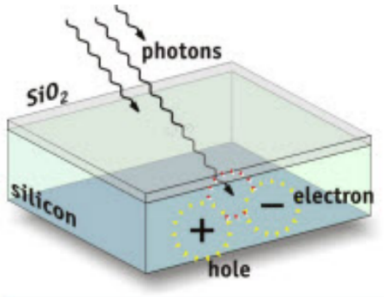


*Figure 1.16: Both CCD and CMOS are based on the so-called photoelectric effect*

*Charge-coupled (CCD) sensors* are composed of thousands (or millions) of light-sensitive cells or pixels, such as silicon (Si), indium arsenide (InAs) or indium gallium arsenide (InGaAs), that are capable of producing an electrical charge proportional to the amount of light they receive. The pixels can be arranged in a single line (linear array CCDs) or in a two-dimensional grid (area array CCDs) [22]. The main features are low dark noise and low signal-to-noise ratio. Silicon CCDs are mostly used due to their high resolution, relatively inexpensive cost, and acceptable quantum efficiency in the spectral range [22]. CCDs have been replaced by photomultiplier tube arrays (PMTs) due to their high speed. Photomultiplier tube arrays (PMTs) are another type of detector that generate an electrical output after a photon hits the photocathode in a few nanoseconds [1]. Light-sensitive cells are made up of different materials depending on the spectral range of interest, for example InAs and GaAs are characterized by a spectral response between 900 and 1700 nm. InGaAs is able to extend the previous range to 2600 nm. The mid-infrared (2500-25000 nm) and NIR (800-2500 nm) spectral regions are covered by mercury cadmium telluride (MCT)[22]. This is shown in fig. 1.17.

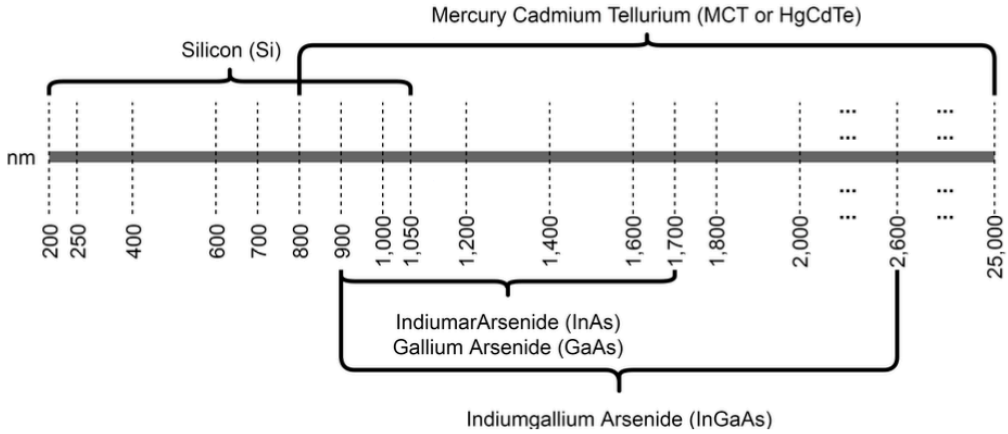


*Figure 1.17: Materials involved in hyperspectral sensors fabrication*

*Complementary metal oxide semiconductor sensors (CMOS)* are characterized by a photodetector and a readout amplifier integrated with each other with the ability also to convert the voltage signal generated by the incoming electrons thanks to an optically intense transistor placed next to the photodiode [22]. As a result, these sensors are able to acquire and measure light intensity very quickly compared to CCDs, but on the other hand their use is limited due to a high dark current and noise. The advantage of the CMOS sensor is its low cost and low power supply [1] [22].

### 1.7.4 Parameters that characterize the performance of detector arrays

a) *Linearity of sensor response:* normally, hyperspectral imagers are characterized by a linearity of sensor response that is good in the relevant types of photodetectors. In NIR spectroscopy, the spectral signatures of a sample are built on the intensity values of the pixels [28]. Consequently, the pixel intensity value at the system output should be a linear function of the input light intensity [28]. Spectral linearity is tested by comparing the actual reflectance and transmittance values of standard lenses with known properties with the values measured using the system [28].

b) *Signal-to-noise ratio:* this parameter is critical for the system and is expressed as the ratio between the actual signal and the noise [28]:

$$SNR = \frac{1}{n}\sum_{i=1}^{n} SNR(\lambda_i) = \frac{1}{n}\sum_{i=1}^{n} \frac{\mu(\lambda_i)}{\sigma(\lambda_i)} \quad (1.11)$$

Where:

- n: number of the spectral bands used
- SNR($\lambda_i$): is the system's SNR at the wavelength $\lambda$
- $\mu(\lambda_i)$: mean deviation of all spectral values in the measured region at the wavelength $\lambda$
- $\sigma(\lambda_i)$: standard deviation of all spectral values in the measured region at the wavelength $\lambda$

The SNR of the imager can be obtained from the noise of a single detector element while a constant light source is displayed. The noise should then be determined for each spectral band used and finally, it should also be measured at various light levels within the dynamic range.

The SNR plays a very important role in the subsequent evaluation of the system's accuracy [28]. Higher SNR values can result in a better calibration [28]. Both SNR and spectral resolution must be matched to the detection system [29]. Three main forms of noise can be distinguished, the readout noise due to the amplifier and electronics, the shot noise from the signal itself and finally, the shot noise from the dark current, which depends on both exposure time and temperature [28].

In NIR systems, selecting a suitable detector, improving the signal transmission capability, adopting a denoising filter in the hardware and ensuring specific working conditions can improve the SNR [28].

c) *Quantum efficiency* is one of the most important characteristics of a detector, and is defined as the ratio of collected electrons (photoelectrons) to the number of incident photons. In fact, not all photons encoding on a generic pixel are used to release electrons:

$$QE = \frac{photoelectrons}{incident\ photons} \quad (1.12)$$

Thanks to the combination of micro lenses and backlighting CMOS are characterized by an high quantum efficiency values with peak sensitivity generally in the green range [22].

The quantum efficiency measured for a given wavelength of incident light is called spectral sensitivity. Quantum efficiency and spectral sensitivity define how much light information is lost and, above all, in what spectral range the sensor can operate [22].

### 1.7.5 Hyperspectral Imaging dispersive devices

Dispersive devices are the central element of an HSI system. These elements can be located in different positions depending on their function [1]. If the dispersive elements have the function of wavelength selection they are placed between the light source and the sample, in case of emission wavelength dispersion function they are located between the sample and the detector arrays. Several types of optical and electro-optical dispersive devices can perform spectral dispersion or selection in HSI systems [1].
Those commonly used are divided into three classes and include monochromators, optical bandpass filters and single shot imagers.

*Monochromators* are used for light scattering, and this is done by employing a grating or a prism. The hyperspectral cube is then formed first along one axis of the sensor and then along the other by coupling the scattering element with a two-dimensional array of detectors [29].

The *prism* scatters light at different angles due to the change in the refractive index of the material itself, which varies with the wavelength of the incident light [1].

Although the prism is characterized by high efficiency and low scattering, it has a much more complex optical design than gratings [1] [29].

The *diffraction grating* consists of a set of diffraction elements, through which it is able to separate polychromatic light into its monochromatic components [30]. A distinction can be made between reflection and transmission gratings, the former being superimposed on a reflective surface and the latter on a transparent surface [30]. At the output of the grating, the electromagnetic wave impinging on the latter will be characterized by diffraction by a different electric field of amplitude or phase or both [30]. This system can achieve a high efficiency. The convex grating with the Offner spectrometer is the most commonly used grating [29].

The last type of monochromator is the *prism-grating-prism (PGP)* which combines both scattering elements of a prism and a grating. This system consists of a transmission grating with a specially designed volume which is inserted between two identical prisms [1][29].Through the entrance slit, which defines both the final geometry of the line and the spectral resolution of the system, light can enter. In this system the central wavelength of the design wavelength range passes directly through, while the other wavelengths, i.e. the shorter and longer ones, are scattered symmetrically on both sides of the central wavelength. The pixels of the line are recorded simultaneously by means of a monochromatic area detector in the image plane, while the spectral distribution of each pixel of the line is recorded in a frame (fig. 1.18) [31]. This technique has the advantage of preserving the optical axis, but the disadvantage of losing transmittance due to the fact that materials with high dispersion also exhibit high absorption, which results in a reduction in overall system performance [29].

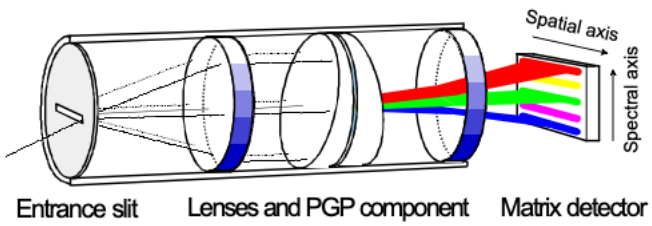


*Figure 1.18: Schematic of the PGP direct sight spectrograph*

### 1.7.6 Hyperspectral Imaging optical bandpass filter

The bandpass optical filters can be fixed or tunable and are widely used in area scan HSI systems [1]. Specifically among the fixed ones the most common are:
*Fixed bandpass filters* are interference filters usually placed in a filter wheel that rotates in front of detector arrays or in front of the light source to transmit the wavelength of interest and reject light out of the passband [1]. Normally these filters since they do not contain more than 10 bandpass filters are used in multispectral techniques [4]. The main disadvantages are:

- Low resolution
- Narrow spectral range
- Mechanical vibration due to moving parts
- Image misregistration due to filter movement

*Tunable bandpass filters* can be mechanically swapped or controlled differently to select a desired spectral range. These types of filters include tunable filters (TFs), which provide an appropriate compromise between spectral bandwidth and acquisition time for wide-field imaging systems [32]. The spectral transmission of these devices can be controlled electronically by a voltage, signal, or filter. In particular are distinguished liquid crystal tunable filters and acoustic optical tunable filters [1].
*Liquid crystal tunable filters (LCTFs)* consist of a linear polarizer, a birefringent quartz element characterized by a fixed delay, a tunable retarder composed by liquid crystal plates, and finally an analyzer oriented with its axis parallel to the initial polarizer [32][33]. The liquid crystal plates of the tunable retarder consist of two transparent electrodes (indium tin oxide) on either side of a cell containing nematic liquid crystals (fig 1.19) [32].

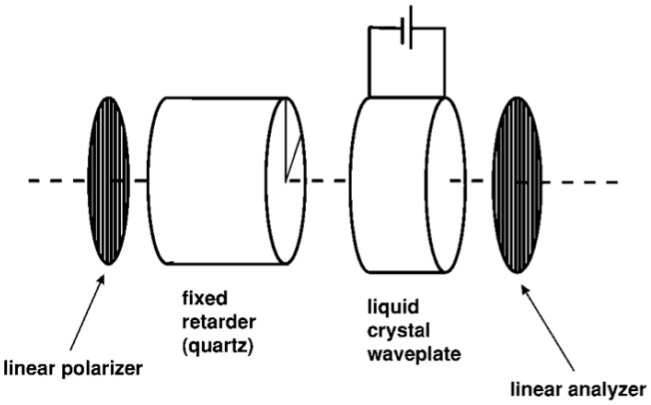


*Figure 1.19: Schematic diagram of a single Lyot-Ohman cell*

The LCTF is polarization sensitive and its switching speed is limited by the crystal relaxation time and is of the order of ~50 msec [32]. This parameter is achieved by appropriate device design with a sequence of short wavelengths [34]. The final images obtained are characterized by a very large number of bands (10-100) with very narrow spectral widths of the individual bands [34][35]. The spectral resolution of these types of filters is generally on the order of a few nm, although it can be narrowed further by a narrower bandpass [34]. Another advantageous parameter is the wide wavelength tuning range, while unfavorable is the not too fast wavelength tuning speed and poor light transmission.

*Acoustic-optical tunable filters* (AOTFs) are based on both photo-acoustic and acoustic-optical interactions. These filters depend primarily on the perturbation applied to the physical structure of the filter caused by a piezoelectric transducer connected to the acoustic-optical medium [36]. The transducers consist of a crystal in which radio-frequency waves (RF) in the range of 20-200 MHz are responsible for separating each wavelength of light from a broadband source [36].

The wavelength of the selected light is a function of the frequency applied to the crystal, consequently, the change in the latter results in a change in the wavelength of the filtered light [34].

Acoustic waves traveling through the transducer cause compression and relaxation in the crystal, the resulting changes in density determine the refractive index [34]. In contrast to a classical diffraction grating, this device acts more like a filter in that it diffracts only a specific wavelength of light [34]. The intensity of the diffracted light

is directed into two first-order beams, called (+) and (-) beams, which are orthogonally polarized and each used in specific applications [34]. In order for the AOTF to be defined as a tunable filter, it is characterized by a beam stop that blocks the undeflected broadband light by directing only the monochromatic light toward the camera [34]. The angle between the (+) and (-) beams is generally a few degrees, and the bandwidth of the selected light depends on both the device and the operating wavelength (fig. 1.20) [34].
The switching speed of these filters is faster than the previous ones with a value between 10 and 30 milliseconds. The main disadvantage is low light transmission and high cost [32].

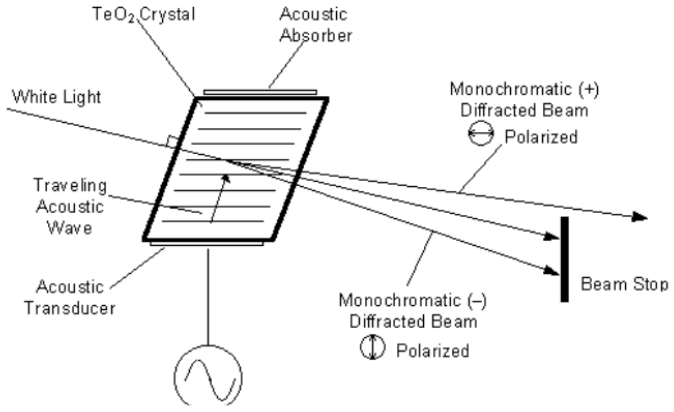


*Figure 1.20: AOTF operations*

Spectral filter technology offers high percentage transmission, high out-of-band Spectral filters are able to offer high transmission rate, high out-of-band blocking power, and high wavelength tuning range [32]. In addition, thanks to their high dynamic range and high sensitivity, they bring a significant improvement in the ability to perform hyperspectral microscopy studies [32].

### 1.7.7 Main parameters of hyperspectral imaging

In the choice of hyperspectral imaging systems device it is important to define the performance since different applications usually require various performance

parameters [37]. The main performance parameters that a spectral imaging system usually refers to include spatial resolution, temporal resolution, radiometric resolution, spectral resolution, dynamic range, sensitivity, etc [37]. These parameters depend primarily on the optical system's ability to produce an undistorted, un-aberrated, and intense data cube of a scene, as well as the detector's ability to convert an image into a digital form with low noise and fine spatial or spectral sampling [37].

The pieces of information contained in an image are stored in grids composed of units called pixels. A pixel is the smallest units of an image, they are normally square and represent a certain area on an image. Pixel represents the average of the light reflectance values of the objects contained in a certain area, depending on the type of sensor used. In the case of optical spectral bands, the latter corresponds to the Instantaneous Field of View (IFOV) of the sensor

a) *Spatial resolution or geometric resolution* is the projection of the detector element, usually coinciding with a Charged Couplet Devices CCD sensor, through the sensor optics within the instantaneous field of view of the sensor. The goodness and level of accuracy of the images are directly proportional to the size of the pixel on the object, or otherwise to the value of the instantaneous field of view of the instrument [37]. In other words, it is the size of the CCD element that determines the spatial resolution. Therefore, the spatial resolution is nothing more than the instrument's ability to discriminate between different objects in the image [37]. Spatial resolution limit is a very important parameter of an imaging system that should be taken into consideration before the examination of any object [37].
b) *Temporal resolution* is determined by the frame rate and exposure time of the camera [37]. Fast dynamic events that occur faster than the cameras frame rate are not visible (or captured incorrectly) in the recorded video sequences (temp).
c) *Radiometric resolution* is defined as the amount of energy levels between a maximum and minimum level that a sensor can discriminate. The energy levels obviously examined by the sensor must be contained in the

wavelengths proper to the target under consideration. Normally the images detected by the sensor are digital images in which the scene detected is represented by a matrix of pixels, each of which is characterized by a positive integer number, the DN (Digital Number) ranging from 0 to a selected power of 1, and corresponds to the average radiance of the area covered by each pixel [23]. The digital number range is the number of bits used to encode numbers in binary format. Therefore, if a sensor used 8 bits to record data, then 28 = 256 digital values, between 0 and 255, would be available. However, if only 4 bits were used, then only 24 = 16 values between 0 and 15 would be available. Therefore, the radiometric resolution would be much lower. The DN can be rendered displayed in a range of gray tones, with black representing a digital number of 0 and white representing the maximum value. So radiometric resolution corresponds to the number of these shades of gray that it can be possible to seen.

d) *Spectral resolution* describes the ability of a biomedical spectral imaging system to distinguish two signals that are separated by a small spectral difference [28][37]. The finer the spectral resolution, the narrower the wavelength range for a particular channel or band [28]. Hyperspectral sensors, detect hundreds of very narrow spectral bands throughout the visible, near infrared and mid-infrared portions of the electromagnetic spectrum. Their very high spectral resolution facilitates fine discrimination between different targets based on their spectral response in each of the narrow bands [28]. Spectral resolution is usually described by the full width at half maximum bandwidth (FWHM), which corresponds to the width of the spectral response function at half its peak height [28]. Spectral resolution can be obtained either by measuring the spectra of a known monochromatic light source and calculating the FWHM, or otherwise can be expressed as a function of the width of the entrance slit:

$$BP = FWHM \approx \frac{d\lambda}{dx}\, x\, w \text{ [nm]} \quad \text{Or} \quad BP = \frac{a\cos\alpha}{nf_2}\, x\, w \text{ [nm]} \qquad (1.13)$$

Where

- $\frac{d\lambda}{dx}$: is the linear dispersion representing how the wavelength increases per sensor distance
- $w$: slit width
- $a$: distance between the grooves in the grating
- $\alpha$: angle of the incident wave
- $n$ is the spectral order
- $f_2$ is the collimator focal length Spectral resolution is normally determined in any instrument using a light source that emits a spectrum with a pure monochromatic line.

A representation of the spectral passband for both a well-aligned and a more realistic instrument can be seen in the fig. 1.21.

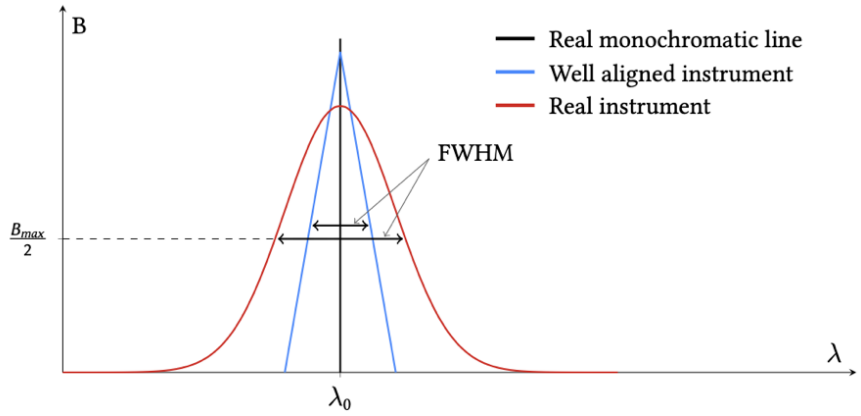


*Figure 1.21: Example of bandpass for a real monochromatic line, for a well aligned instrument, and for a real instrument*

The spectral resolution of a spectral imaging system usually depends on the type of spectral dispersion element the system employs [37].

*e)* *Dynamic range* is the ratio between the maximum and minimum values that can be recorded in the same scan. This parameter depends on the number of bits of the converter used [37].

*f)* The *sensitivity* of a camera is quantifiable as the minimum amount of light that can be detected and depends mainly on the noise floor of the sensor.

### 1.7.8 Noise in digital image processing

When a sensor captures an image, noise is also acquired with it, which degrades the performance of both video and photographic footage and reduces image quality. Much of this noise is random and therefore impossible to remove completely. The main types of noise:

- *Shot Noise or Photon noise*
- *Thermally generated noise*
- *Reset noise or Reading noise*
- *Dark current noise*

*Shot noise* is the one present in the image itself. If the images are taken at different times, the intensity, which corresponds to the number of photons recorded, will not be the same for each image, but will vary slightly. The deviation of the image intensity follows the law of Poisson distribution [38][39]. The noise associated with the image itself coincides with this intensity deviation. Poisson's law allows us to know the value of this parameter, which can be obtained as the square root of the measured signal intensity [38]. This type of noise represents one of the main natural limits as it is associated with the random arrival of photons towards each type of detector [38].
Within the CCD itself, additional electrons are generated as a result of the physical process within the CCD. This noise is called *thermal noise* because the amount of electrons depends on the operating temperature of the CCD.
*Dark current* corresponds to the generation rate of thermal electrons at a specific temperature [40]. This parameter increases with increasing exposure length and decreases with decreasing temperature [37][38]. Similarly to photon noise, dark noise follows Poisson's relation that the dark current is equivalent to the square root of the number of thermal electrons generated within the image exposure time [40]. This type of noise is relatively easy to handle either by cooling the CCD, or by stripping the electrons of the heat energy needed to reach an intermediate state [41].

*Reset noise* is related to the amplifier inside the chip whose function is to convert electrical charge into voltage [38][42]. The electrical charge present in a pixel is transferred to the output node where the conversion to volts takes place using the sense capacitor and the output amplifier [41]. The CCD capacitor is reset to the reference value, which is characterized by a certain uncertainty due to the thermal noise generated by the channels resistance, before measuring each charge packet of the pixel [37][41]. This reset process produces about 50 electrons, which is why many CCD camera manufacturers include circuitry that eliminates reset noise [41].

### 1.7.9 Hyperspectral Imaging applications

The use of hyperspectral imaging with the passage of time has rapidly spread, thanks to its ability to identify and discriminate different materials, in many different fields, such as [29]:

- **Mining and geological applications**: these types of fields were one of the first in which spectral imaging was of great importance. [42]
- **Military sector**: thanks to the ability of this technique to discriminate between materials [42].
- **Remote sensing**: in this area it is very important to distinguish the characteristics of the Earth's surface, each characterized by different spectrum bands. The multi spectral satellite can capture images on few bands, for example Landsat 7 has 8 bands. But the multi-spectral imaging satellite can capture the Earth's surface in more than 200 bands. In this way obviously many more objects can be differentiated. [43]
- **Environmental monitoring**: has become popular in this area to track changes in the environment. It is used to understand surface CO2 emissions, to map hydrological formations, and also to track pollution levels [pollution].
- **Food**: Hyperspectral imaging is widely used in the food industry, some examples refer to the detection of bruises in apples, fish freshness, citrus inspection and sugar distribution [22] [44].

- **Study of seed viability:** Using this technique and then plotting the reflectance spectrum of the seeds, one can conclude whether the seeds are viable or non-viable. The benefit of hyperspectral imaging is that with naked eyes the seed might look the same [45].
- **Forensic science**: hyperspectral imaging in this area can be used in a variety of ways: analysis of questioned documents, arson investigation, bloodstain visualization and differentiation between dark marks, fiber comparison, gunshot residue, visualization, tape examination, fingerprint enhancement, and TLC plate visualization [46].
- **Oil and gas**: Hyperspectral imaging technology is widely used in gas exploration and to detect possible onshore oil seeps [47].
- **Thin films**: Due to the ability of hyperspectral imaging to distinguish tiny objects, it has been widely used in quality control of thin film production process [48].
- **Pharmaceuticals**: Hyperspectral imaging technique is widely used in the control of counterfeit or illegal drugs by handling medicine packaging and powder mixing. [46]
- **Biotechnology:** Hyperspectral technology has become popular in this area due to its ability to rapidly acquire data that can be used in the laboratory. Mostly they are used in the study of wound analysis, fluorescence microscopy and cell biology.
- **Medical Diagnosis**: In this area, hyperspectral imaging plays an important role in the early detection of diseases and their prevention, due to the ability to identify potential biochemical changes related to disease progression. Hyperspectral imaging technology can be used to detect various types of cancer at an early stage, and in the last period as we will see below it has assumed great importance in ophthalmology, and in particular in the diagnosis of retinal diseases [4].

## 1.8 Hyperspectral imaging in ophthalmology

Hyperspectral imaging is an emerging modality for a large number of medical applications, such as ophthalmology. It is especially used for non-invasive diagnosis of diseases and in guiding surgery thanks to the images it can obtain [1]. For example, one of the main purpose in the ophthalmological field is to try to follow the molecular and cellular development of the retina in vivo [49]. The light affecting biological tissues undergoes a scattering due to the inhomogeneity of the latter and an absorption in specific structures such as hemoglobin, melanin and water. With the aim of identifying quantitative diagnostic information from the light that returns to the sensors of the hyperspectral chamber it is hypothesized that the absorption, fluorescence and scattering characteristics of a tissue change during the progression and evolution of the disease.

Fluorescence refers to the ability of some substances to re-emit received electromagnetic radiation, generally in the ultraviolet range, at a longer wavelength, generally in the visible spectrum. This property is not permanent and continuous in the tissue, but generally stops when the excitation ends. In the pigment epithelium of the retina can be found some components with these properties such as melanin (excited at wavelengths of 787 nm) and lipofuscin (excited at wavelengths of 470 nm) [50]. In this paper, as we will see later, a slit lamp was used in an eyepiece of which a hyperspectral camera was mounted.

### 1.8.1 Eye Anatomy

The eye is one of the most important sensory organs, unparalleled in complexity, capable of absorbing and processing more than ten million pieces of information per second. This organ focuses light on a light sensitive surface (the *retina*) using a lens and an aperture or opening (the *pupil*) whose size can be adjusted to change the amount of entering light [51]. The human eye can be compared to a sphere that can be divided into an anterior and posterior segment (fig. 1.13) [51]. The first one, which occupies the anterior and most superficial portion of the eye, comprises the

conjunctiva, the cornea, the anterior chamber of the eye, the iris with the pupil and the crystalline lens. The second segment covers the remaining space of the eye and consists of the vitreous body, the sclera, the uvea and the retina. The eyeball is made up of three superimposed membranes, which are called ocular membranes, starting from the outside to the inside of the eye, these membranes differ not only in their function but also in their composition [51]. The most superficial membrane is the tunica fibrosa. In the anterior part it is transparent and is called the cornea, while in the posterior part it is opaque and is called the sclera[51]. These two areas are not communicating, they are separated by the furrow of the sclera. The second membrane is the vascular tunica, rich in blood vessels and dark pigment, and containing smooth muscular elements. In the anterior part it has a complex structure and together with the retina it forms first the ciliary body and then the iris. In the posterior, larger part, where it assumes a regular arrangement it is called the choroid [51]. The deeper membrane, called retina, is nervous in nature and the optic nerve originates from it [51]. The anterior part of the retina contributes to the formation of the iris and the ciliary body. This area is not characterized by components of a nervous nature, is not responsible for the formation of the optic nerve and is called the blind part of the retina. The regularly arranged posterior part, on the other hand, is very wide and is called the optic part of the retina, since it is responsible for visual function.

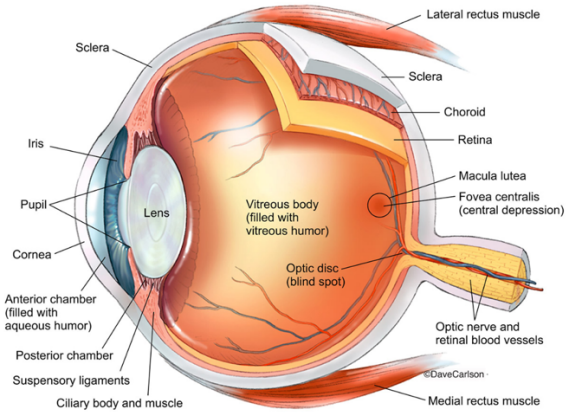


*Figure 1.22: Eye's anatomy*

### 1.8.2 Anterior segment of eye

The anterior segment of the eyeball is the visible part and includes the cornea, the anterior chamber, the iris, the central pupillary foramen, the crystalline lens with the structures that support it, i.e. the zonular apparatus, the ciliary body that continues anteriorly with the iris and posteriorly with the choroid.

*The cornea* is the first natural lens that light encounters in its path, measuring about 0.5 mm thick and is the front portion of the ocular fibrous tunic, which is opaque and takes the name of sclera [52]. The cornea is composed from the outside to the inside by five layers, such as the stratified floor epithelium, Bowman's membrane, stroma, Descemet's membrane and endothelium [53][52]. It is a transparent membrane without vessels but rich in nerve fibers for this reason even the smallest trauma causes violent pain [52]. This organ has a more or less spherical shape, and its various curvature in the different arcs for 360° of the circumference determines astigmatism, the visual defect that does not allow a clear vision. Its average power is about 43 diopters.

It is continuously wetted by the tear film that adheres to its anterior surface and is nourished by the aqueous humor from which it draws contacts in its posterior surface. The tear film protects the cornea from both substances and external damage [53]. The tear film-corneal surface interface constitutes the most powerful converging lens in the human eye. The stability of the tear film and the transparency of the cornea are essential for vision.

The cornea has a double role, the first is to allow the passage and convergence of light to the internal structures of the eye, in particular to the fovea, the second is to protect the eye from abrasive trauma and pathogens such as viruses, germs and bacteria [52].

*The anterior chamber* is a cavity containing aqueous humor, a substance that generates important nutrients for both the crystalline lens and the cornea. This chamber is delimited anteriorly by the cornea and posteriorly by the ciliary body, for a short distance by the iris in its entirety, and by the crystalline lens for that portion that faces the pupillary foramen [52].

It is about 3.4 mm deep at the center and flattens out towards the periphery with a narrow sinus called the anterior chamber angle.
The angle of the anterior chamber, together with the neighboring structures, constitutes the so-called region of the angle of the chamber, seat of the delicate processes of drainage of aqueous humor.

*The iris* is a circular membrane located between the anterior chamber and the crystalline lens. This structure gives color to our eyes and surrounds the pupil, a small central hole varying in width from 2 to 8 mm depending on the amount of light reaching it [53][54]. The iris is composed of the stroma from the vessels and two muscles, the radial muscle and the sphincter muscle, which allow dilation and constriction of the iris, respectively [52]. It can be either clear or brown, but actually its coloring depends both on the amount of pigment and on optical phenomena of reflection and diffraction of light in the iris stroma.
In light irises with little pigment, light passes through to the deep layers where it is reflected, assuming a light color. On the contrary, in brown irises, rich in pigment, light does not penetrate to the deep layers and is neither reflected nor diffracted.

*The crystalline* lens is the second natural lens that light encounters before reaching the retina. It is a biconvex elastic lens that can vary its thickness and shape thanks to a ring of muscle fibers arranged around it, called the ciliary body, in order to increase or decrease its power of convergence. When the eye looks at an object in the distance (6 m) , the crystalline lens flattens and decreases its curvature; when, on the other hand, it looks at a near object, it becomes more convex and increases its curvature [52]. Over the years, the crystalline lens can lose its elasticity, becoming stiffer, and in this case corrective glasses are needed for near vision; if, on the other hand, it loses its normal transparency, becoming opaque, it develops what is called a cataract.

*The posterior chamber* is a much smaller cavity when compared to the anterior chamber, and also contains aqueous humor. It has an annular shape, bounded

anteriorly by the iris, laterally by the ciliary body, and posteriorly by the zonular fibers and the lenticular equator.
On the medial side it progressively narrows into the irid-lenticular space and through the latter it communicates with the anterior chamber.

### 1.8.3 Posterior segment of the eye

*The posterior segment* of the eye is the most important part because within it, it is possible to anatomically identify structures like macula and fovea that allow us to see.
Diagnostics of this segment, and even more so surgery, make use of the most sophisticated and elective instruments and techniques, suitable for observing and intervening on very delicate and extremely vulnerable structures.

*The uvea* is the vascular layer of the eye, interposed between the sclera and the retina. This is the membrane designed to provide nourishment to all the structures that are part of the eye, and can be divided into three parts that, from the posterior to the anterior part are, the choroid, the ciliary body and the iris, respectively.

*The choroid* is a richly vascularized tissue structure, located between the sclera and the retina and is divided from the retinal nerve tissue by Bruch's membrane and the retinal pigment epithelium [52]. Posteriorly, the choroid adheres to the sclera through the suprachoroidal lamina; anteriorly, it consists of a more densely vascularized layer called the choriocapillaris lamina.
The choroid is characterized by large and medium-sized veins with numerous branches and arteries with the main function to oxygenate and nourish the outermost layers of the retina [52] [54]. Choroid is also responsible of maintenance of a constant temperature of the retina and at the end participates in the adaptation of the eye, like the transition between near and far vision.

*The sclera* is one of three membranes along with the choroid and retina that line and protect the inside of the eyeball from internal and external forces, and it maintains its shape [53]. This white-colored membrane, composed of collagen and elastic fibers, covers the entire eye with different densities, extending from the optic nerve to the cornea, and is thinner at the front of the eye than at the back [52].

*The vitreous cavity* fills the space between the lens and the back of the eye [51][52]. This area is filled with a gelatinous substance called the vitreous humor, the transparency of which allows a clear vision at all distances [52]

*The retina* is the innermost membrane of the eye and has the function of transforming the rays of light focused into it through the cornea, pupil and lens into impulses that travel via the optic nerve to the brain, where they are interpreted as the images one views [52] [53].

The retina is a very thin layer of transparent nerve tissue (500 μ thick at the periphery to 250 μ thick at the fovea) that rests on a pigment layer, called the retinal pigment epithelium (EPR), which is responsible for both the nutrition and the disposal of the products of metabolism of the photoreceptors (cones and rods) (fig. 1.24) [6]. In addition to the photoreceptors, that composed the outermost layer neural retina, this latter is characterized by a considerable number of cells with the function of amplifying, modulating and distributing the visual stimulus: bipolar, amacrine and horizontal cells [7]. Light passing through the retina causes chemical changes in the photoreceptors, which transform the signal into a nerve impulse [52]. This is transferred via the ganglion cell endings (binds to others to form the optic nerve) to the brain [52].

The zone in which about 95% of all sensory cells are located is the center of the retina, the macula, an area of about 5 square millimeters, densely packed with con cone photoreceptors that make the visual image more detailed [7][54]. It is so called due to the presence of a particular pigment with a slightly yellowish color, xanthophyll [52]. The macula is particularly susceptible to metabolic changes in the body and even minimal structural damage is responsible for serious visual impairment. The fovea is the central portion of the macula, with a diameter of 1.0

mm, and is the point in which the optical system converges vertical and horizontal light rays [52]. There are no rods in this area, but cones are very numerous, and since these cells not only allow us to perceive the colors of our surroundings, but are also responsible for sharp vision, this area represents the sharpest point of vision in the macula [7][52]. Within the fovea it is possible to distinguish an even smaller, vessel-less area called the foveola, just 0.35 mm in diameter densely packed with cones [7]. The retina is crossed by small arteries and veins that radiate from one point, the optic disc [7].

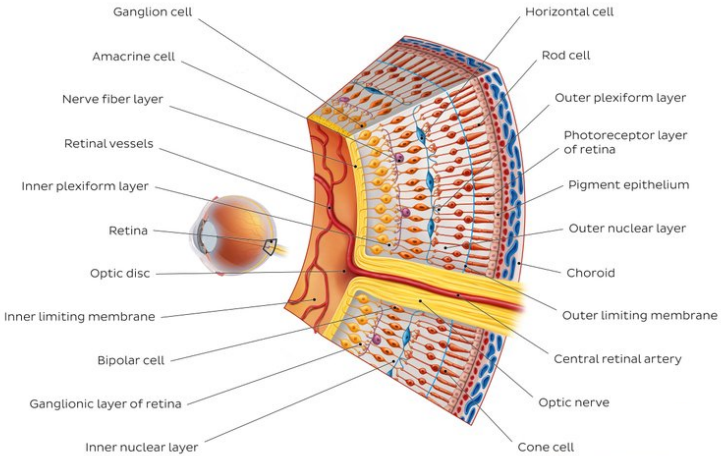


*Figure 1.23: Layer of rods and cones*

*The optic nerve*, is the II pair of cranial nerves, is about 5 cm long and is wrapped around the meninges, the dura mater, arachnoid and pia mater respectively. It is composed of many fibers within it, each of which is protected by a myelin sheath. Each individual fiber corresponds to a small area of the retina, while each bundle corresponds to a retinal area. At the center of the optic nerve are fibers that carry bioelectric signals from the macula. The nerve fibers originate from the retinal ganglion cells and form a bridge that connects the eyeball to the diencephalon. The function of the optic nerve is to transmit electrical impulses from the retina to the visual center of the brain [52]. These impulses are then processed and transformed into images.

*The Retinal Pigment Epithelium (EPR)* is an integral part of the retina and consists of pigmented cells, called melanocytes characterized by prolongations, enriched with melanin, that branch between the cones and rods, and in particular they stretch in the presence of large amounts of light and retract in dark moments [52]. The main function of these filaments is therefore to carry the necessary nutritional materials, repair the losses that the cones and rods undergo in their functional activity and it is involved in ocular immune response [53] [55]. This epithelium is located between Bruch's membrane and the outer layer of the photoreceptors (neuroretina) [52]. The retinal pigment epithelium is defined as the external blood-retinal barrier, as it performs many functions such as promoting the selective exchange of molecules between the photoreceptors and the choroid, and at the same time preventing the passage of liquids from the choroid to the retina [52][53]. Its integrity and its adhesion to the retinal cells is therefore an essential condition for the proper functioning of the complex retinal balance. In the presence of retinal pathologies, it is precisely this that is affected [52].

Lipofuscin is one of the main substances that represents the waste product of the metabolism of cones and rods and is accumulated, with the passage of age, in the retinal pigment epithelium [56]. This substance is not homogenous, but is formed by different materials such as lipids, proteins, and different fluorophores [57] Lipofuscin, therefore, is an important fluorophore, with significant absorption around 470 nm and emitting in the yellow-green region with a peak near 600-610 nm (fig. 1.25) [50].

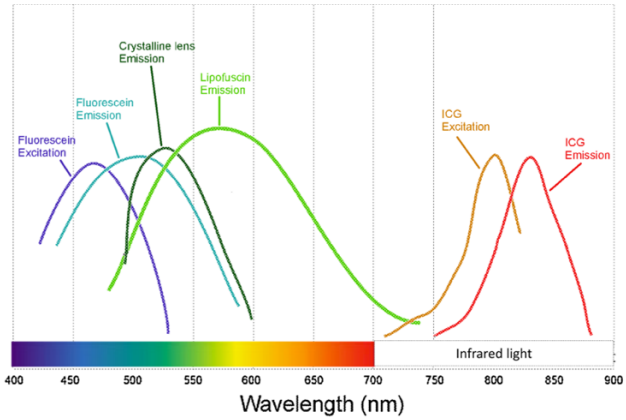


*Figure 1.24: Emission spectrum of lipofuscin*

### 1.8.4 Slit camera or biomicroscope

Slit-lamp examination, also called "biomicroscope" is a diagnostic examination that is generally performed during an eye examination.
Thanks to this examination, the eyelids, conjunctiva, sclera, cornea, anterior chamber, iris and crystalline lens are all observed at high magnification [58]. Using additional lenses, it also allows the examination of the iridocorneal angle, the vitreous body, the retina and the optic nerve head [58][59]. In addition to physical examination, the slit lamp allow to identify and suspect many ocular pathologies, and it is often used for tonometry, linear measurement of tissue or lesions, and ophthalmic photography [58]. This instrument is composed of a illumination system, supporting system, observation system and a joystick [60].

#### *1.8.4.1 Illumination system*

Illumination system provides a precise and an adjustable source of light. The lighting system consists of a halogen light source that can be placed either at the top or at the bottom depending on the model of the slit lamp [60]. The light emitted by the light source is passed through the condenser lens system, that consists of a couple of planoconvex lenses with their convex surfaces in opposition and are able to create a collimated light beam or a flat wavefront [60]. The light is passed through a regulable slit, which size, direction and shape can be varied using two knobs. In the illumination system there are also filters that allow a better evaluation of the anterior segment. In particular three filters are identified, and are cobalt blue filter, red free (green filter) and Neutral density filter (fig. 1.26) [61].

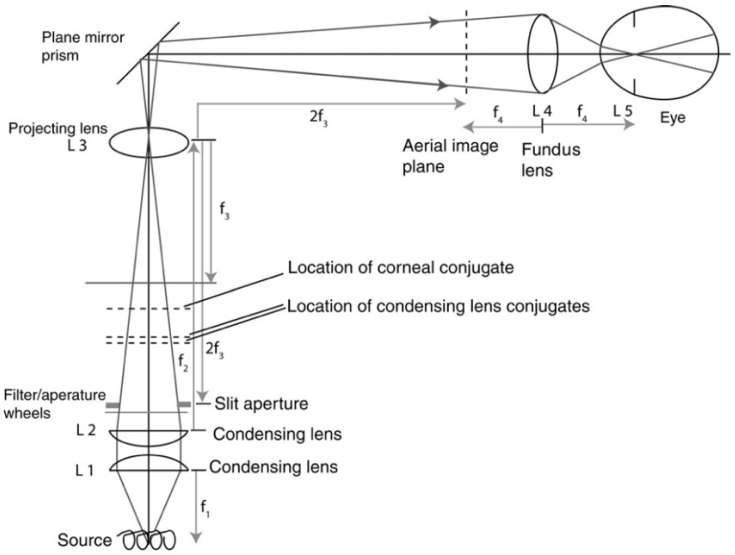


*Figure 1.25: Schematic of the illumination system during slit lamp assisted ophthalmoscopy*

a) *Cobalt blue filter* produce light of the wavelength 450 to 500 nm. This filter is useful for looking problem, like the status of the cornea and any corneal abrasions, in eye once it has been stained with fluorescein [62]. The cobalt blue filter is able to enhance the dye first introduced, which in case of corneal alteration is accumulated. Fluorescein is the most widely used dye and it is characterized by a maximum absorption at 490 nm (blue), and a maximum exposure at 520 nm (green) (fig. 1.26).
b) *Red free (green) filter* is used to observe the blood vessels of the sclera, conjunctiva and iris, as it increases the contrast of the image and brings out the capillaries. This filter obscure anything that is red hence the red free light, thus blood vessels or hemorrhages appears black. So, this filter increases the contrast between the structures and the tissues. [62]
c) *Neutral density filter* decreases maximum brightness for photosensitive patients, so reduce the light intensity without lowering the light, so it avoids the glare of the subject examined.

Then the projection lens allows an image of the slit to be formed to the eye. The diameter of the projection lens is usually quite small. This has two advantages, the first is to keep lens aberrations low, which results in better image quality, and the

second is to increase the depth of focus of the slit and thus produces a better optical section of the eye.

Finally, the illumination system of a slit lamp must be able to switch relatively easily from one side of the microscope to the other. To allow this, the projection system is usually arranged along a vertical axis, with a mirror or a prism with an inclination of 45 degrees, allowing to direct the light beam along a horizontal axis, then towards the eye. There are also rings in the illumination system that allow you to change the size of the slit in relation to width, shape and orientation (fig. 1.27) [60].

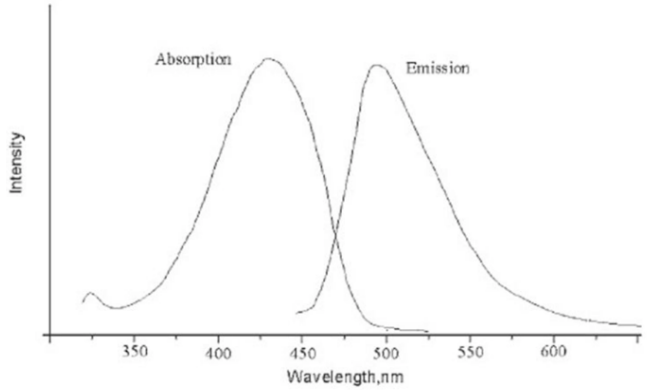


*Figure 1.26: Fluorescein spectrum*

*Figure 1.27: Slight width and shape*

Depending on the type of illumination, particular details of the tissue under examination can be visualized and studied.

In *direct illumination* the light beam is directly aimed at the focused object (coupled mode). In this case a distinction is made between diffuse illumination, focal (sectional or parallelepiped) and specular reflection:

- *Diffuse direct illumination:* magnification is low or medium, the illumination should be medium to high and the slit is fully open to

perform a panoramic assessment of ocular surface tissue (e.g., the bulbar and palpebral conjunctiva) [58][60] . The angle between the microscope and illumination system should be 30°- 45° (fig. 1.28) [59]. This type of illumination also used to examine size and shape, transparency and any foreign bodies or opacities present, and also it is used to observe contact lens fitting performance. Diffuse direct illumination it can be used in combination with:

- White light: this light requires the use of a wide, full-height beam that is directed onto the surface of the eye or adnexa from the temporal or nasal side. In order for the wide beam not to be too bright for the patient the brightness level site must be lowered [61].
- Cobalt-blue filter: produces blue light in which the fluorescein dye becomes yellow-green. This type of illumination is used to evaluate fluorescein staining of ocular surface tissues or the tear film and to distinguish the fluorescein pattern during Goldmann applanation tonometry [61].
- Red-free filter produces light green light, facilitating the evaluation of blood vessels and hemorrhages [61].

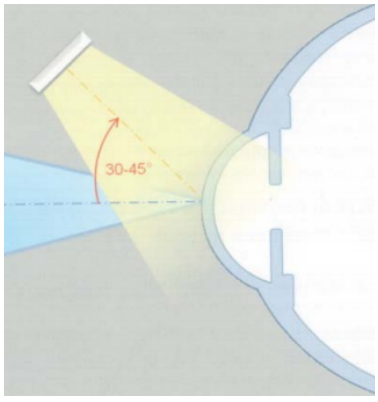


*Figure 1.28: Diffuse direct illumination*

- *Direct Focal illumination*: magnification is low or medium and the slit is narrow (<0.5mm for the section) or medium (between 0.5mm and 2 mm for the parallelepiped [58]. This illumination is achieved by

directing a full-height, medium-width, medium-bright beam obliquely (30°- 45°) into the eye and directing it on the cornea so that a quadrilateral block of light (parallelepiped or corneal prism) illuminates it (fig. 1.29) [60]. The parallelepiped consists of a "curved cube" that is useful for assessing the epithelium, stroma, Descemet's membrane, and the possible presence of edema [58]. The anterior surface of the parallelepiped represents the anterior surface of the cornea; the posterior surface represents the behind; and the other two faces of the parallelepiped show the cornea in cross-section. Corneal scars or infiltrates appear brighter than surroundings because they have more density [61]. After direct focal examination with the medium beam, the parallelepiped is narrowed so that its anterior and posterior surfaces become very thin, leaving only illumination of the cross-section of the cornea. This thin beam, called the optical section, is particularly useful for judging the depth of lesions and examining the crystalline lens [59] [60]. The whole tissue can be examined by moving simultaneous focus of the microscope across the surface. The conical beam together optic section and parallelepiped is another type. Conical beam is observe using small and circular pattern beam light source 45°-60° temporally from the microscope and directed into the pupil [61]. The biomicroscope is in front of the eye, and the magnification is high [61]. The first step is to adjust the light source aperture size to smallest one or by reducing the area of the parallelepiped until it becomes a small spot. The beam is focused between the cornea and the anterior the lens surface, and the dark zone between the cornea and the lens is observed by [61]. This zone is normally optically empty and appears black. Flare appears grey or milky and cells may be facilitated by gently oscillating the illuminator.

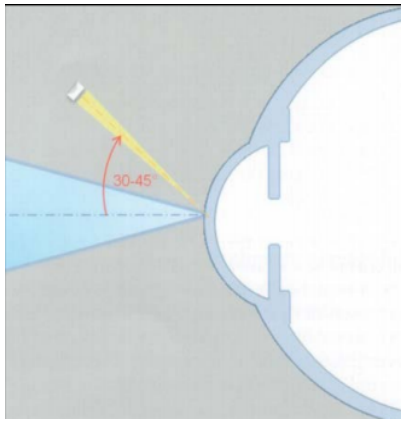


*Figure 1.29: Direct Focal illumination*

- *Specular reflection direct illumination*: the magnification is high and the slit is a small, short parallelepiped: the angle of incidence of the light beam (usually should be 50-60 degrees wide with respect to the axis of observation of the examiner) on the cornea is equal to the angle of reflection of light in the biomicroscope [60] (fig. 1.30). This type of illumination depends on the creation of a specular reflection zone, which is an area of very bright illumination produced by the reflection of light directly on the examiner's eyes [58]. A bright area of specular reflection will be most evident on the temporal and mid-peripheral corneal epithelium. Positioning the surface of the parallelepiped over this zone will produce a specular reflection zone on both the epithelial (anterior) and endothelial (posterior) faces of the parallelepiped. This technique allows you to evaluate mainly the endothelium, highlighting both its cells and cell margins and the possible presence of guttae, but it is also used to examine the anterior surface of the cornea or lens [59] [61]. Thanks to this illumination in the endothelium, each structures looks like a mosaic pattern.

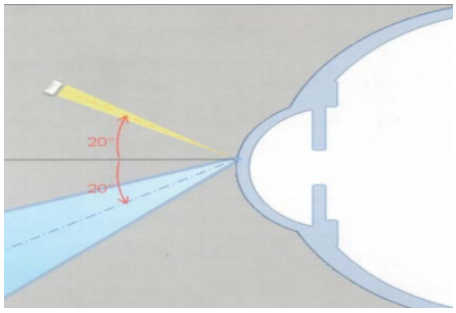


*Figure 1.30: Specular reflection direct illumination*

In *indirect illumination* the light beam is off-center to illuminate behind the focused object (decoupled mode). In this case it is possible to talk about backlighting or sclerotic scattering [59].

- *Transillumination, or backlighting*: the magnification is low or medium and the slit is a small parallelepiped [60]. This illumination backlights the tissues being examined. In this case, a medium-amplitude beam of light is projected onto a part of the eye that is deeper than the area to be studied, so that the latter can be seen by the reflected light while the examiner focuses on the tissues to be examined (fig. 1.31) [59]. This technique makes it easy to detect vacuoles of edema in the corneal epithelium, blood vessels in the cornea, deposits or other abnormalities on the posterior surface of the cornea, and tears or areas of atrophy in the iris [58].

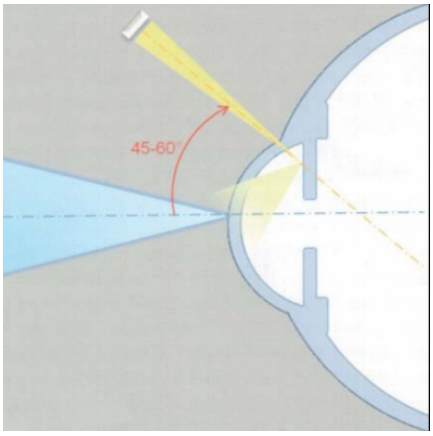


*Figure 1.31: Transillumination*

- *Sclerotic scatter lighting:* magnification is low and the slit is a small parallelepiped: the off-center (fig. 1.32). The off-center, medium-amplitude light beam is projected at the limbus and internally reflected through the corneal tissue (internal reflection similar to light propagation through an optical fiber), revealing low-optical-density changes such as dystrophy, epithelial edema, and Descemet's membrane rupture [60]. Less transparent areas in this type of illumination are highlighted because they scatter internally reflected light [60].

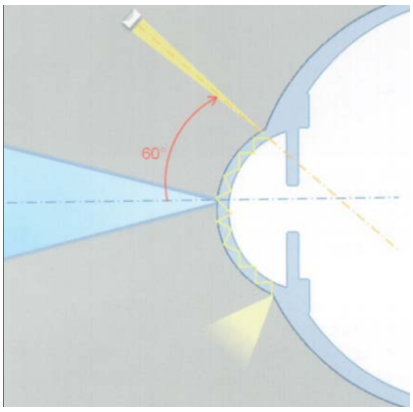


*Figure 1.32: Sclerotic scatter lighting*

Either epithelial-side or endothelial-side illumination techniques can be applied in the evaluation of a cornea.

#### 1.8.4.2 *Supporting system*

The moving stand is the mechanical system that allows the microscope and illumination system to be hinged on the same axis around which they rotate independently to create different angles between illumination and observation system that allow different examination technique possible. This allows both to focus on the same plane, in the same point but with different inclinations on the horizontal axis

#### 1.8.4.3 *Observation system*

The observation system consists of two parts:

- *Galilean-type biomicroscope*: that allows the evaluation of ocular structures in three dimensions, thus in a stereoscopic environment. This system can be adapted to the needs of the examiner, as the inter-pupillary distance and optical compensation through the eyepieces can be modified. To examine both anterior segment structures in greater detail and to allow better judgment of depth
- *Magnification system* ranging from 6X to 40X. Ideally, the practitioner should be able to change magnification easily and this gives slit lamps with four or five different objectives an advantage [58].

The biomicroscope together with the different magnifications provide best view of stereoscopic images.

#### *1.8.4.4 Joystick and additional photographic elements*

Joystick allows the movement of the microscope and illumination system towards or away from the eye and from side to side [60]. The up and down movement is obtained via some sort of screw device that moves the whole illumination and viewing system up and down relative to the chin rest.

Additional photographic elements may include a:

- Digital camera: CCD (video camera) capable of filming what is being framed [60].
- Beam splitter capable of providing a coaxial view

electronic flash to reproduce the effect of lighting [60].

- Fill light that consists of an auxiliary source of diffuse illumination to obtain general information about the context highlighted by the slit [58].

- Wratten filter (yellow) that when used in combination with the blue filter of the illumination system, improves the evaluation of the contact lens or the anterior segment in the fluoroscopic examination [60].

#### 1.8.4.5 *Patient support arrangement*

The arrangement of the patient support is a chin rest that moves vertically. The arrangement for adjusting the height of the table has been made to accommodate the person of all sizes [58].
During the course of the examination, should be positioned comfortably in front of the slit lamp with his or her chin resting on the chin rest and forehead opposed to head rest.
The microscope and illumination system should be aligned with the patient's eye to be examined. Fixation target should be place at the required position. Examination should be carried out in semi dark room so that the examiner's eye are partially dark-adapted to ensure sensitivity to low intensities of light. There should be a minimum exposure of retina to light. Low magnification should be first used to locate the pathology and higher magnification should then be used to examine it.

### 1.8.5 Eye disease

The retina is one of the most metabolically active tissues in the human body. Consequently, a possible imbalance between oxygen supply and demand following ischemia is thought to play a key role in the pathogenesis of diseases of the eye posterior segment such as diabetic retinopathy, glaucoma, age-related macular degeneration [63]. Nowadays, technologies for the measurement of oxygen tension in retinal vessels and the successive diagnosis and effective therapy monitoring are based on optical imaging methods and, in particular, some of them are realized by integrating a hyperspectral imaging system with a fundus camera. Through this integration it becomes possible to keep track of spatial changes in oxygen saturation

in retinal structures and the optic nerve head by exploiting the differential spectral absorption characteristics of the two main derivatives of hemoglobin, oxy- and deoxyhemoglobin [63] .

*Glaucoma* is a damage on the optic nerve, often due to elevated eye pressure, leading to irreversible vision loss. Normally, intraocular pressure is kept constant by a precise balance between the aqueous humor and the amount of fluid escaping from the eyeball. The aqueous humor is the fluid produced in the posterior chamber of the eye by specific structures called ciliary processes, then circulates between the iris and lens entering through the pupil in the anterior chamber (space in front of the iris), and is drained from there to the external venous system by a filtering structure called trabecularis, which is located at the angle between the cornea and iris (irid-corneal angle). In glaucoma, the drainage channels or uveoscleral pathway become obstructed, blocked or covered and fluid is unable to pass producing a compression on ocular structures, especially in the optic nerve head. The pressure of the eye under normal conditions is 16 mmHg, the upper limit of this variable according to statistical considerations is set at 21 mmHg.
Two different types of primary glaucoma, related to difficult drainage pathways, can be distinguished, the open-angle glaucoma and angle closure glaucoma.
*Primary open-angle glaucoma* is the most common syndrome caused by optic nerve damage characterized by an open anterior chamber angle and elevated or sometimes average intraocular pressure (IOP). Risk factors for this disease include older age, African ethnicity, thinner central corneal thickness, myopia, diabetes, and systemic hypertension, and it is strongly conditioned by hereditary factors. The optic nerve head is normally a slightly elongated circular shape, with a depression of the central area. The region between the rim of the cup and the rim of the disc is called the neurosensory rim and consists of the axons of retinal ganglion cells. Thinning of this area, hemorrhage of the nerve fiber layer across the edge of the disc, vertical elongation of the pair, and rapid angulations in the course of the blood vessels are the main changes in the optic nerve that lead to the development of this disease.
*Angle-closure glaucoma* is linked to more or less circumferential irid-trabecular contact with acute, intermittent or chronic closure of the irid-corneal angle

Intravascular oxygenation of the retinal vessels, retina, and optic nerve by hyperspectral imaging are currently the most widely used informative methods to investigate it [64]. Oxygen saturation levels are calculated after hyperspectral cube preprocessing by a formula using the Lambert-Beer law that links the ratio of the optical density of the vessels to the saturation-sensitive wavelength and the other isobestic.[64].

*Age-related macular degeneration* (AMD) affects the retina, in particular the central portion, the macula. AMD is a disease associated with advancing age and is one of the main causes blindness after 55 years, so a timely diagnosis is of necessary importance [54]. The retina and particularly the cells of the retinal pigment epithelium are exposed to high oxidative stress. Over time, antioxidants decrease leading to the formation, in the basal surface of the retinal pigmented epithelium (RPE), of drusen and degradation products even in the Brunch membrane [65]. Of consequence, the aging process of the eye alters the physiology of the macula leading to the death of the sensible cells of the retina (the photoreceptors) either slowly or otherwise dramatically and rapidly. Drusen are deposits of hyaline material generated as a result of altered metabolism of photoreceptor cells. Drusen can be hard or soft. Hard drusen are the least dangerous types with round, small, well-delineated shapes, while soft drusen are risky, wider, and inaccurately delineated. In fact, the drusen diameter (small < 63 μm in diameter), medium (63 to 124 μm), or large (<124 μm) classify the degree of disease evolution [66]. The dry or atrophic form and the wet or exudative form of AMD can be distinguished [54]. In the former case there is slower atrophy of the central retina due to poor nutrition by the capillaries, causing possible scar formation in the macula with a "map" appearance. At the same time if compared to exudative AMD is characterized by a better preservation of visual acuity. Generally affects both eyes, but can also occur asymmetrically and at the macular level involves the presentation of drusen.  The second form is more severe characterized by the presence of new subretinal abnormal capillaries, that being permeable to plasma, can originate the appearance of subretinal fluid that can lead to detachment or serous retinal pigment epithelium or otherwise breaking

generate a retinal hemorrhage. Cellular protein cytochrome-c has been found to be a key signaling molecule in degeneration and apoptosis processes. [4]

*Diabetic retinopathy* (DB) is a microvascular complication of the retina that can develop in those people who have type 1 diabetes and type 2 diabetes. This disease is also a major cause of cecity, and its diagnosis is not simple as there is no loss of vision even in advanced stages. Two different types of retinopathy can be discriminated: the first type is early diabetic retinopathy characterized by a weakening of the blood vessel walls that can lead to bulges that when damaged cause bleeding. The consequence is the formation of edema, an accumulation of fluid, in the macula.
The second type is proliferative diabetic retinopathy, which develops later than previous retinopathy and is more serious because it is caused by an abnormal growth of blood vessels on the inner surface of the retina, causing possible detachment or glaucoma. It is important to have an early diagnosis of this disease in order to anticipate even the worst cases and to be able to treat it successfully.

## 1.9 Hyperspectral imaging in dermatology

In the present work, in addition to the field of ophthalmology, it has been gone to examine how hyperspectral imaging systems are able to discriminate a mole from the skin.
Recently, traditional digital imaging based on measurements of light spectrum only in in the red, green, and blue region has been replaced by the use of hyperspectral imaging, which provides continuous spectral sampling not only in the part of the light spectrum visible to humans, but also in the ultraviolet and infrared range.
A mole is a pigmented, flat or fleshy skin lesion composed of pituitary glands, known as melanocytes, cells that are located in the lower part of the epidermis, just above the dermis and are able to activate genes to encode RNA necessary for melanin synthesis [67]. Melanocytes are not only found on the epidermis, but are also distributed in the hair follicle, in the mucosa, in the cochlea of the ear, in the eye and

in particular in the iris and midbrain [68]. Melanin is a pigment found in our body that gives color to the skin and produce two types of pigments based on the biosynthetic pathways, eumelanin and pheomelanin [68]. Eumelanin provides a dark, long-lasting pigmentation, in fact it is typically found more abundantly in individuals with brown or black skin, while pheomelanin being a red-yellow pigment enhances light color and it is abundant in fair-skinned individuals with red hair.

Melanoma originates from melanocytes and is the most serious form of skin cancer, that results in an uncontrolled division of cells in the epidermis, which can lead to malignant formation [67].

Examination of the skin and early detection of melanoma traditionally is performed using a magnifying lens with optimal lighting conditions.

To identify the suspicious changes of a mole it has been referred to the ABCDE criteria, where A indicates the asymmetry of the melanoma, B refers to the edges, C denotes the color of the mole, D is used to describe the size and finally letter E stands for its evolution, in particular about its size, shape and color.

High spectral resolution systems can eliminate traditional subjective interpretations and it is able to offer objective diagnostic accuracy, in fact, based on specific spectral characteristics of the chromophores of the skin tissue such as melanin or hemoglobin, it is able to discriminate these targets from others [69] [70].

Melanin is the major chromophore in the visible range and contributes to the optical properties of the skin by absorbing and scattering light. This pigment primarily absorbs energy in the UV and blue areas of the electromagnetic spectrum with a subsequent decay to red. The scattering of melanin is instead generated by the small vesicles (1 micron size ) that are located inside, called melanosomes, characterized by a different refractive index between their membrane and the melanin polymer [71].

Considering that the spectral absorption range of the melanin causes not only the fluorescence of itself, but also of other organic molecules such as NADH/NAD(P)H, β-carotene, hemoglobin, and flavin, which are characterized by a higher quantum yield than melanin, the fluorescence of the latter ones becomes undetectable [72] [73]. To overcome this problem the fluorescence of melanin is generated thanks to

an excitation peak at a wavelength of 787 nm, and in fact this pigment, is one of the main fluorophores in near-infrared autofluorescence [50]

## 1.10 Hyperspectral imaging for wound healing

The most common types of wounds are those caused by pressure ulcers and vascular, arterial, venous, or mixed problems [74]. Venous leg ulcers are a consequence of chronic venous insufficiency that afflicts 1-2% of the population over 65 years of age in the U.S., U.K., Europe, and Australia [75][76]. Arterial ulcers are due to reduced or eventual occlusion of flow to the lower extremity, and the major cause is atherosclerosis of the medium to large veins [75]. Venous ulcers are a consequence of the inability of the legs to force the passage of blood through the venous conduits of the bicuspid valve by contraction of the muscles leading to the formation of edema [77].

Pressure ulcers are defined as localized damage to the skin and underlying tissues caused by various factors such as friction, shear, and pressure that, over time, lead to a progressive decrease in capillary blood flow, occlusion of blood and lymph vessels, ischemia of dermis, epidermis and subcutaneous tissues [78][79]. For the healing of these wounds, regular changes in the position assumed, suitable mattresses to decrease pressure and specific medications are recommended. For this last reason, it is essential to initially determine the cause that led to the generation of the wound, then it is important to identify factors that exert a positive influence on healing and subsequently, the increasingly important challenge is decision making in wound treatment. Keeping track on wound healing and on many cells and tissues structures that are involved, is an important step because, depending on the condition of the patient and the treatment of the wound, a chronic disease can be generated [77]. The wound area, size and perimeter and their respective progression, should be recorded during time, at the initial time and at regular intervals in order to follow the process of evolution to cures and medications that is different depending on the wound and to understand if the appropriate treatment is being taken or not [74].

There are several methods to determine the area of the wound. The simplest one, from a practical point of view, is to consider the wound as rectangular shape and then measure its size with a ruler. A second method is to trace the edge of the wound on a transparent grid sheet and the total area is derived either from the sum of the squares or by means of an electronic device. With developments related to technology, the image of the wound is photographed and then, using software, the area is obtained. Wound measurements are being developed not only in two-dimension but also in three-dimensional measurements (stereovision, photogrammetry, laser light) that allow the determination of area, volume and perimeter. It is essential to use the same method to coding the area for all acquisitions, with the patient always in the same position.

The potential of hyperspectral imaging in determining tissue oxygen levels is not only employed in ophthalmology, as reported in 1.8.5, but also in wound healing [80]. This technique has the great advantage to provide doctors images with important informative and quantitative spectral content of the wound healing in order to recognize and differentiate materials, and allows the creation of data collections that can be used for educational, diagnostic, research purposes and for the validation of a clinical approach [80].

# CHAPTER 2 MATERIALS AND METHODS

## 2.1 Introduction

This chapter presents the hyperspectral imaging systems used to acquire images throughout this thesis. In particular are reported the functions, configurations and technical specifications of the instruments used and the calibration procedure to be carried out before taking data and the subsequent management of acquired data. The first lamp was used in combination with the slit lamp, while the second was used in order to detect both traces of melanin in the skin and the spectral characteristic of the wound in the skin. To obtain images of adequate quality and reliable data, a characterization was initially performed to identify the performance of the system.
It is important to note that neither radiometric nor spectral calibration was performed during the activity, since on the one hand the imager, claimed to be of high precision, is already sold with a radiometric-spectral calibration certificate, and on the other hand because operating by relative reflectance measurements, no absolute radiance values are detected in the non-remote hyperspectral technique.
Paragraph 2.9 describes the samples used in this work, and then the data processing in the MATLAB environment was described.

## 2.2 Slit Lamp

The slit lamp provided for the present work by the DIISM of the Università Politecnica delle Marche is the Haag-Streit, model BD-900, on which the hyperspectral camera was then installed on an eyepiece (fig. 2.1). This machine (BD 900) is mainly used to investigate the anterior segment of the eye. Its main features are 10-16 times magnification due to the lever located under the microscope. The slit length is 1- 14 mm, and it has a yellow filter that allows additional contrast to the images when using fluorescence and it is activated by simply rotating the filter located at the front of the microscope. All other features of this slit lamp are described in fig. 2.2. Patient

access in this type of lamp is aided by the single support column present. The slit lamp features a continuously adjustable potentiometer conveniently located next to the joystick that allows you to adjust the level of light intensity in four main levels: 0, 1/2, 1/4, 1. For the ultimate goal of this thesis work, this slit lamp was modified not only with the addition of the hyperspectral camera on an eyepiece, but also with the integration of video port with C-mount optics, connected to the computer, to show the area in real time as seen by the specialist.

*Figure 2.1: Haag-Streit, model BD-900*

| | |
|---|---|
| **Slit Lamp Illuminator** | |
| Slit image width | 0 – 14 mm continuous |
| Slit image length | 1 - 14 mm continuous |
| Max aperture diameter | 14 mm |
| Slit image radial range | ± 90° |
| Radial movement of the slit light illumination relative to the microscope axis | Horizontal ± 90° |
| Filters | Blue, red-free, grey (10 %), yellow<br>The UV filter and the heat absorption filter are permanently mounted |
| Light source | Halogen lamp bulb 12 V / 2.5A |
| Illumination intensity: | 75 000 Lux at position 1/4<br>150 000 Lux at position 1/2<br>300 000 Lux at position 1 |
| Working temperature | 10° to 35° C |
| **Stereo-Microscope** | |
| Stereo angle | 13° |
| Magnification changer | 1x and 1.6x |
| Magnification:<br>with ocular 10x (standard)<br>with ocular 25x | <br>10x and 16x<br>25x and 40x |
| Range of adjusting eye-pieces | +6 to -6 diopters |
| Inter pupillary distance | 54 - 94 mm |
| **Instrument base** | |
| Operation | Single handed 3-dimensional operation of the guide lever |
| Adjustment of the instrument base | 100 mm (length), 100 mm (side), 30 mm (height) |
| **Power supply** | Input AC 115V, ±10% / 0.25 – 0.42A<br>AC 230V, ±10% / 0.13 - 0.21A<br>50 – 600Hz<br>Output 1 DC 7 – 14.4V / max. 36W<br>Output 2 DC 5V / 1W |
| **Net weight** | 8.1 kg (without power supply, headrest and options) |

*Figure 2.2: Data sheet the Haag-Streit, model BD-900*

## 2.3 Senop HSC-2 hyperspectral camera

The HSI instrument supplied for the current work by work by the DIISM of the Università Politecnica delle Marche consists of a high-precision HSC-2 hyperspectral camera (serial number 7002486) (fig. 2.3).

*Figure 2.3: Senop HSC-2 hyperspectral camera*

The Senop HSC-2 Hyperspectral Camera is a frame-based spectral system, sensitive to the spectral range between 512 and 900 nm, with the possibility of acquiring up to 1000 bands. In the present camera, each pixel is associated with a real value measured at a resolution corresponding to 1 megapixel without using interpolation. HSC-2 camera is equipped by different types of connectors, such as the Ethernet port, the power connector, the USB type C connector and the connection for the external GPS antenna. This device also has a user interface where you can change the script, for example, or adjust the exposure time. The data sheet of hyperspectral camera is reported in fig. 2.5. It is possible to change the focus of the camera by simply rotating the lens, and also on the back is a standard unc quarter 20 mounting thread that allows the camera to be mounted on a tripod for example or on other systems such as the slit lamp in this work. The hyperspectral sensor is integrated with position sensor and IMU for proper high resolution image processing. For the ultimate goal of this activity this camera was integrated on a slit lamp, Haag-Streit, model BD-900. An adjustable mounting and centering bracket was designed so that the objective of the camera coincided with an eyepiece of the microscope, in afocal mode, in order to exploit the magnification capacity and the high quality optical path (fig 2.4- 2.6).

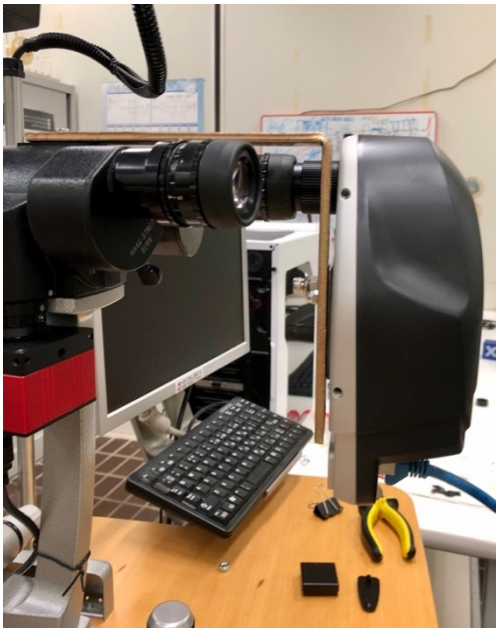

*Figure 2.4: Hyperspectral camera mounted in the slit lamp*

| PARAMETER | SPECIFICATION | REMARKS |
|---|---|---|
| Camera versions | HSC-2.1-B: 450-800 nm<br>HSC-2.1-C: 500-900 nm<br>HSC-2.3-C: 500-900 nm C-mount | HSC-2.3-C is a C-mount camera for example microscopical imaging. |
| Spectral FWHM | 6-18 nm | |
| Spectral Step | 0.1 nm | |
| Spectral Bands | up to 1000 | The bands are freely selectable/programmable. |
| Horizontal FOV | 36.8° | Diagonal 52.0° |
| Vertical FOV | 36.8° | Diagonal 52.0° |
| Image Sensor | CMOS | Pixel size is 5.5 µm x 5.5 µm. |
| Dynamic Range | 10/12 bits | |
| Max Image Rate (frames / s) | 74 (12 bit)<br>149 (10 bit) | The camera exposures each band separately. |
| Image Resolutions | 1024x1024 | All pixels are true image pixels. No interpolation used. |
| Exposure time | Adjustable | Maximum frame rate may be limited if exposure time is long. |
| Memory | 1TB | Shooting time with max frame rate 12 bit: 1h 45min &<br>10 bit: 1h 17min. |
| Connections | GigE RJ-45<br>Mini-Displayport v1.2<br>IO port with UART and 4GPIO pins<br>MMCX for external GPS antenna (if needed)<br>USB-C for irradiance sensor | |
| Weight | 990 g | |
| Dimensions (l x w x h) | 199 mm x 131 mm x 97 mm | |
| Positioning | GPS and BeiDou | With external antenna also Glonass and Galileo. |
| Voltage supply | 7-17 VDC | Set includes AC/DC adapter with cable. |
| Inertial Measurement Unit | Gyroscope and<br>3 axis accelerometer | |
| Adjustable optics | Focus distance: 30 cm - ∞ | FOV is limited with less than 30 cm distances. |
| Live Use | External display can be attached | |
| PC-software | Senop HSI-2 | Windows 7 & 10 |
| Data export | Standard ENVI | |
| Connectivity | Open API | |

*Figure 2.5: Senop HSC-2 data sheet*

*Figure 2.6: Hyperspectral system and slit lamp*

From the data sheet there is not much information regarding the characteristics of the monochromator. However, thanks to a thorough spectral analysis of the operating modes of the chamber, performed with the different filters characteristic of the latter, it was found an unnatural peak recorded at 640 nm . As an example of the previously mentioned discontinuity, fig. 2.7, shows the Spectralon trends acquired with the three different characteristic filters of the slit lamp.

The spectral investigation showed, also, that in the use of the yellow filter of the slit lamp, in addition to the previous discontinuity point, it present a saturation point at 820 nm.

The Senop HSC-2 is capable of being used in both stand-alone and snapshot modes. The former is a pre-programmed mode that employs scripts loaded into on-board memory. In the scripts are configured in addition to the sequences of wavelengths to be acquired and their order, the spectral resolution and exposure time. The second mode is connected via Giga Ethernet link to a computer and is controlled by the control application installable in Miscrosoft, Apple or Linuz operating systems.

The acquired data are stored either in the form of small monochrome images of each spectral band acquired (tumbnail) or as two files:

- the first file, called *data,* with .dat extension contains the acquired radiance data on the scanned wavelengths digitized in DN
- the second file, called *header*, with extension .hdr contains both the information relating to the capture and recording conditions of the data essential for the spatial and spectral reconstruction of the image under examination. This file can be used in all software capable of working with this type of extension. In this work they have been exported and processed in MATLAB environment.

The acquisition system is controlled by a PC which, by means of a specialized acquisition software , allows both to manage the different units of the measurement system and to perform the acquisition of the spectra and finally to collect them.
A mask simulating the patient's face with an optical cavity was made to acquire a flat-field reference image. To achieve this, a PLA additively printed Spectralon was inserted into the optical cavity (fig 2.8).

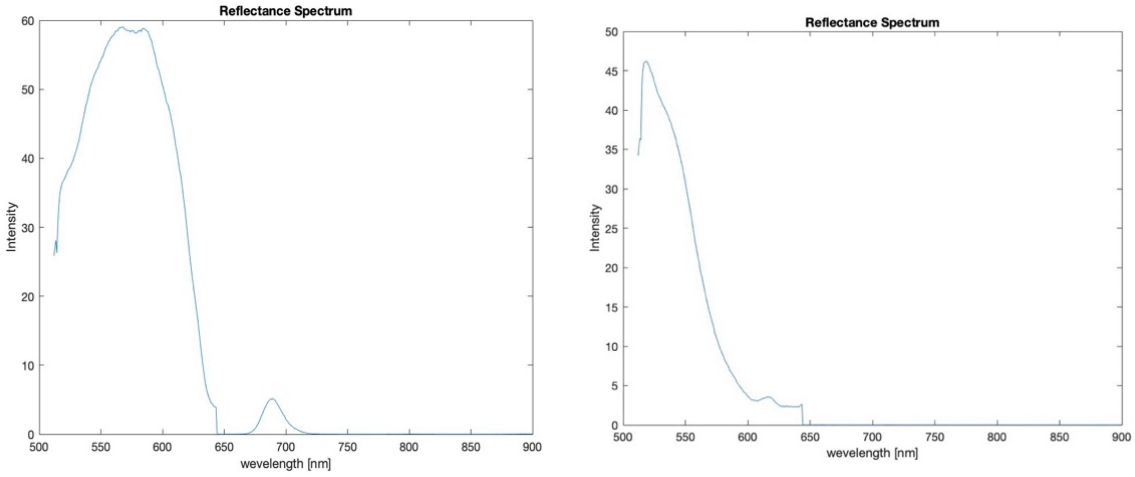

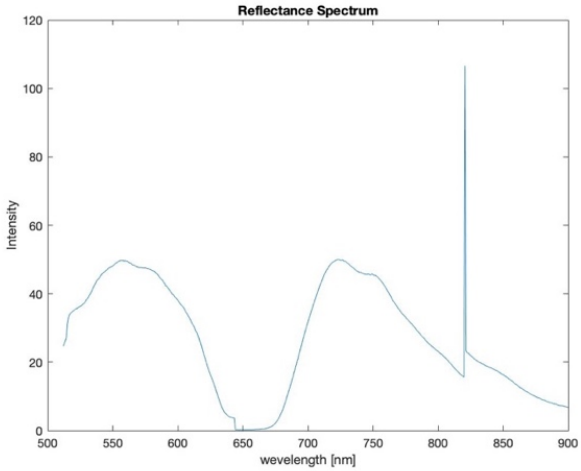


*Figure 2.7: Slit lamp spectrum without filter (left), with blue filter (right), and yellow filter (bottom)*

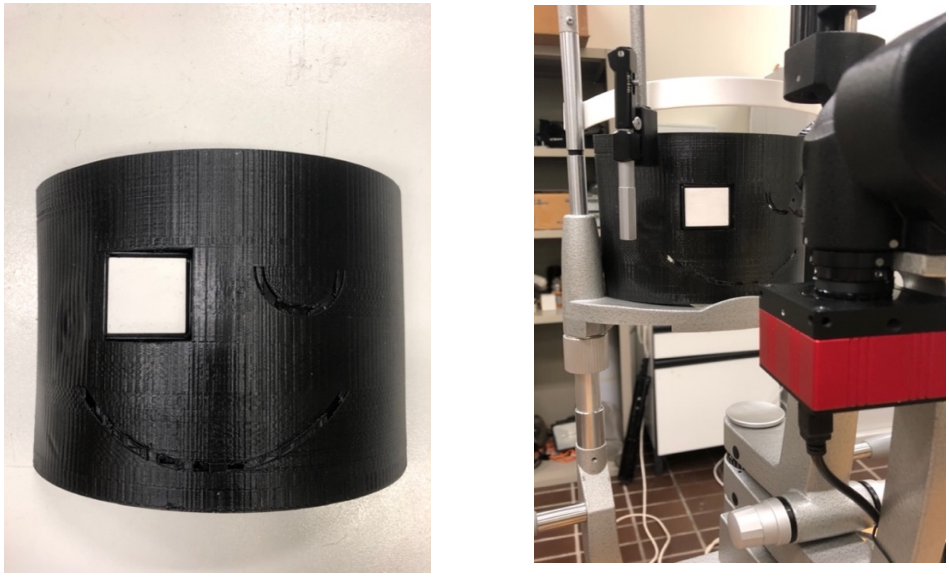

*Figure 2.8: Spectralon inserted in the mask (left). The mask on the slit lamp (right)*

## 2.4 Spectrometer

The spectrometer connected to a PC, with Microsoft Windows 10 and controlled via the proprietary software SM32ProForUSB version 2.9, was used in auto-configured mode without binning (fig. 2.9). The basic function of spectrometers is to collect light from a light source, divide it into its spectral components, digitize the signal according to wavelength and display it on the computer. A fiber optic cable is

connected to the spectrometer through a small opening. The probe at the end of the fiber has the task of acquiring light, which is then directed to the spectrometer. Normally spectrometers are formed by two concave mirrors, the first has the function to collimate the divergent light and direct it to a grating that then disperses the spectral components of light at variable angles. The light is then focused on the second mirror and finally displayed on the detector where the photons are converted into electrons.


*Figure 2.9: SM442 spectrometer, used for spectral characterization of illumination sources in combination with different slit lamp filters*

This instrument was used to characterize the spectrum of the filters, described in section 1.8.4.1, characteristic of the slit lamp, obviously taking into account the halogen lamp illumination featured by the slit lamp. The spectral range defined in the spectrometer software was set from 300 to 1000 nm. Both the slit lamp potentiometer and the spectrometer's do integration time were set to avoid any form of saturation (fig 2.10).

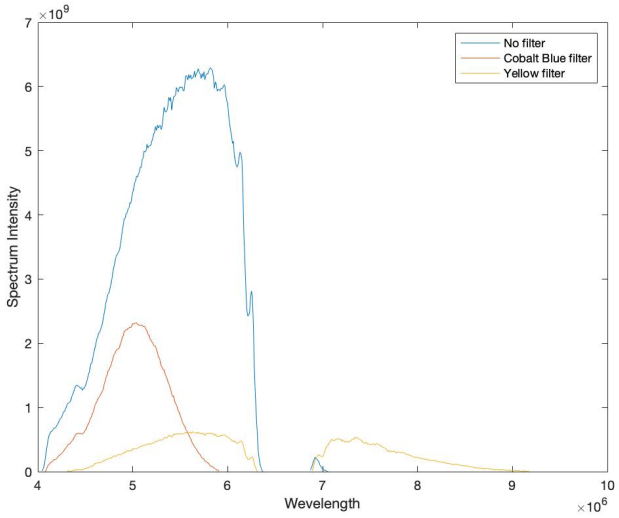


*Figure 2.10: Spectra acquired with the spectrometer*

## 2.5 HinaLea Hyperspectral camera

The second HSI instrument supplied for the current work by DIISM of the Università Politecnica delle Marche consists of The HinaLea® 4250 (serial number 637427), that it is sensitive to the spectral range between 400 and 1000 nm, with the possibility of acquiring 300 bands (fig 2.11) . This system represents a breakthrough in hyperspectral imaging, including the hardware and software needed to support a very wide range of applications. No mechanical scanning required due to patented Fabry-Pèrot interferometer technology.

This camera is composed of a tunable filter placed in front of the sensor that is able to sequentially select spectral bands and acquire for each of them the corresponding hyperspectral cube. The data sheet of this camera is shown in fig. 2.12.

Also in this case the acquisition system is controlled by a PC using HinaLEa's proprietary software, TrueScope Windows 10 Version 1.1.6, that allows:

- quick and easy hypercube acquisition of both the reference target and the test sample
- intuitive image classification and segmentation as part of a suite of powerful spectral image exploration tools
- storage and re-load

The illumination source used in this work is a LED lamp for the acquisition skin, and an halogen lamp for wound acquisition.

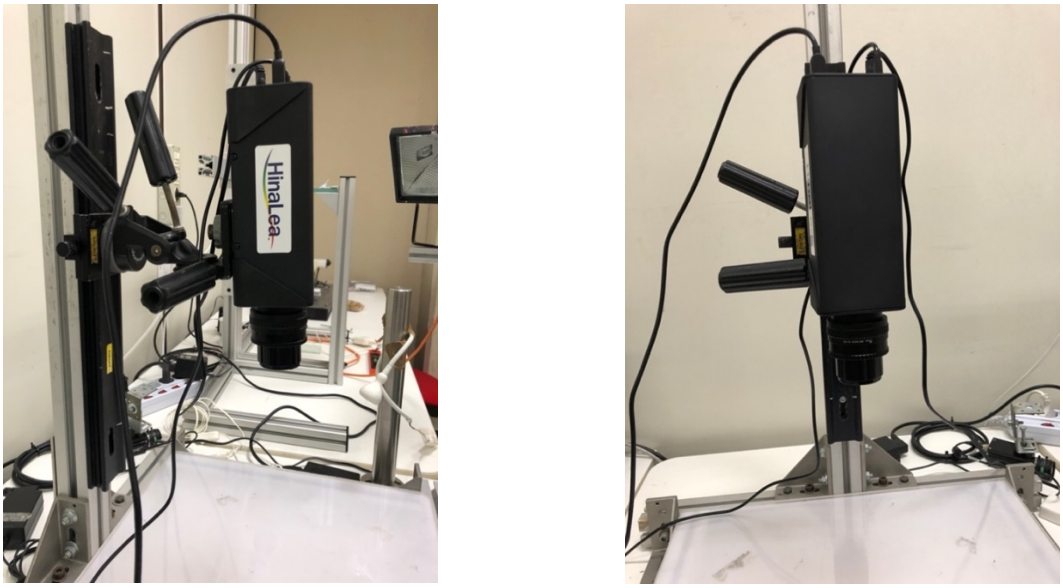


*Figure 2.11: HinaLea® 4250 Hyperspectral Camera*

| | |
|---|---|
| **Mechanical** | |
| **Dimensions (LxWxH)** | 197.7mm (7.78") x 81mm (3.19") x 78mm (3.07")<br>15° FOV lenses add 45.5mm (1.79") when focused at infinity (see below)<br>30° FOV lenses add 130.7mm (5.15") when focused at infinity (see below) |
| **Mass (Weight)** | 1.25 kg (2.75 lbs.) |
| **Electrical** | |
| **Input Voltage** | 110 VAC at 60Hz / 220 VAC at 50Hz |
| **Data Interfaces** | USB 2.0, 3.0 |
| **Environmental** | |
| **Operating Temperature** | 20°C ± 5°C |
| **Humidity** | 65% non-condensing |
| **Scan Performance** | |
| **Standard Lens** | 15° Field of View (FOV) – 150 mm to ∞<br>30° Field of View (FOV) – 150 mm to ∞ |
| **Sensor Spatial Resolution** | 2.3 MP+ |
| **Spectral Range** | 400 – 1,000 nm |
| **Spectral Bands** | 300 nominal |
| **Spectral Resolution** | 4 nm (FWHM) |
| **Dynamic Range** | User selectable 8 or 16 bit |
| **Spatial Resolution** | 2.3 MP with demosaicing |
| **Illumination** | Optional |

*Figure 2.12: HinaLea® 4250 Data Sheet*

### 2.5.1 HinaLea Hyperspectral camera calibration

The calibration phase must be carried out before the acquisition and subsequent management of the acquired data. Instrument calibration from a practical point of view in this hyperspectral camera was performed by acquiring two images.

- The first is the *black reference image (Di)*, which is acquired with the camera lens completely closed, with the aim of removing the effect of the dark current of the CCD.
- The second is the *white reference image* (*Wi*), captured using a reference standard given by the manufacturer of the machine.

After this calibration phase the raw hyperspectral image (*Roi*) is acquired and consequently the reflectance image (*Ri*) of the obtained image is calculated thanks to the following eq. (2.1):

$$Ri = \frac{\mathrm{Roi}-\mathrm{Di}}{\mathrm{Wi}-\mathrm{Di}} \tag{2.1}$$

The procedure described above is carried out using the appropriate software. In the same way as for the hyperspectral camera, data is stored in the form of both a tumbnail sequence and two files, data file and header file respectively. Finally the hyperspectral images are saved in reflectance format with the extension .hdr to be processed later in MATLAB environment.

## 2.6 Acquisition modes of the Senop HSC-2 Hyperspectral Camera

A univocal procedure has been defined for image acquisition in the hyperspectral camera Senop HSC-2:

1. *Position the slit lamp integrated to the hyperspectral camera* in order to frame the desired scene with an appropriate focus. This operation is done manually by first selecting the live button of the software relative to the hyperspectral camera and then observing the live image of the framed area on the PC

screen. If the region taken is not the one of interest, it is modified using the joystick of the slit lamp; if it is not correctly focused, it is improved by moving the slit lamp closer or further away.

2. *Position the white reference* of known reflectance signature in the framed area in order to obtain the flat field image.
3. In the *software* corresponding to the hyperspectral camera it is necessary both to define the wavelength range to be analyzed, obviously included between the range present in the machine (512nm and 900 nm), and the step with which the wavelengths are taken.
4. The software it is also necessary to define the exposure time that has to be used. The first way is simply to look at the illumination of the region of interest and if it is too bright you need to reduce the exposure time or lower the slit lamp potentiometer value. The second way that gives a more quantitative information is to analyze the shape of the histogram of the live scene (located in the bottom panel of the software) and see if it has high values in the final part, if there are high values you need to reduce it. A correct exposure time is essential to get the spectrum of the framed image without saturation.
5. Select the icon in the software that allows you to capture the image.
6. Wait for the taking *snapshot process.*
7. Click anywhere on the image to *see the spectrum*.
8. Save the obtained hyperspectral data cube with .hdr extension in order to export it in MATLAB environment.

This procedure was repeated for each sample that was analyzed, and the reference blank image was again recorded and saved whenever the slit lamp filter needed to be changed.

Specifically throughout this activity, the spectral range has always been chosen between 512 nanometers and 900 nanometers, and the number of wavelengths has been 500. The exposure time relative to the three filters of the slit lamp was varied to reach an optimal situation, and was set to:

- The slit lamp potentiometer was set to 1/4 and the exposure time in the relative software of the hyperspectral camera to 15 ms for the normal light without filter
- The slit lamp potentiometer was set to 1/2 and the exposure time in the relative software of the hyperspectral camera to 40 ms for the cobalt blue filter
- The slit lamp potentiometer was set to 1 and the exposure time in the relative software of the hyperspectral camera to 30 ms for the yellow filter

## 2.7 Acquisition modes of the HinaLea® 4250 Hyperspectral Camera

A unique procedure is also defined for the second hyperspectral camera HinaLea® 4250.

1. Prior to any operation, an *auto expose* was resorted to by pressing the appropriate button in the hyperspectral camera software.
2. Once the autoexposure is finished, it is proceed with the acquisition of *the dark reference image,* closing the lens of the camera and then with the *white reference image*, thanks to the appropriate white target given by the company of the hyperspectral camera. The calibration procedure is performed each time the software is switched on.
3. *Position the target* to be analyzed, choosing the desired range. The spectral range can be chosen between 400 nm and 1000 nm.

This hyperspectral camera was used to examine the skin, and for this reason a red filter was applied in the LED illumination system, with the ultimate aim of highlighting the wavelengths related to melanin, while for the wound acquisition is used an halogen lamp.

4. The acquisition of the image takes place through the relative button.
5. In the software the visualization of the spectra is made possible either:
    - selecting a specific area of interest using predefined geometric shapes such as rectangle or ellipse or drawing it manually
    - selecting a single point.

6. Save the obtained hyperspectral data cube with .hdr extension in order to export it in MATLAB environment.

## 2.8 Employed software

The data in this work were analyzed using a personal computer with cpu i5 6600k, 16 GB RAM and Windows 10 64 bit operating system, connected to the camera via Gigabit Ethernet connection.
Proprietary Senop HSC-2 and HinaLea® 4250 control software (True Scope) were used to program, write and load operation scripts onto the camera, and respectively this software are:
For the analysis and extraction of information and subsequent processing of the results was used the commercial software MATLAB_R2020b with Image Processing Toolbox.
Microsoft Excel, a spreadsheet of the Microsoft 365 suite developed and produced by Microsoft Corporation, was used for data storage and development of graphs derived from spectrometer measurements.

## 2.9 Samples used in hyperspectral analysis

This paragraph describes the samples that have been analyzed during this activity, taking into account that melanin is a pigment found not only in the skin, but also in the retina as reported in the first chapter. For this reason the first sample analyzed is a crystal, the alexandrite, characterized by spectral properties close to melanin and then it has been examined the content of this pigment in the skin. The wound acquisition, instead, is performed directly in vivo on the skin of an elderly person at the Torrette Hospital in Ancona.

### 2.9.1 Alexandrite sample

In the retina, especially in the retinal pigmented epithelium, as reported in paragraph [1.8], the substances involved in fluorescence are lipofuscin and melanin. In particular, in the course of this activity it has been initially tried to simulate the fluorescent attitude of melanin by means of a substance characterized by a similar behavior to avoid direct exposure of retinal tissue to light intensity as we did not have the technical and medical competence suitable. Melanin is produced by melanocytes via ribosomes in the rough endoplasmic reticulum and the Golgi apparatus. The melanosome is generated after several stages from the premelanosome vesicles. Melanin absorbs both ultraviolet and visible, increasing linearly from 800 nm to 400 nm (fig 2.13).

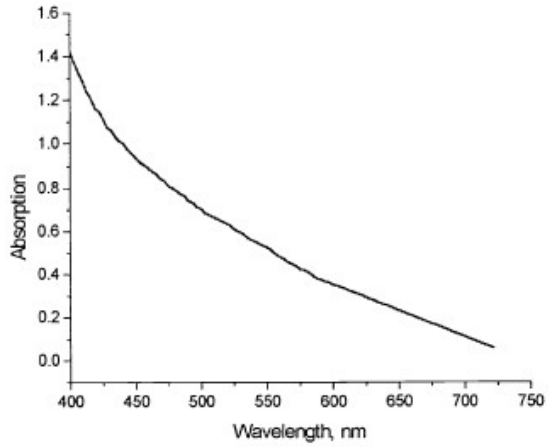


*Figure 2.13: Absorption spectrum of Melanin*

Alexandrite is a natural mineral with the property of changing color depending on the brightness of light, in fact this stone belongs to the anisotropic crystals with the characteristic that can change their color the black rays of light that pass through it with respect to the optical axes. In the presence of light this mineral is colored with shades of verse, in the evening it takes on shades of purple. This crystal is characterized by low symmetry and strong birefringence that allows for linear polarized emission without significant loss of depolarization. The absorption range of this crystal is included in the spectral range of 380-630 nm with characteristic

peaks at 410 nm and 590 nm, while it is characterized by emission in the range of 700 nm to 860 nm, with the main peak at 755 nm (fig. 2.14) [81]. During the activity a piece of alexandrite crystal present in the SIMAU department of the Università Politecnica delle Marche was used. The alexandrite crystal used was inserted into the cavity of the mask built for the insertion of the Spectralon, and has been held steady thanks to some pongo stuck in the back of the sample.

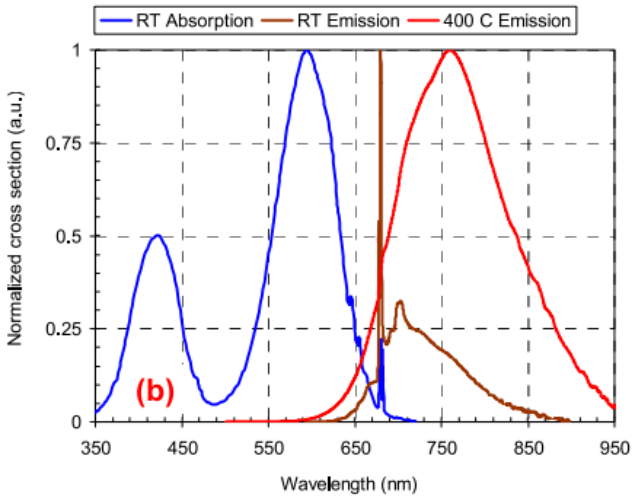


*Figure 2.14: Absorption and Emission spectrum of Alexandrite*

### 2.9.2 Skin sample

The skin study, was initially conducted via the Senop HSC-2 hyperspectral camera integrated with the slit lamp, with the aim of investigating how melanin content, both in the absorption and emission wavelengths, differed between a light and dark skinned person. In the slit lamp was employed the yellow filter because it is characterized by a spectral content that extends throughout the range of interest. Subsequently, a portion of skin characterized by a mole was examined using the HinaLea 4250 hyperspectral camera mounted on a special stand.

Since the camera must necessarily be at least 15 centimeters away from the sample under examination and since no substantial spectral differences were found between the mole and the skin, both lenses provided by the HinaLea company were

used with the ultimate goal of having better discrimination. It was subsequently demonstrated that the images obtained were specular.

### 2.9.3 Wound healing sample

The study on wounds was conducted at the Torrette Hospital of Ancona, in collaboration with Dr. Alessandro Scalise, specialist in plastic, aesthetic and repair surgery.

In particular, in the course of this work, a wound was examined, both in the initial stage and in the final stage of healing, caused by a vascular ulcer. The wound has been treated by the doctor with advanced techniques, in particular using the Aquacel medical device, consisting of Hydrofiber with silver, in which the fibers that compose it, in contact with the wound, adapt to the surface expanding and creating, consequently, a cohesive and strong gel structure [82]. This texture has a dual function, the first is to adhere to the wound eliminating the possibility of creating areas where bacteria can proliferate and the second is to retain and store the exudate, produced by the body as a result of the inflammatory process, without the chance of further migration [82].

In particular, in the work of this thesis, the variation of the spectral content of the wound and its healing process compared to healthy skin was analyzed using the HinaLea 4250 hyperspectral camera, operating in the range between 400 nm and 1000 nm and acquiring 300 wavelengths. Before performing the acquisitions on the patient, the white calibration procedure was performed with a halogen source, whose spectrum is shown in fig. 2.15, also used for the succession analysis of the lesions. Subsequently, both the halogen lamp and the hyperspectral camera, mounted on the two tripods, were positioned with the aim of framing and illuminating the desired scene. The patient appropriately lying on the couch, initially was in supine position, for the acquisition of the lesion healed in the left leg, fig. 2.16, left, then was turned on its side for the lesion present in the right leg, fig. 2.16, right.

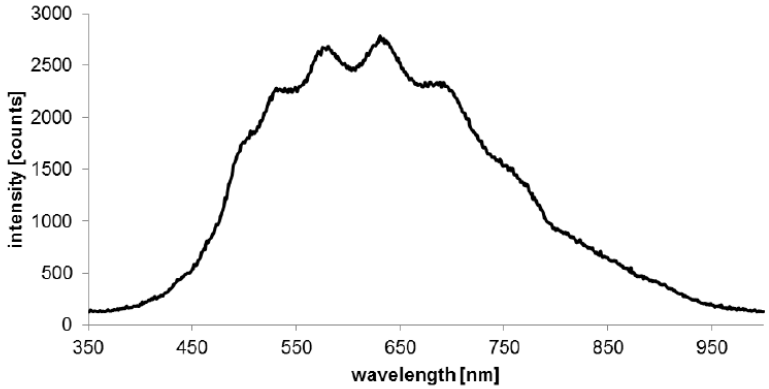


*Figure 2.15: Halogen Lamp spectrum*

*Figure 2.16: Photos of the healed wound (left), and the wound (right)*

In fig. 2.17, the analyzed lesion is shown, where it is possible to see different regions that have been analyzed from the spectral point of view:

- the  red rectangle represents the wound, dark in color, which occupies a very large portion of the skin
- the green rectangle, above the lesion, indicates the area with blood
- the green rectangle indexes the portion of skin where the healing process is taking place in an advanced stage
- the blue rectangle denotes the healthy skin

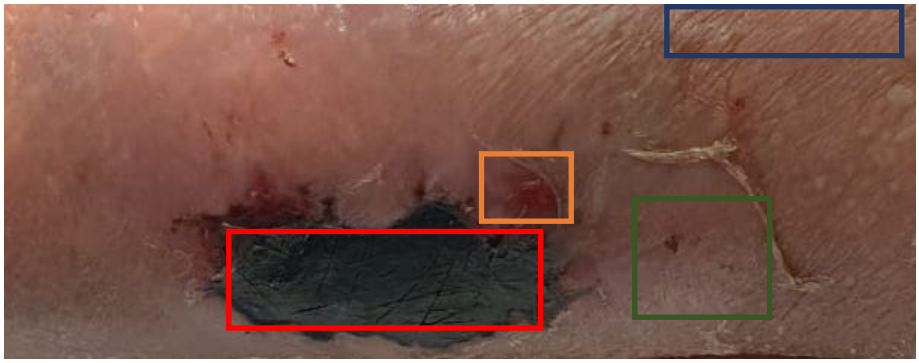

*Figure 2.17: Magnification of the lesion where four zones have been extracted: red indicates the wound, the orange indicates the skin with blood, the blue the healthy skin, the green the healed wound*

## 2.10 Data processing in MATLAB

After the acquisition of the hyperspectral data cube with the software related to the camera used, it was necessary to define a unique procedure for processing them once exported to the MATLAB environment. Initially, work was done on the alexandrite and then on the skin and the wound:

i. Hypercube of data saved in .hdr format was opened in MATLAB using the function read_envihdr
ii. The first step was to obtain the relative spectrum of the Spectralon and of the sample under examination. In both cases a restricted region was first selected with respect to the total one with the ultimate aim of not including those components which did not belong to the area of interest and thus having a characteristic and specific spectrum of the Spectralon and/or the sample.
iii. The spectrum was obtained by summing the value of all the pixels of the cube for each wavelength, then normalized for the size of the cube.
iv. Since the software of the Senop camera does not determine the reflectance of the image as a function of the Spectralon it becomes necessary in these data to normalize them with respect to the Spectralon acquired with the same type of illumination. Since very often the exposure time of the sample and the

Spectralon were not equal, the normalization was then multiplied by the ratio between the exposure time of the Spectral and the sample.

v. Subsequently we went to work on the real images with the ultimate goal of ensuring the user both a higher quality of the latter and the possible features. This was done through the generation of different masks:

    i. The first type of mask was initially obtained by choosing from the histogram (histogram function of MATLAB) of the sample image the discriminatory value (coinciding with the first peak), then used as a threshold for the mask. All pixels of the hyperspectral cube greater than the threshold were set equal to 1 and the others equal to 0.

    ii. The subsequent masks were obtained to improve the previous one, for example by removing all the imperfections present in the first mask using a median filter. This was accomplished by:

        1. Initially the points that had no value and generated white points in the image were removed and replaced with a value coinciding with 0 .This was accomplished thanks to MATLAB's isnan function which returns a vector of equal size to the original one by assigning a value coincident with 1 to all those values without value.
        2. The median filter performs a non-linear operation on the pixels belonging to the mask: the values are sorted and then the value that is in the middle position of the sorting (median value) is calculated. This filter can very effectively remove impulsive salt-and-pepper noise, a noise characterized by some pixels in the image becoming white or black. In particular the function medfilt2(I) of MATLAB was used, which performs exactly a median filtering in the two-dimensional image. In output of this function each output pixel contains the median value in a n for n around the corresponding pixel

in the input image. In order to obtain the optimal value of n different tests have been performed.

3. The last type of mask allows the selection of a specific area of interest (the ROI), more or less large. The area can be chosen directly by the user by selecting three points that generate a circle (using the fit_circle_through_3_points function). Then the mask is generated by setting equal to 1 all those points whose difference between their position and the center of the circle is less than the radius of the circle and 0 all others.

iii. The histograms for the three masks were also subsequently reported in a single window. And since both were characterized by a first peak coinciding with the value 0, this value was removed and it went to see how the second and third mask were similar among themselves.

vi. Subsequently always working with the hyperspectral image obtained was performed the ratio between bands, calculating consequently the image of the scene acquired as a ratio between the acquisition two different wavelengths. This operation allows to obtain images that have the advantage of suppressing the effects of non-uniform illumination, of patterns present in the substrate. During the activity we tried to identify which image could be better both from a visual and computational point of view and therefore operational. The image obtained from the ratio of the bands was initially performed as a ratio between the wavelength of emission (680 nm) compared to those of absorption of the sample (550 nm). Subsequently, other tests were performed both obtaining the image between other wavelengths close to those previously mentioned and selecting spectral ranges around emission and absorption to see if better results could be obtained.

Regarding skin acquisitions with Senop HSC-2 initially, spectral analysis of the samples taken into consideration was performed, obtaining both relative spectra and normalized spectra with the reference white image. Subsequently it has been gone to select the ROI of interest from the image of the sample, and then execute all the

steps previously mentioned. For the captures, by employing the HinaLea hyperspectral camera both for skin and wound acquisition, the spectral analysis of samples were investigated in the wavelengths at the wavelengths of interest.

# CHAPTER 3 RESULTS

## 3.1 Introduction

This chapter reports the results obtained from the use of the Senop HSC and HinaLea 4250 hyperspectral chambers in the VIS and NIR wavelengths, in the case of the samples presented in section 2.9.

## 3.2 Alexandrite acquisition Results

Fig. 3.1, left and right, show, respectively, Spectron's acquired with the blue and yellow slit lamp filters that were employed as target images during this activity. The first Spectralon was used as a reference for alexandrite, while the second was taken for skin. The figures indicate the area that was selected in MATLAB environment in order to have characteristic spectrum without the acquisition of points of no interest.

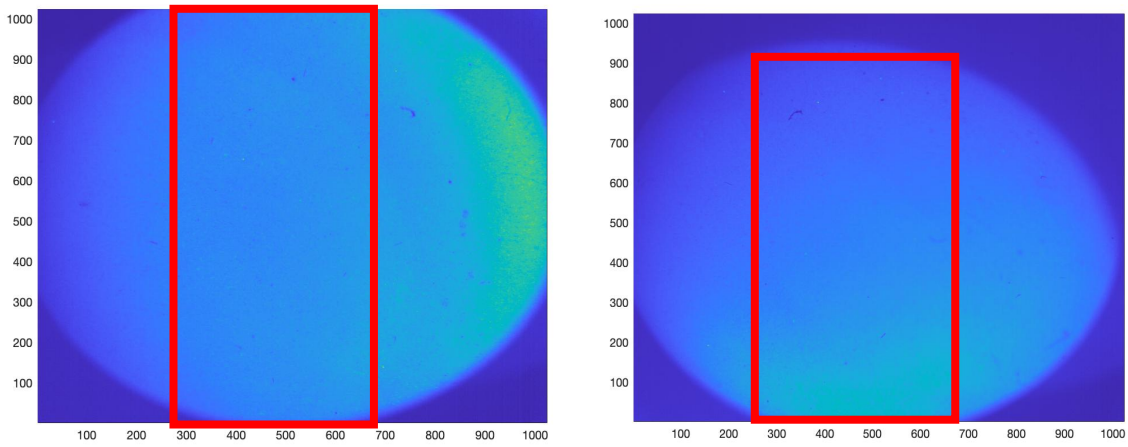


*Figure 3.1: ROI of the blue filter (left) and yellow filter (right)*

The resultant hyperspectral cubes for the Spectralon acquired with the blue filter is 301x900x500, while the second obtained with the yellow filter is 401x900x500.
The alexandrite was acquired with an exposure time of 25 ms and the potentiometer coincident with the value of 1.
Fig. 3.2 shows in the right part the reflectance alexandrite spectrum and the subsequent normalization, in the left side, performed in relation to the white

reference image obtained using the blue filter of the slit lamp. From the right figure it can be seen that contrary to the literature, the characteristic peak of the alexandrite is not at 755 nm, but at 680 nm. From the left image it can be observed that since the blue filter is devoid of spectral content after 644 nm, the characteristic range of alexandrite (650 nm-750 nm) is identified by an high spectral component that decreases after 800 nm.

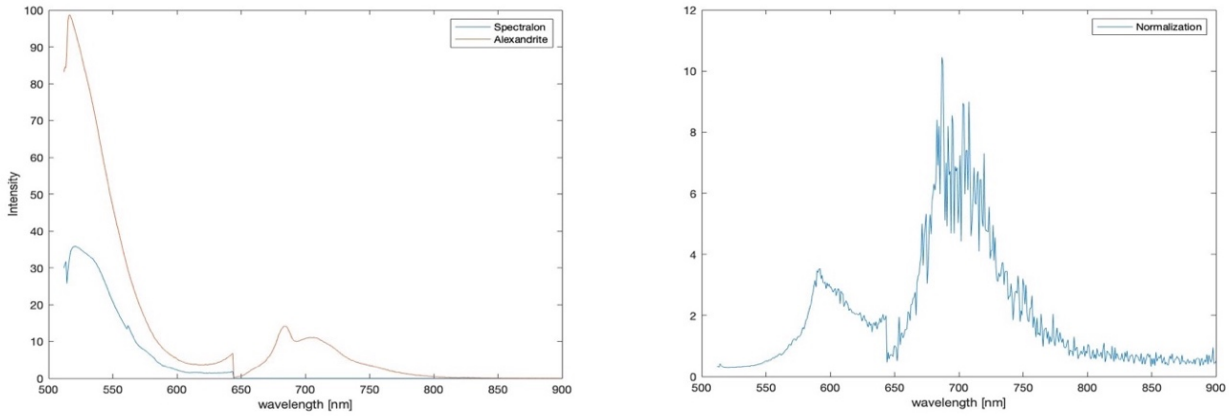


*Figure 3.2: Alexandrite spectrum (left), and its respective normalization (right)*

Fig. 3.3 shows, in the right side, the alexandrite image acquired at the absorption wavelength coincident with the 550 nm, from which the respective histogram was obtained as it can be possible to seen in the right side. Subsequently for the determination of the primary mask, the characteristic value of the first peak was extracted from the histogram, with a value of is $0.4*10^4$. The mask obtained is reported in fig. 3.4.

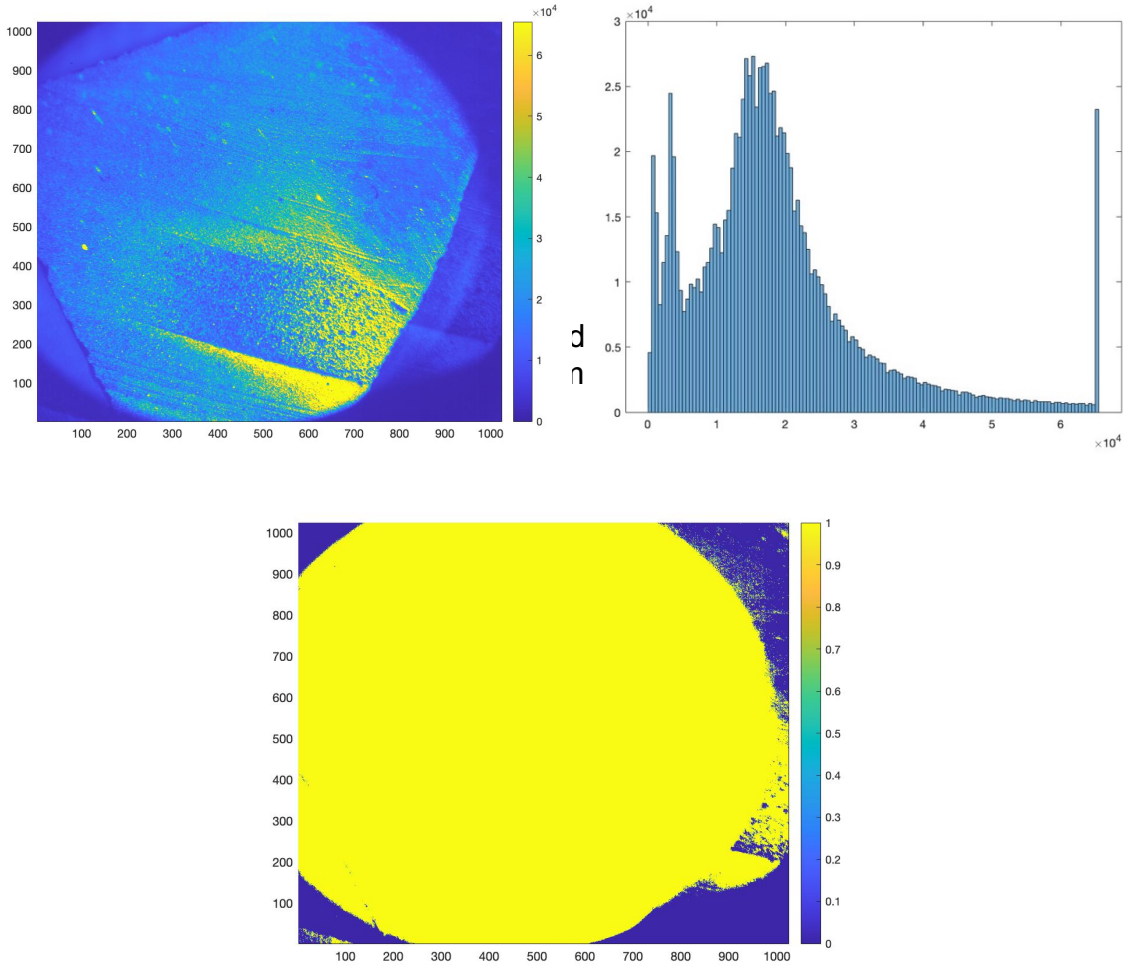


*Figure 3.4: First mask of Alexandrite*

It is possible to observe from fig. 3.4 the functionality of the mask is lost in the borders of the sample under examination and consequently a clear and good quality image is not obtained. Below, in fig. 3. 5, are reported some attempts to improve the mask by applying median filters where the number of points averaged between them is increased in order to have a mask of good quality: 2, 3, 7, 9.

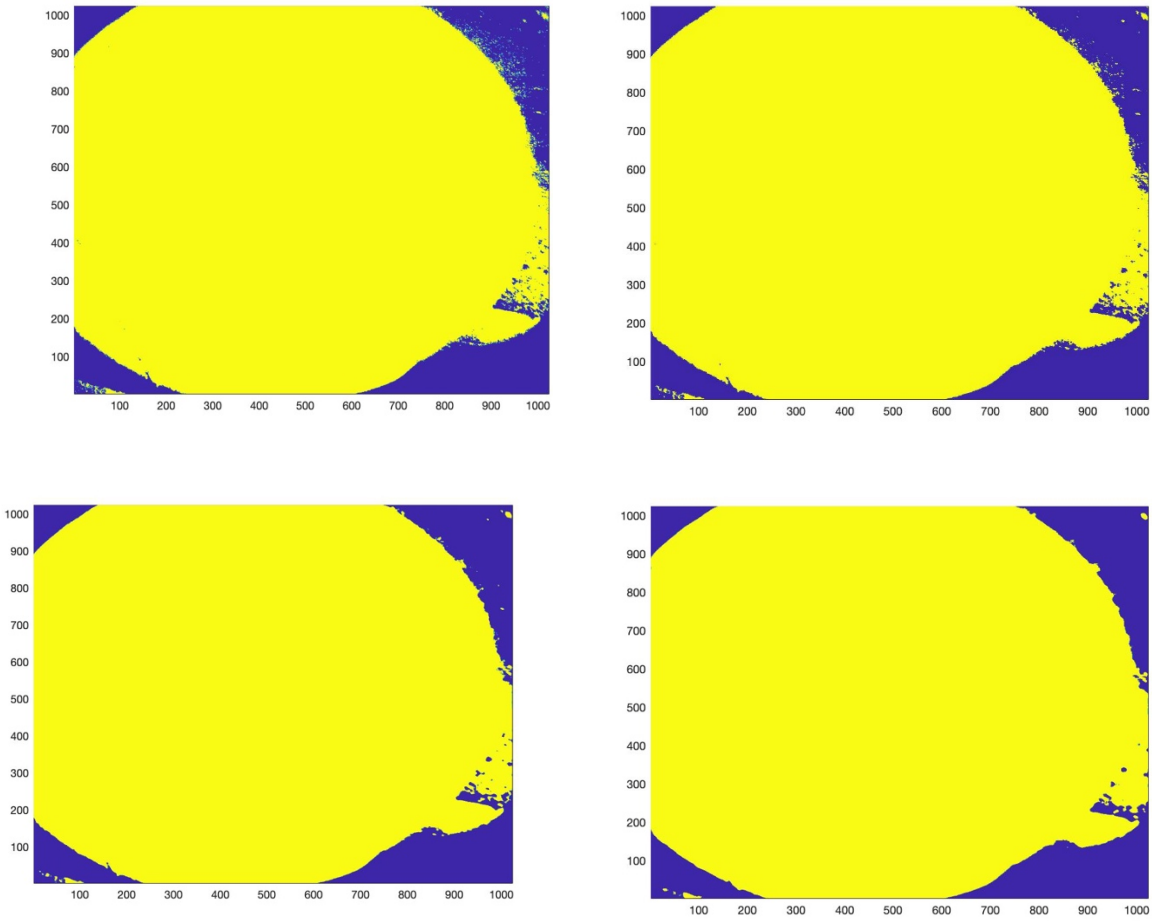


*Figure 3.5: Alexandrite image trough the median filter with 2 (left top), 3 (right top), 7 (left bottom), 9 (right bottom)*

The coming mask was developed with the ultimate purpose of investigating a specific area of interest. Fig. 3.6 shows, starting from the mask obtained previously, the image in shades of gray. In particular through the selection of three points that delimit a specific area, the relative mask is obtained (fig. 3.7 left). The right side of the fig. 3.7 shows in a single window the three masks achieved, the last mask present in the rightmost side, is obviously characterized by higher accuracy and precision.

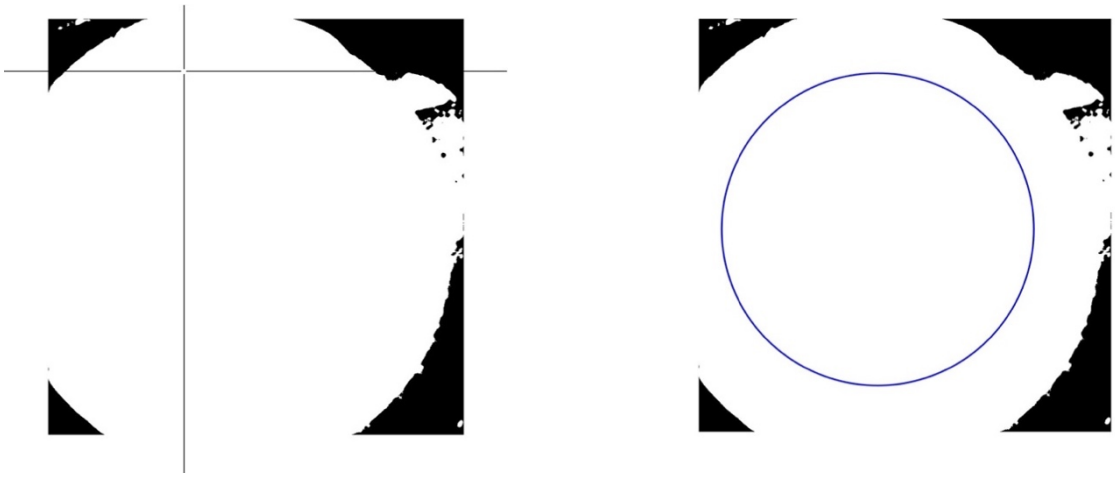

*Figure 3.6: Alexandrite image in gray shadow (left), and the selection of three points (right)*

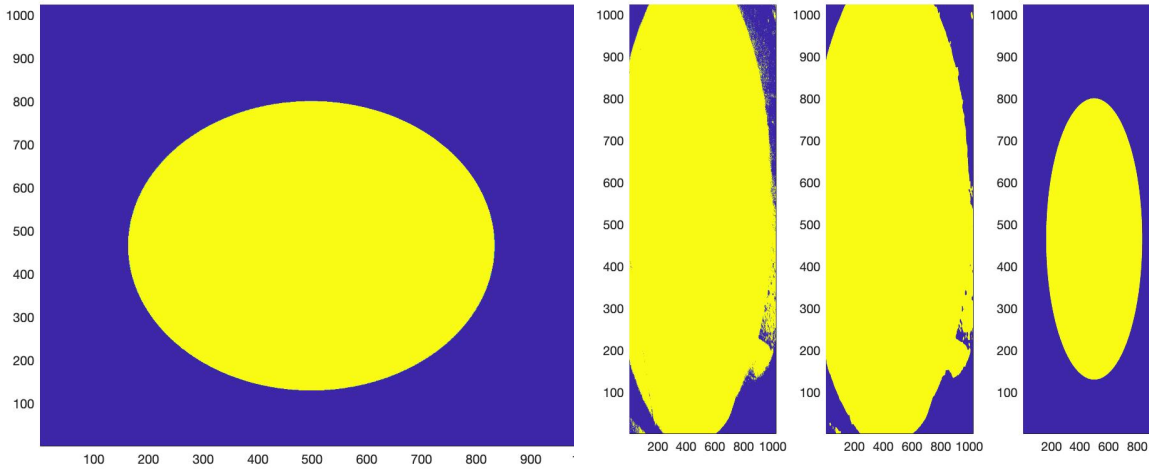


*Figure 3.7: Mask of the Alexandrite by selecting three points (left), and the three successive mask (right)*

The creation of the three masks was then applied to the image of the alexandrite obtained from the ratio between the emission (680 nm) and absorption (550 nm) wavelengths. Fig. 3.8 represents the sample under examination, and it is possible to note, the presence of white dots especially in the top and bottom boards of the image, resulting from the absence of value between the ratios of wavelengths. The points once corrected in MATLAB environment led to an image of good quality without imperfections.

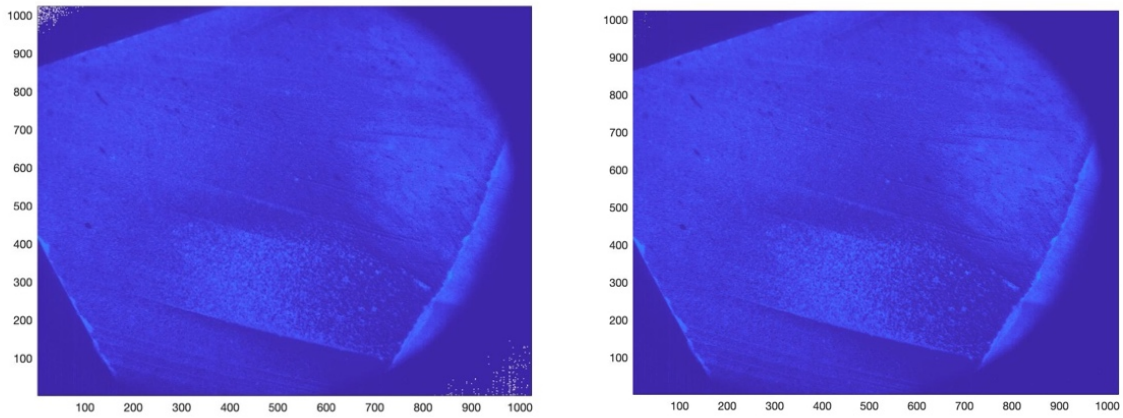


*Figure 3.8: Alexandrite image without correction (left), and with correction (right)*

It is evident from fig. 3.9 that through the application of masks the image undergoes a gradual improvement in both accuracy and contrast. Fig. 3.10 shows the histograms of the previously reported image, and it is possible to observe that when the peak at value 0 is removed, the histograms of the sample taken with the median filter and the round filter are very similar to each other (fig 3.11).

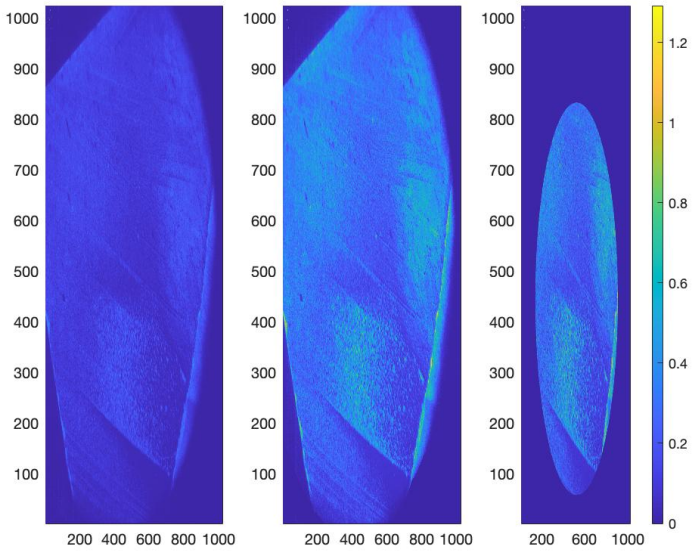


*Figure 3.9: Alexandrite masks*

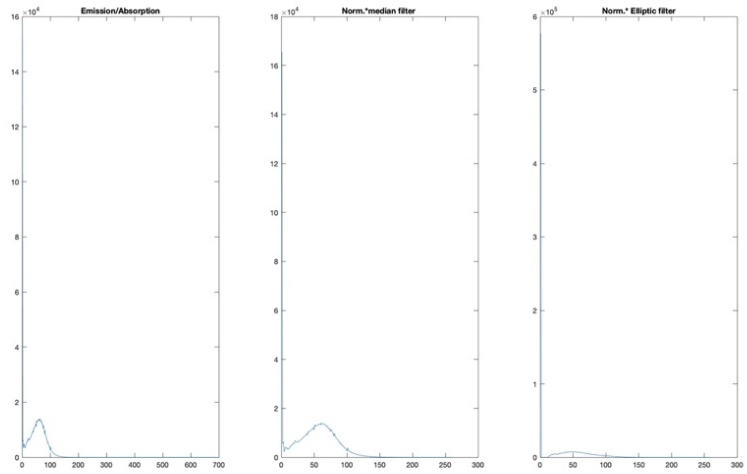


*Figure 3.10: Alexandrite histogram*

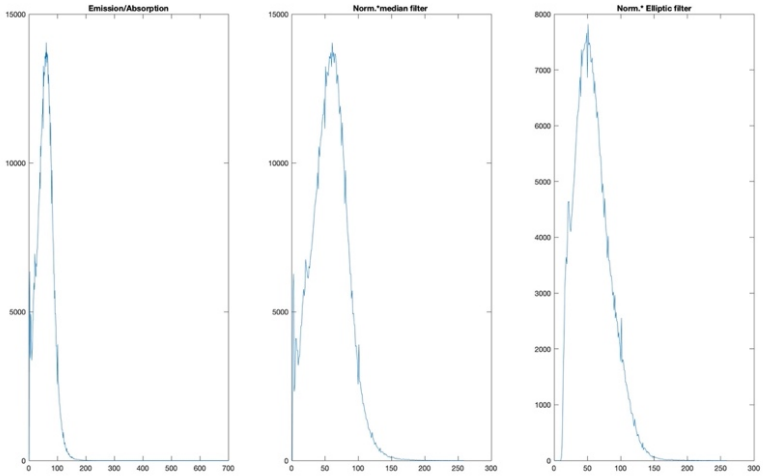


*Figure 3.11: Alexandrite mask without zero value*

The last step taken in image processing is illustrated in fig. 3.12, which in a single window shows the alexandrite at emission wavelength, absorption wavelength, and that obtained as a ratio of the reference emission wavelength (680 nm) and absorption wavelength (550 nm), respectively. Fig. 3.13, left side, shows the images obtained as a result of the ratio between the values near the emission and absorption wavelengths, respectively:

- 683 / 553 nm
- 677 / 547 nm
- 667 / 537 nm

Fig. 3.13, right side, illustrates the second attempt to increase image quality by reporting the relationship between the emission and absorption bands, respectively:

- A range of twenty wavelengths centered on the reference wavelengths
- A range of ten wavelengths before the reference wavelengths
- A range of thirty wavelengths before the reference wavelengths
- A range of thirty wavelengths following the reference wavelengths.

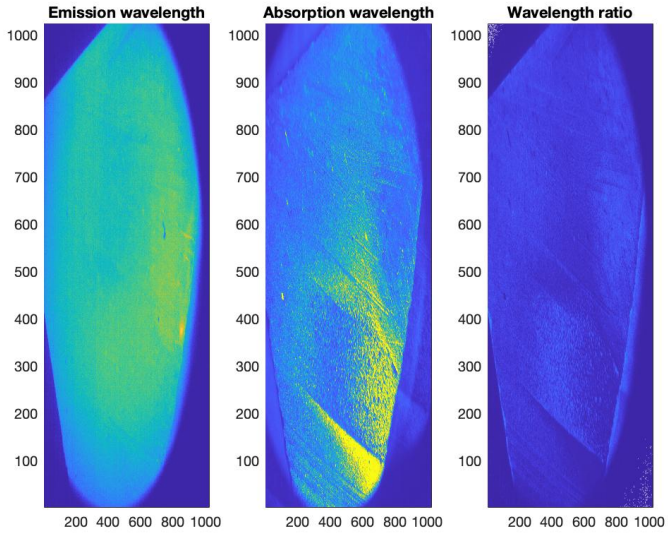


*Figure 3.12: Alexandrite acquisition at emission, absorption, and ratio wavelength*

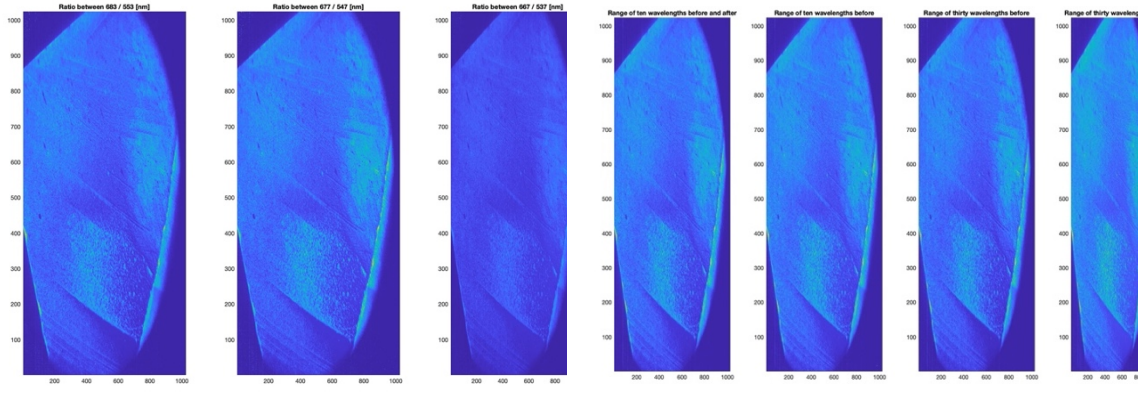

*Figure 3.13: Different attempts to obtain a good contrast image*

## 3.3 Skin acquisition results with Senop HSC-2 Camera

Fig. 3.14, left, shows the reflectance spectra obtained on both light and dark skin. The features used for the acquisition are:

- Slit lamp: yellow filter
- Exposure time: 50 ms
- Potentiometer intensity: 1

Fig. 3.14, right, represents the normalization of the different skins with respect to the reference target obtained using the yellow slit lamp filter.

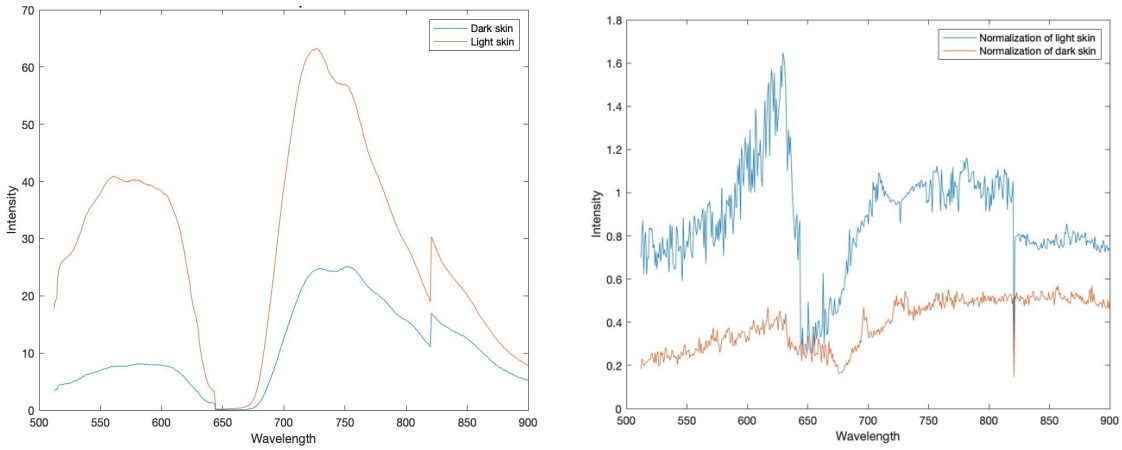


*Figure 3.14: Skin Spectrum (left) and normalization (right)*

It is easily observable that the content of melanin is characterized by a greater absorption in the case of dark skin than in the case of light skin, in fact the reflectance spectrum is characterized by a lower intensity. The same phenomenon was also found in the following wavelengths. This result must be related to the fact that in wavelengths towards 500 nm, besides melanin, other substances with a higher quantum content are excited, as reported in paragraph 1.9.

Fig. 3.15 shows the light skin acquisition at the absorption wavelength (550 nm), in which the ROI of interest, coincident with the mole, was selected (34x60x500). Fig. 3.16. left and right, shows the spectrum of the skin and mole, respectively, and the subsequent normalization with respect to the Spectralon acquired using the yellow filter of the slit lamp. The figure for the spectrum of the mole shows greater

absorption in the region between 550nm and 650nm, and higher emission from 720 nm than the surrounding skin.

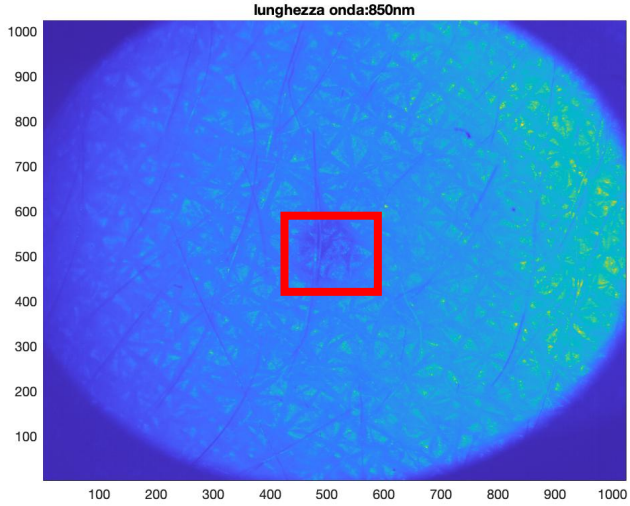


*Figure 3.15: Skin acquisition*

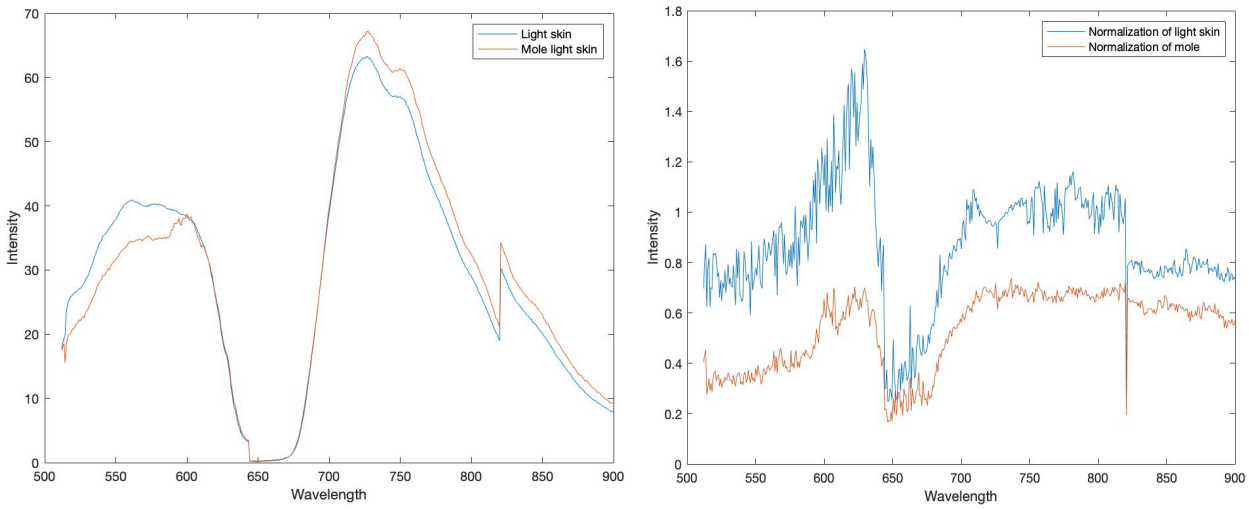


*Figure 3.16 :Spectrum of mole and skin (left), and the successive normalization (right)*

Fig. 3.17 illustrates the image of the skin with the presence of the mole with the application of the three previously described mask obtained through the histogram value. Also in this case, as done previously, the selection of three points gives rise to the generation of the last mask.

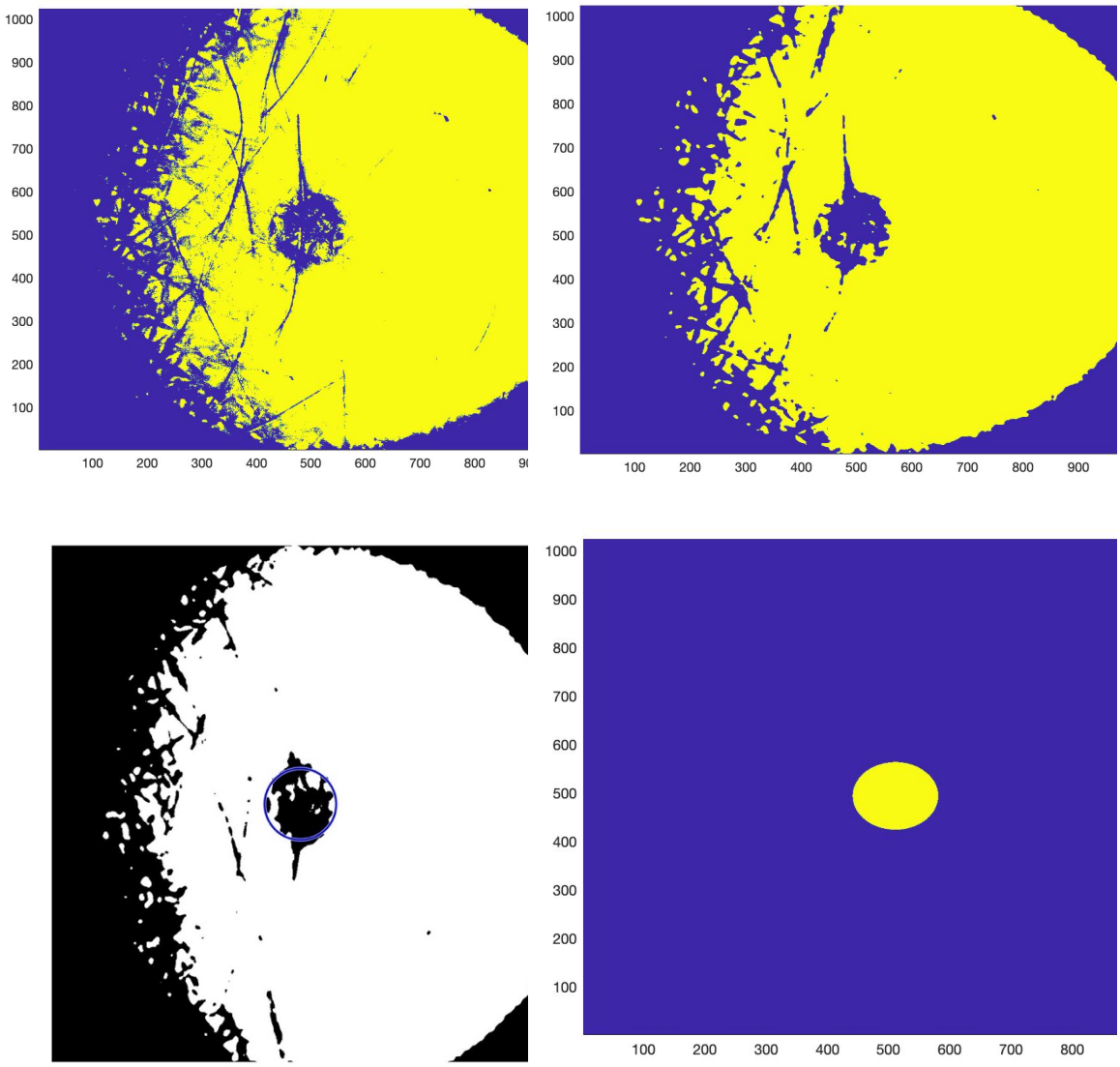


*Figure 3.17 : Generation of the mask on the skin*

Fig. 3.18 shows the skin at the emission wavelength of melanin, in which, according to the theory, the mole should have emerged compared to the surrounding skin because it is characterized by a higher content of this substance. This instead is not confirmed, in fact it is found that the mole assumes a behavior similar to that of the skin. Possible explanations for this can be attributed either to the phenomena of reflection and diffusion, or otherwise to the possible composition of the mole and its small size, and finally, it is attributed to the presence of many other substances with a quantum range greater than melanin. It could be useful to analyze and excite the skin at higher wavelengths such as 780 nm.

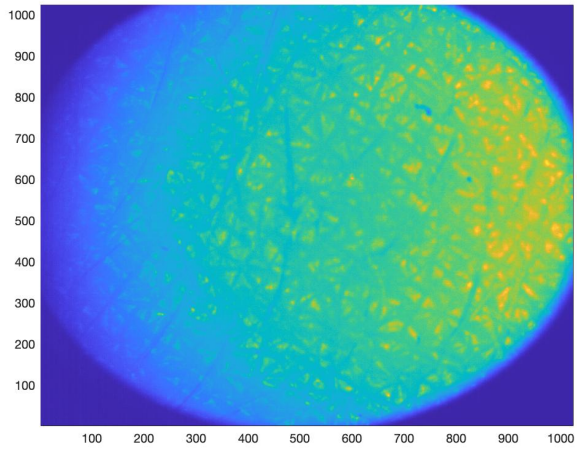


*Figure 3.18: Skin and mole at emission wavelength*

## 3.4 Skin acquisition results with HinaLea Camera

Fig. 3.19 reports the acquisition of a portion of skin with the presence of the mole with the HinaLea hyperspectral camera, in combination with an LED lamp to which a red filter was applied (fig 3.20).

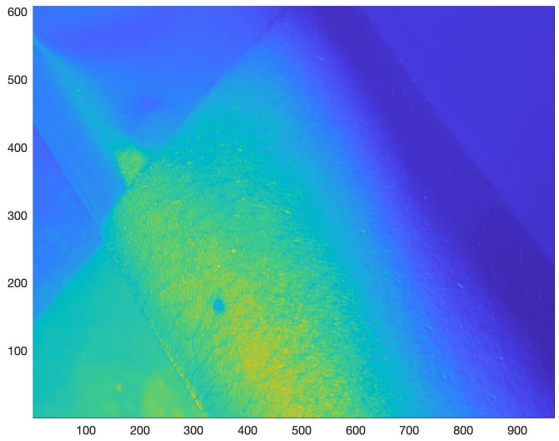


*Figure 3.19: Skin acquisition*

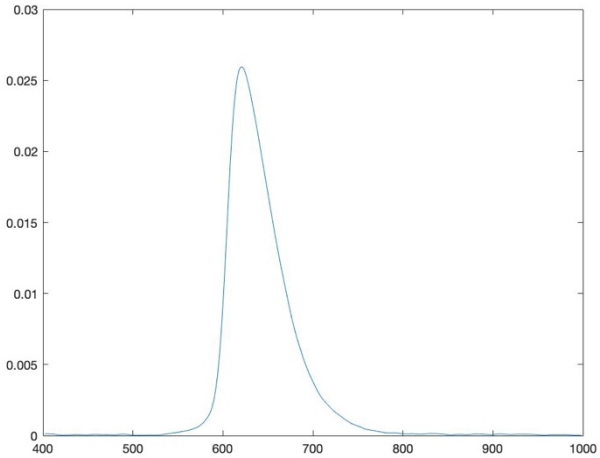


*Figure 3.20: Red filter*

Fig. 3.21, left, shows the average reflectance spectrum of the skin and mole, and subsequent normalization with the red filter in the right. For better analysis, the spectra of each individual pixel of the mole ROI (10 pixels x 7 pixels x 400 wavelengths) are shown in fig 3.22.

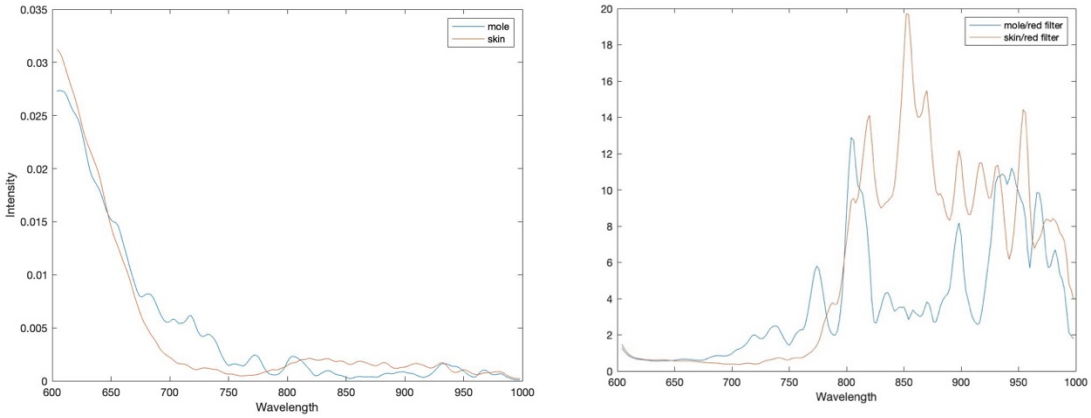


*Figure 3.21: Mole and skin spectrum (left), and normalization (right)*

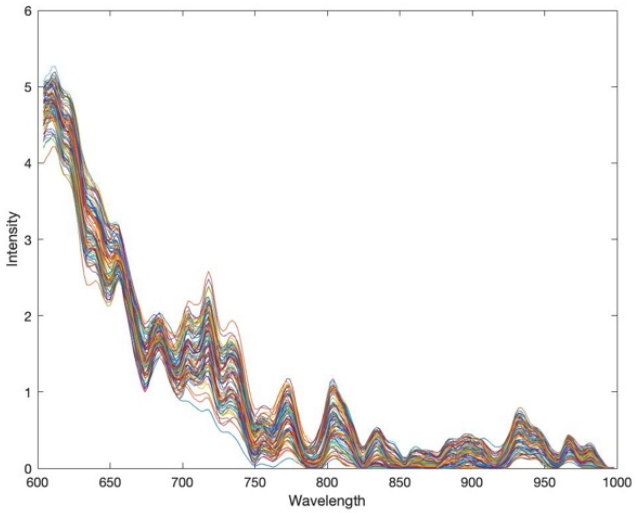


*Figure 3.22: Mole spectrum pixel for pixel*

At this point it went to see from a visual point of view, as was done with the previous hyperspectral camera, if the mole, at a wavelength of 750 nm, emerged from the surrounding skin characterized by a lower spectral content. As illustrated, from fig. 3.23, this does not happen, and this phenomenon can be attributed either to the texture of the skin, or to the direction of illumination.

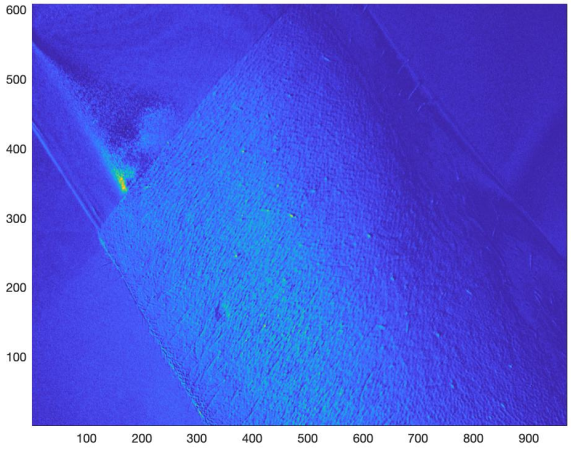


*Figure 3.23: Skin and mole acquisition at 750 nm*

In this case the main limitation of the hyperspectral camera is given by the fact that for a correct focusing of the sample under examination, it is necessary to position it at a minimum distance of 15 cm.

## 3.5 Eye acquisition results "in vivo"

This part reports the findings of the eye, appropriately dilated with eye drops, of the anterior segment, in particularly the cornea.

For a faster acquisition of the scene in vivo, without causing any kind of damage to the examined eye, the spectral range of the camera between 512 nm and 800 nm was divided into 30 spectral lines, with the aim of having at the same time both a rapid acquisition and information with a sufficient information content. Neither the yellow or the blue filter, but only the normal light filter of the slit lamp was used during the course of this examination.

Fig. 3.24 shows the cornea, on the left is reported the image obtained from the integrated camera of the slit lamp, while on the right is depicted the same image achieved in MATLAB, without any processing, at a wavelength of 613 nm.

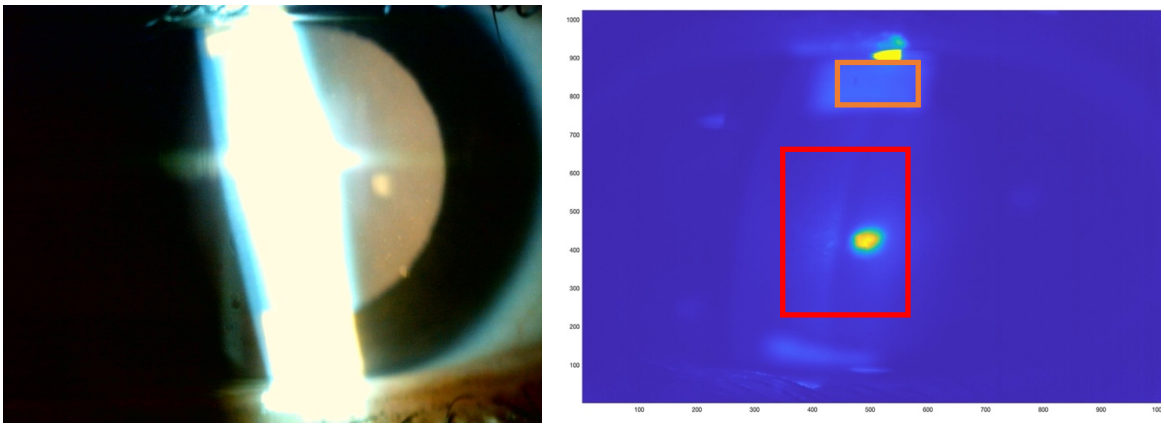

*Figure 3.24: Eye image acquired with the camera (left), and hyperspectral camera (right)*

Regarding the spectral study of the eye, from fig. 3.24 (right), two different regions were successively extracted. The first extrapolated corresponds to the iris (orange rectangle), the area above the white colored cornea, while the second is the cornea itself (red rectangle). As shown in fig. 3.25, it was possible to obtain both the spectrum of the anterior segment (right) and the posterior segment (left). This means, that even omitting the use of the lenses used by the specialist for the

visualization of the posterior segment of the eye, this camera is able to provide a spectral analysis of it.

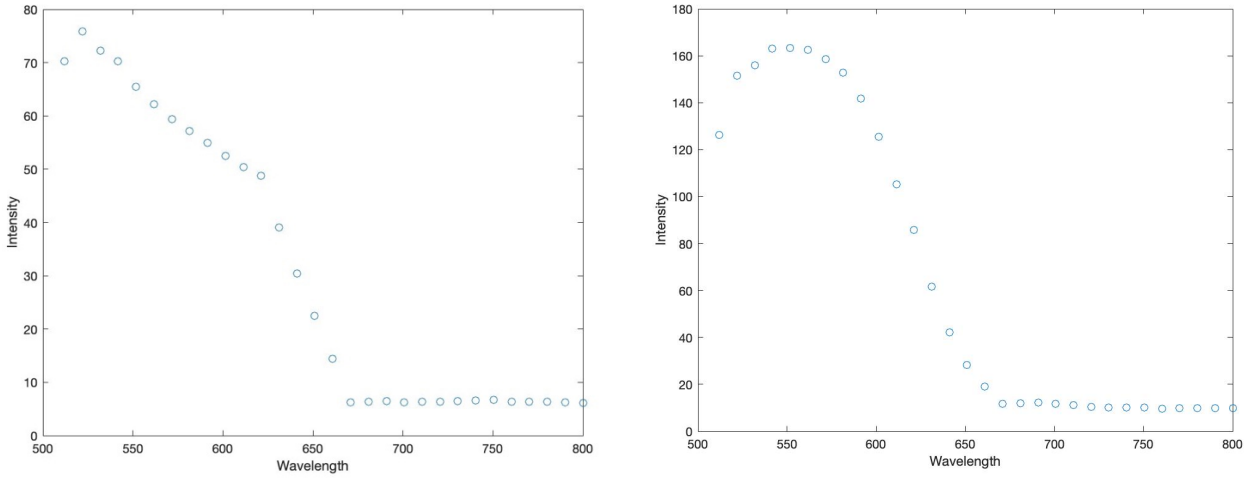


*Figure 3.25: Irid spectrum (left), cornea spectrum (right)*

## 3.6 Wound healing acquisition results "in vivo"

Fig. 3.26, on the left, shows the photo of the healed wound, while on the right it is possible to observe the image in MATLAB, extracted at a wavelength of 502 nm. The image on the left, does not show marked differences between the healthy skin and the healed wound, there is only a slightly darker region in the central area.

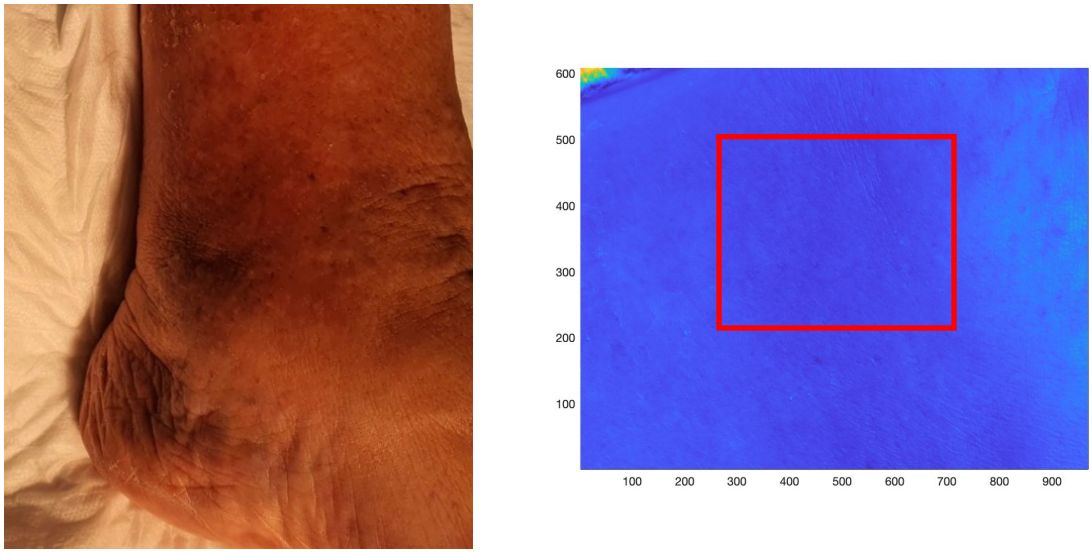


*Figure 3.26: Photos of the healed wound (left), and its implementation in MATLAB (right)*

Fig. 3.27, on the left, in the same way as the previous acquisition, shows the photo of the healed wound, while on the right the image in MATLAB extracted at a wavelength of 620 nm. In this case the red arrow indicates the portion of skin with the wound, the orange arrow the section with blood, the green arrow the healed wound and finally the blue arrow points to the section of healthy skin.

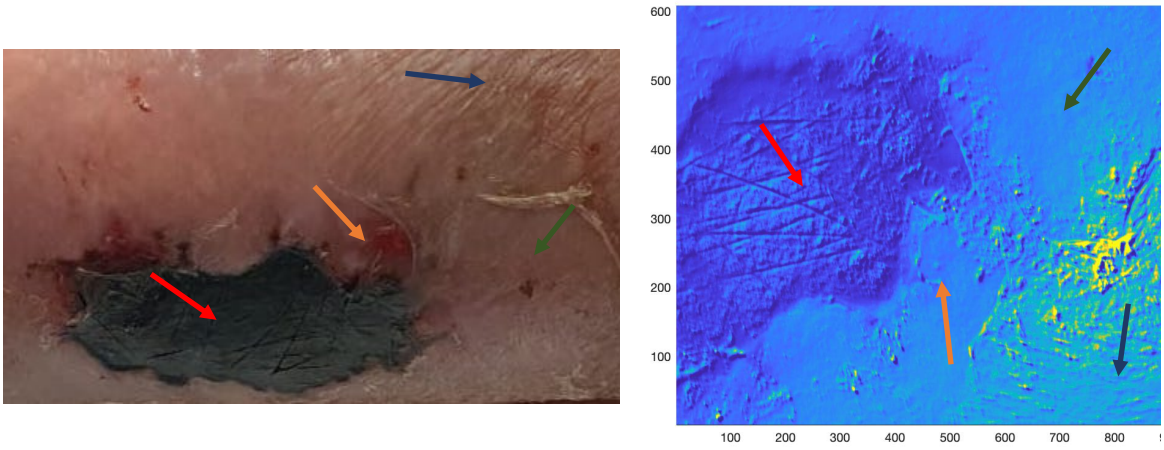


*Figure 3.27: Photos of the wound (left), and its implementation in MATLAB (right). The red row indicates the wound, the orange row points towards blood zone, blue row refers to the healthy skin, and the green row indicates the healed wound*

Before performing the spectral processing of the data in MATLAB, in the True Scope software a segmentation procedure was executed thanks to the classification option which, taking into consideration all the wavelengths, clusters those portions of skin with similar features, both for fig. 3.26 and fig. 3.27. If in the first case it is obtained an image that appropriately classifies the healed wound from the surrounding healthy skin (fig. 3. 28, top) , in the second case (fig 3.28, bottom) , probably due to the presence of shadows, of not perfectly smooth surface of skin (fig. 3.27, left), of not uniform illumination at the moment of the acquisition and finally of high number of classes defined in input to the function, it is obtained a result not perfectly analogous and traceable to the data of the image subsequently elaborated in MATLAB.

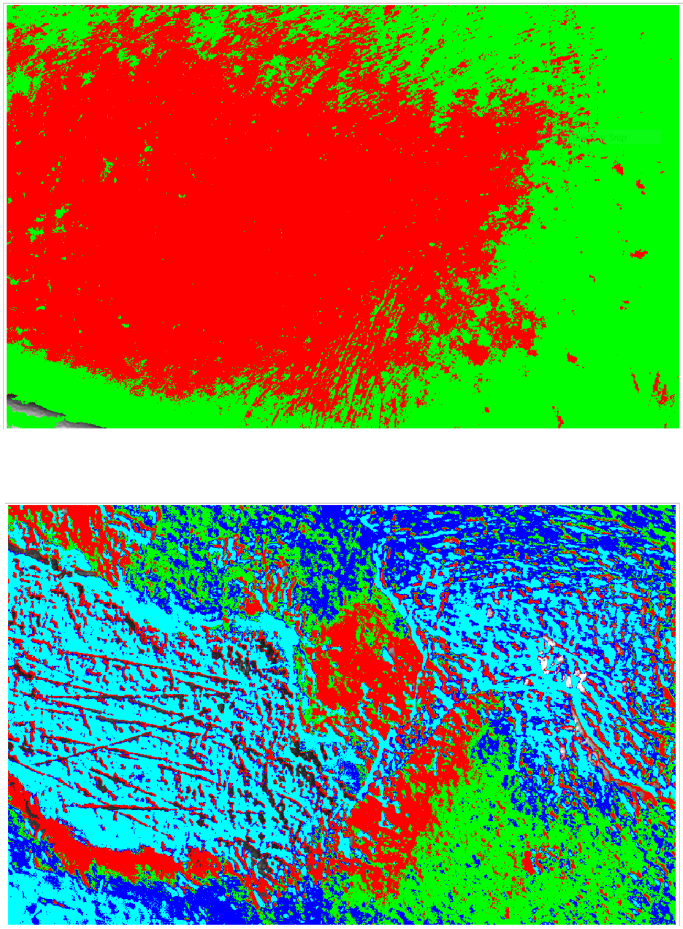

*Figure 3.28: Clustering with TrueScope software of the healed wound (top), and of the wound (bottom)*

Fig. 3.29, shows on the left the spectrum of the healed wound and healthy skin while on the right four distinct spectra are illustrated with the goal of seeing how the healing process is distinguishable and identifiable using the hyperspectral camera. Specifically, the first extracted region is at the wound, the second is at the presence of blood accumulation near the wound, the third is at the wound healing tract, and the last is extrapolated from the healthy skin. From the spectral analysis, characteristic peaks (544 nm, 614 nm, 642 nm, and 658 nm) are identifiable, not related to the composition of the skin, but to the spectral characteristics of the halogen lamp, fig. 2.15, used in the course of this analysis. It is visible, that the spectral content of the wound still under treatment is characterized by a totally different spectral content and with a much lower intensity, if compared both to the healthy skin, and to the almost healed one.

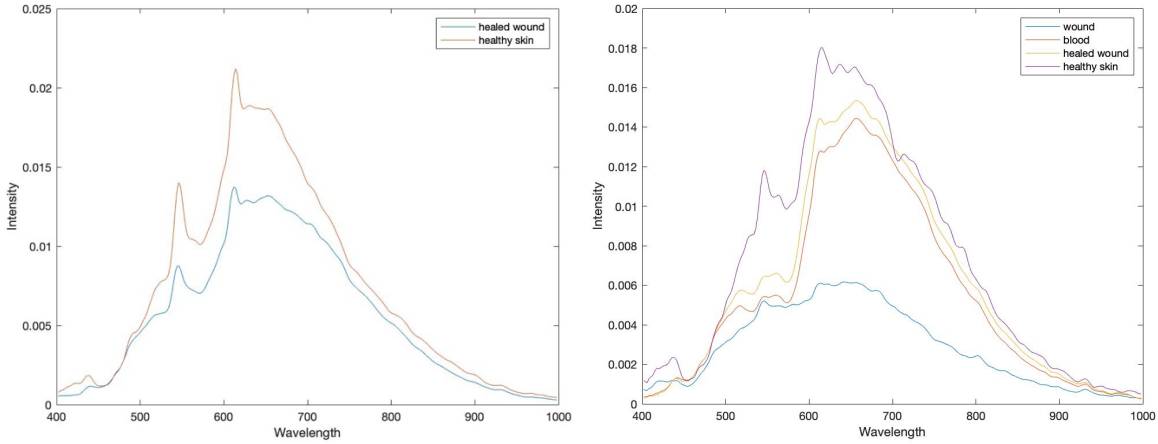


*Figure 3.29: Healed wound and healthy skin (left), wound spectrum (right)*

# CHAPTER 4 CONCLUSIONS

The objectives of this thesis work were several: first of all, the design and development of a calibration procedure of a hyperspectral imaging system, operating between 512 nm and 900 nm, integrated with a slit lamp and the subsequent evaluation of the functionality of the whole system from a medical point of view; secondly, the analysis of the hyperspectral system from a dermatological point of view in the evaluation and identification of the melanin content between a mole and the skin; finally, to verify how a hyperspectral system can be useful in the diagnosis and in the decision-making and treatment process of wound healing.
Regarding the first point, after the development of the calibration system, the final objective was to understand, together with a specialist in the field of ophthalmology, if such a system could be actually used as a biomedical device capable of providing a greater discriminatory capacity or additional information for early diagnosis of diseases affecting the eye, compared to the traditional instruments used. The slit lamp, was born primarily as optical coherence tomography (OCT) of the anterior segment, but at the same time thanks to the use of secondary lenses used by the ophthalmologist at the time of the examination allows to analyze the posterior segment, such as the macula, fovea and optic nerve. The slit lamp in this work has been modified not only with the addition of the hyperspectral chamber, Senop HSC-2, mounted in afocal mode on a slit lamp eyepiece, but also with a camera, in order to have a correct view of the desired sample. Initially it was essential to perform a calibration procedure, thanks to the use of a Spectralon, inserted into the mask cavity appropriately created to simulate the patient's face. The Spectralon made it possible to have a white reference image, the baseline target for all acquisitions. During the discussion with the expert, it first emerged, how the addition of the camera at the time of the examination was indispensable, and also, as was reported in the results, a good quality of the image obtained by the hyperspectral system with regard to the cornea and the anterior segment. The utility of the camera is to provide an instantaneous image, in color, of the scene framed by the specialist, and being characterized by the same path as the hyperspectral camera provides the same sample scene that can be seen "live" in the Senop-HSC 2 camera system, in black

and white. From the spectral survey, it was possible to see that the spectral information content of the front segment is actually not the only one. This detail was observed once fig. 3.24 was processed in MATLAB; in fact, it was possible to extract from the ROI coinciding with the iris its average spectrum.

In the future, with the aim of having a correct biomedical device, it will probably be necessary to modify the optical path of the slit lamp considering the degree of magnification of the lenses used by the specialist within the set-up of the slit lamp, so as to be able to obtain not only the spectral information content, but also a live image with sufficient illumination to identify the framed region.

Regarding the dermatological hyperspectral analysis conducted on the skin, it has been reported that this hyperspectral system provides an excellent discriminatory capacity for light and dark skin, making visible that the spectral content of dark skin is always lower than the light skin. This phenomenon is due to the fact that melanin, as reported in the literature, has its maximum absorption peak, around 780 nm, and consequently the spectral content of dark skin in the whole range prior to this wavelength is lower. The variation of the content of this pigment in the emission range, in the course of this thesis has not been examined; in fact, being melanin a fluorophore, emits at wavelengths longer than those of absorption, wavelengths that do not fall within the spectral range of the Senop-HSC chamber.

Focusing on the hyperspectral survey of the mole, two main peculiarities emerged. The first is related to the fact that even a healthy and small mole can be analyzed without difficulty with a hyperspectral camera. The second is concerning the higher spectral content of this pigment in the range extending from 700 nm to 750 nm compared to the surrounding skin. This result was demonstrated by both hyperspectral cameras. In the Senop-HSC hyperspectral camera, it is possible to notice in this range, a trend of the spectral content greater than that of the skin, while with the HinaLea camera, the behavior of the mole analyzed pixel by pixel, unlike the skin which decreases and fades after 700 nm, is characterized by a more pronounced and distinctive attitude. The result not expected from this thesis, but attributable to both skin texture and illumination, was that at the characteristic wavelength of the mole, coinciding with 720 nm, the latter behaves in the same way as the skin. A limitation in the work of this thesis in the use of the hyperspectral

camera HinaLea, is due to the fact that for a correct focus, the camera must necessarily be at least 15 centimeters away from the sample examined. To overcome this problem and achieve even better results, the traditional objectives that characterize this hyperspectral camera supplied by the manufacturer can be replaced, using appropriate adapters, by objectives with a higher magnification power. The result, brought in this study, on the discriminatory capacity of the hyperspectral system is very important because in the future, thanks to a more careful and precise analysis, taking into consideration not only healthy moles, but also melanomas, to the traditional law that regulates moles, such as "ABCDE", a new letter regarding the spectral content of the latter can be added.

Unlike the Senop-HSC hyperspectral camera, where before the analysis a careful process of calibration and subsequent implementation of the target in MATLAB was carried out, the second hyperspectral camera HinaLea 4250 was used alone, so the calibration process, thanks also to the advanced capabilities of the software related to the camera itself, was much easier and faster.

The last biomedical field in which the hyperspectral camera was used in the work of this thesis was the analysis of a wound caused by a vascular ulcer on an elderly person at the Torrette Hospital of Ancona. The monitoring and treatment of wounds is covering an increasingly important area thanks to the new dressings offered by the engineering field, for a correct and early healing of the patient. Hyperspectral analysis is essential to monitor over weeks the size, area and content of the wound compared to healthy skin. The hyperspectral investigation was performed in this work on a wound, treated with the Aquacel medical device, with the HinaLea 4250 hyperspectral camera. From the results that emerged from this study, it can be deduced how this technology allows to obtain, in a short time, reliable results that enable to understand if it is analyzing a wound, a portion of healing skin or a section of healthy skin.

For future studies, concerning this field, it would be useful to investigate the course and process of a wound healing, from the initial to the final state, at periodic and regular intervals, with the ultimate goal of collecting both a large number of data and spectral information that would allow the doctors to understand both in which stage it is and to determine unequivocally the treatment to be followed.

In conclusion of this study it can be deduced how the investigation with a hyperspectral camera can be useful in different biomedical fields to detect in an early way any pathologies not distinguishable to the naked eye and with other devices now in use by specialists in the sector. At the same time, this technology can also be considered as a valid tool to help guide and decide on the treatment of diseases. Employing in this study two different hyperspectral cameras, it emerged as the main limitation, how the desired scene acquisition is compromised by the acquisition time of the data, considering the fact that this technique does not acquire only the spatial content of a data, but also the spectral one, identified by a number of wavelengths. Consequently, before each acquisition it is important to define, according to the sample under examination, both the spectral range of interest and a limited number of bands in order to have at the same time an acquisition as useful as possible, but also fast in order to not have distortions due to artifacts of patient movement.

# REFERENCES


[1] Guolan L., Baowei F. Medical hyperspectral imaging: a review. 2014

[2] Cenni di storia della spettroscopia. http://spettroscopia.uai.it/Cenni%20di%20storia%20della%20spettroscopia.htm

[3] La nascita della spettroscopia: aspetti teorici e applicativi. https://www.google.com/url?q=https://elearning.uniroma1.it/pluginfile.php/602286/mod_folder/content/0/SDC%2520Lezione%252010%2520Bubsen%2520Kirchoff%2520e%2520le%2520origini%2520della%2520spettroscopia%2520di%2520emissione%253B%2520Il%2520sistema%2520periodico%2520di%2520D.%2520Mendeleev/SDC%252010a%2520Origini%2520della%2520spettroscopia.pdf%3Fforcedownload%3D1&sa=U&ved=2ahUKEwiIm5mn38TxAhVBuKQKHbQSA3UQFjAAegQIAxAB&usg=AOvVaw0stIB1Cv7ueMF2K49z0B9W

[4] Che cos'è la spettroscopia http://xoomer.virgilio.it/ggsbel/Teoria1/Introduzione.htm

[5] Spettrofotometria https://www.e-santoni.edu.it/wp-content/uploads/2019/10/qacs_spettrofotometria.pdf

[6] Barbur J.L., Stockman A. Photopic, Mesopic and Scotopic Vision and Changes in Visual Performance. 2010

[7] Lanaro M.P., Bonanomi C., Rizzi A. Open issues in the study of human retina. 2017

[8] MaO W., Miyagishima K.J., Yao Y., Soreghan B., Sampath A.P., Chen J. Functional Comparison of Rod and Cone G$_t$ on the Regulation of Light Sensitivity. 2012

[9] Zhang F., Kurokawa k., Bernucci M.T., Won Jung H., Lassoued A., Crowell J.A., JNeitz J., Neitz M., Miller D.T. Revealing How Color Vision Phenotype and Genotype Manifest in Individual Cone Cells. 2021

[10] Lewis A., Zhaoping L. Are cone sensitivities determined by natural color statistics?. 2006

[11] Stockman A., Sharpe L.T , Fach C. The spectral sensitivity of the human short-wavelength sensitive cones derived from thresholds and color matches.1998

[12] Zele A.J., Cao D. Vision under mesopic and scotopic illumination. 2015

[13] Min L., Peiyu W. , Jianhua D., Qi Y., Jiaqi J. The Circadian Effect Versus Mesopic Vision Effect in Road Lighting Applications. 2020

[14] Bradbury S., Evenne P.J. Absorption, Transmission And Reflection Of Light By The Specimen, Handbook Contrast Techniques in Light Microscopy.

[15] Bass M., Van Stryland E.W., Williams D.R., Wolfe W.L., Handbook of optics, devices, measurements, & properties. Second edition. Chapter 25. 1995
[16] Nayar S., K.Ikeuchi K., Kanade T. Surface reflection: Physical and geometrical perspective. 1991
[17] Kelley E.F., George R. Jones G.R., Germer T.A. The Three Components of Reflection. 1998
[18] Li Y., Zhang Y. , Rong Z., Wang W, Xie D. A Novel Microfacet Cosine Linear Kernel-Driven Bidirectional Reflectance Distribution Function Model. 2021
[19] Jones R.R., Hooper D.C., Zhang L., Daniel Wolverson D., Valev V.K. Raman Techniques: Fundamentals and Frontiers. 2019
[20] Xingcai L. , Xie L. , Zheng X. The comparison between the Mie theory and the Rayleigh approximation to calculate the EM scattering by partially charged sand. 2011
[21] Verhoeven J.W., Gossary of terms used in photochemistry. 1996
[22] Adão T., Hruška J., Pádua L., Bessa J., Peres E., Morais R., Sousa J., Hyperspectral Imaging: A Review on UAV-Based Sensors, Data Processing and Applications for Agriculture and Forestry. 2017
[23] Marvin E. Klein, Bernard J. Aalderink , Roberto Padoan , Gerrit de Bruin, Ted A.G. Steemers. Quantitative Hyperspectral Reflectance Imaging. 2008
[24] Signoroni A. , Savardi M. , Baronio A. , Benini S. Deep Learning Meets Hyperspectral Image Analysis: A Multidisciplinary Review. 2019
[25] Abdo M., Badilita V., Korvink J. Spatial scanning hyperspectral imaging combining a rotating slit with a Dove prism. 2019
[26] Hyperspectral and Multispectral Imaging. https://www.photonics.com/Articles/Hyperspectral_and_Multispectral_Imaging/a65595
[27] Grusche S. Basic slit spectroscope reveals three-dimensional scenes through diagonal slices of hyperspectral cubes. 2014
[28] Xie L.J., Wang A.C., Xu H.R, Fu X.P., Ying Y.B. Applications of near-infrared systems for quality evaluation of fruits: a review. 2016
[29] Yuen P. WT., Richardson M. An introduction to hyperspectral imaging and its application for security, surveillance and target acquisition. 2010
[30] Loewen E. Diffraction grating handbook. 2002
[31] Hyvarinen T., Herrala E., Dall'Ava A. Direct sight imaging spectrograph: a unique add-on component brings spectral imaging to industrial applications. 1998

[32] Favreau P., Hernandez C., Lindsey A.S., Alvarez D.F., Rich T., Prabhat P., Leavesley S.J. Thin-film tunable filters for hyperspectral fluorescence microscopy. 2014
[33] Slawson R.W., Ninkov Z., Horch E.P. Hyperspectral Imaging : Wide-Area Spectrophotometry Using a Liquid-Crystal Tunable Filter. 1999
[34] Gat N. Imaging Spectroscopy Using Tunable Filters: A Review. 2000
[35] Roth F. , Abbadi A., Herman O., Pavelek M., Prenosil V. Compact hybrid real-time hyperspectral imaging system with high effective spatial, spectral, and temporal resolution. 2016
[36] Abdlaty R., Sahli S., Hayward J., Fang Q. Hyperspectral imaging: comparison of acousto-optic and liquid crystal tunable filters. 2018
[37] Qingli L., Xiaofu H., Yiting W., Hongying L., Dongrong X., Fangmin G. Review of spectral imaging technology in biomedical engineering: achievements and challenges. 2013
[38] Irie K., McKinnon A.E., Unsworth K., Woodhead I.M. A model for measurement of noise in CCD digital video cameras. 2014
[39] Jedidi W., Poisson Shot Noise Traffic Model and Approximation of Significant Functionals. 2014
[40] Konnik M., Welsh J. High-level numerical simulations of noise in CCD and CMOS photosensors: review and tutorial. 2014
[41] CCD Image sensor noise Sources https://www.onsemi.com/pub/Collateral/AND9189-D.PDF
[42] Anderson R., Malila W., Maxwell R. ,Reed L., Military Utility of Multispectral and Hyperspectral Sensors. 1994
[43] Ren J., Zabalza J., Marshall S., Zheng J. Effective Feature Extraction and Data Reduction in Remote Sensing Using Hyperspectral Imaging
[44] Ravikanth L. , Jayas D.S., White N.D.G., Fields P.G., & Sun D.W. Extraction of Spectral Information from Hyperspectral Data and Application of Hyperspectral Imaging for Food and Agricultural Products. 2016
[45] Wang D., Dowell F.E., Ram M.S., Schapaugh W.T., Classification of Fungal-Damaged Soybean Seeds Using Near-Infrared Spectroscopy. 2004
[46] Edelman G.J., Gaston E., Van Leeuwen T.G., Cullen P.J., Aalders M.C.G. Hyperspectral imaging for non-contact analysis of forensic traces. 2012
[47] Funk C.C., Theiler J., Roberts D.A., Borel C.C., Clustering to Improve Matched Filter Detection of Weak Gas Plumes in Hyperspectral Thermal Imagery. 2001

[48] Suja V.C., Sentmanat J., Hofmann G.,Scales C., Fuller G.G. Hyperspectral imaging for dynamic thin film interferometry. 2020
[49] Carvalho E.R., Hoveling R.J.M., Noorden C.J.F , Schlingemann R.O, Aalders M.C.G., Functional Imaging of the Ocular Fundus Using an 8-Band Retinal Multispectral Imaging System. 2020
[50] Yung M., Klufas M.A., Sarraf D. Clinical applications of fundus autofluorescence in retinal disease. 2016
[51] Kolb H. Gross Anatomy of the eye. 2007
[52] Zhu J., Zhang E., Del Rio- Tsonis K., Eye Antomy. 2002
[53] Willoughby C.E., Ponzin D., Ferrari S., Lobo A., Anatomy and physiology of the human eye: effects of mucopolysaccharidoses disease on structure and function – a review. 2010.
[54] Ehrlich R., Harris A., Kheradiya N.S., Winston D.M., Ciulla T.A., Wirostko B. Age-related macular degeneration and the aging eye. 2008
[55] Joseph F., Rizzo I.I.I. Embryology, Anatomy, and Physiology of the Afferent Visual Pathway.
[56] Wing G.L., Blanchard G.C., Weiter JJ. The topography and age relationship of lipofuscin concentration in the retinal pigment epithelium. 1977
[57] Kennedy C.J., Rakoczy P.E., Constable J.J. Lipofuscin of the retinal pigment epithelium: a review. 1995
[58] Slit-Lamp Biomicroscopy. Chapter 10. https://chicago.medicine.uic.edu/wp-content/uploads/sites/6/2018/04/Workshop-Slit-Lamp.pdf
[59] Anteprima dell'atlante di Eye-Banking http://www.bancheocchi.it/pdf/corso16/Pagani.pdf
[60] Evaluation atlas of cornea https://www.bancheocchi.it/pdf/atlanteSIBO/Evaluation_atlas_of_corneas.pdf
[61] Advanced Slit Lamp skills https://www.healthpartners.com/institute/wp-content/uploads/2018/05/3-SA-45-SLE-Handouts-new.pdf
[62] Rediscover Your Red- Free https://www.healthpartners.com/institute/wp-content/uploads/2018/05/3-SA-45-SLE-Handouts-new.pdf
[63] Mordant D.J., Al-Abboud L., Muyo G., Gorman A., Sallam A., Rodmell P., Crowe J., Morgan S., Ritchie P., Harvey A.R., McNaughtA.I. Validation of Human Whole Blood Oximetry, Using a Hyperspectral Fundus Camera with a Model Eye. 2011

[64] Mordant D.J., Al-Abboud I. , Muyo G.,, Gorman A., Harvey A.R., McNaught AI. Oxygen saturation measurements of the retinal vasculature in treated asymmetrical primary open-angle glaucoma using hyperspectral imaging. 2013
[65] Mullins R.F., Russell S.R., Anderson D.H., Hageman G.S. Drusen associated with aging and age-related macular degeneration contain proteins common to extracellular deposits associated with atherosclerosis, elastosis, amyloidosis, and dense deposit disease. 2000
[66] Rama D. Jager R.D., Mieler W.F., Miller J.W. Age-Related Macular Degeneration. 2009
[67] Abbas K., Qadir M.I., Anwar S., The role of melanin in skin cancer. 2018
[68] Yamaguchi Y., Hearing V.J. Melanocytes and Their Diseases. 2014
[69] Dicker D.T, Lerner J., Van Belle P., Guerry D., Herlyn M., Elder D.E., El-Deiry W.S. Differentiation of normal skin and melanoma using high resolution hyperspectral imaging. 2006
[70] Qinghua H., Ruikang W. Hyperspectral imaging enabled by an unmodified smartphone for analyzing skin morphological features and monitoring hemodynamics. 2020
[71] Stamatas G.N., Balas C., Kollias N. Hyperspectral Image Acquisition and Analysis of Skin. 2014
[72] Dimitrow E., Riemann I., Ehlers A., Koehler M.J., Norgauer J., Elsner P., Konig K., Kaatz M. Spectral fluorescence lifetime detection and selective melanin imaging by multiphoton laser tomography for melanoma diagnosis. 2008
[73] Leupold D., Pfeifer L., Hofmann M., Forschner A. , Wessler G., Haenssle H. From Melanocytes to Melanoma Cells: Characterization of the Malignant Transformation by Four Distinctly Different
[74] Pavlovčič U., Diaci J., Možina J., Jezeršek M., Wound perimeter, area, and volume measurement based on laser 3D and color acquisition. 2015
[75] Grey J.E., Enoch S., Harding K.G. Venous and arterial leg ulcers. 2006
[76] Finlayson K., Edwards H., Courtney M. Factors associated with recurrence of venous leg ulcers: A survey and retrospective chart review. 2009
[77] Sussman G. Ulcer dressings and management. 2014
[78] Joseph E Grey J.E., Enoch S., Harding K.G. ABC of wound healing Pressure ulcers. 2006
[79] Sorg H., Tilkorn D.J., Hager S. Hauser J., MirastschijskI U., Skin Wound Healing: An Update on the Current Knowledge and Concepts. 2016

[80] Saiko G., Lombardi P., Armstrong D., Harding K., Hyperspectral imaging in wound care: A systematic review. 2020
[81] Demirbas U., Sennaroglu A., Kartner F.X., Temperature dependence of Alexandrite effective emission cross section and small signal gain over the 25-450 °C range. 2019
[82] Walker M., Hobot J.A., Newman G.R., Bowler P.G. Scanning electron microscopic examination of bacterial immobilisation in a carboxymethyl cellulose (AQUACELS) and alginate dressings. 2002